MONASH University

Fabrication of Axi-symmetric Hybrid Materials Using Combination of Shear and Pressure

A thesis submitted in fulfilment of the requirements

for the award of the degree of

Doctor of Philosophy

by

Thaneshan Sapanathan

Department of Mechanical and Aerospace Engineering

Monash University

2014

Acronyms

AFSCE	Axi-symmetric Forward spiral composite extrusion
AFSE	Axi-symmetric Forward spiral extrusion
Al/Cu	aluminum/copper
BSE	backscattered electron
CHPT	Confined High Pressure Torsion
DBT	Dedicated Blanking Test
DBTT	ductile–brittle transition temperature
DFB	Diffusion bonding
DFW	Diffusion welding
EBSD	Electron backscatter diffraction
ECAE	Equal channel angular extrusion
ECAP	Equal Channel Angular Pressing
EDM	Electric discharge machining
EDX	Energy-dispersive X-ray spectroscopy
FE	Finite Element
FIB	Focused ion beam
HAGB	High-Angle Grain Boundary
HIP	Hot Isostatic Pressing
HPT	High Pressure Torsion
I-ECAP	Incremental-Equal Channel Angular Pressing
IMC	Intermetallic Compound
LAGB	Low-Angle Grain Boundary
MSPT	Micro shear punch test
OM	Optical microscopy
Pt	Platinum
SE	Secondary electron
SEM	scanning electron microscope
SPD	Severe Plastic Deformation
TE	Twist Extrusion

T-ECAP	Torsional-Equal Channel Angular Pressing
Tm	Melting temperature
UFG	Ultra-fined grain
VLAFSE	Variable Lead Axi-symmetric Forward spiral composite extrusion
XRD	X-ray diffraction spectroscopy

Declaration Statement

I, Thaneshan Sapanathan, declare that the thesis entitled "Fabrication of Axi-symmetric Hybrid Materials Using Combination of Shear and Pressure" submitted in the fulfilment of the requirements for the award of the degree of Doctor of Philosophy, at the department of Mechanical and Aerospace Engineering, Monash University, is entirely my own work.

I affirm to the best of my knowledge, the thesis does not contain any material that has been submitted or accepted for the award of another degree, diploma or qualification in any other university or institution of learning. I also certify that the thesis contains no material previously published or written by another person, except where due reference is made in the text of the thesis.

(Thaneshan Sapanathan)

Date:

This thesis is lovingly dedicated to my parents

for their love, encouragement and support

Abstract

Innovative manufacturing processes are considered as the alternate solutions to produce materials for the growing demand. Hybrid materials become attractive alternatives in engineering applications; they can provide multiple attributes in a single solution. Cladded hybrid rods and tubes, a special type of hybrid metals are fabricated using various techniques, such as extrusion, drawing, hydrostatic extrusion processes.

From a literature survey, it was identified that new sophisticated processes are required to eliminate the existing issues in those hybrid metals manufacturing methods and to obtain the product with multiple attributes. Meanwhile, severe plastic deformation (SPD) processes are well known for delivering high strength processed materials because of their capability of producing materials with significant grain refinement. Therefore, two novel axi-symmetric SPD processes were investigated by utilizing the synergic effect of these processes in hybrid materials fabrications.

Firstly, the axi-symmetric forward spiral composite extrusion process (AFSCE) was investigated for a fabrication of Al/Cu clad rods which produces the hybrid rods with good quality bond with bonding shear strength of ~50.5MPa. A dedicated blanking test was designed to evaluate the bond strength of the processed samples. AFSCE is also a near-zero shape change process and has better dimensional control on the core and clad of the products. The extruded samples were investigated using FIB, SEM, EDX, XRD, EBSD and micro-hardness test to characterize the bonded interface and parent materials. A cup shape hardness behavior of hardness was identified in both materials and ultrafine grain formation was confirmed in the copper region at the interface.

Then a confined high pressure torsion process (CHPT), was used to fabricate Al/Cu cladded discs are presented in the 2nd part of the thesis. The CHPT process showed a significant improvement in the compacted aluminum powder samples and the powder regions of the Al/Cu clad components. The compacted Al powder samples have higher shear strength than Al alloy "AA5005-H34" and 5 times higher shear strength than pure bulk aluminum. The effective compaction of this process is promising for fabrication of high strength materials in an economical way which can eliminate the sintering process which is required for the traditional powder processing methods.

Acknowledgments

I would like to express my sincere gratitude for my supervisors A/Prof. Raafat Ibrahim, Dr. Saden H Zahiri and Dr. Shahin Khoddam for their valuable support for my project. I do not have words to explain their continuous support and valuable discussions which make the project to move in the right direction. Not only I appreciate their support on the project aspects, but also I have to thank for their roles as good mentors and guides whenever I was having problems in my project.

I also acknowledge Prof. Raman Singh for giving permission to use cold mounting, grinding and polishing facilities in the corrosion lab located in Room 37 and Prof. Jianfeng Nie allowing access to the Micro Hardness Tester in the metallography lab in Room 186/Building 37.

My PhD involves a lot of experimental work which required a lot of assistance from mechanical and Aerospace Engineering workshop staff. In particular, I should thank to Mr.Hugh Venables, Mr.Nat Derose, Mr.Narendra Babu and Mr. Santhosh Babu for their assistance in manufacturing parts and setting up equipments.

I also acknowledge the use of the facilities and assistance of Mr. David Vowles, Dr.Flame Burgmann and Dr. Xi-Ya Fang and at the Monash Centre for Electron Microscopy. This research used equipment funded by Australian Research Council Grant LE0882821.

I would like to acknowledge Mr. Rod Mackie for conducting XRD on my samples and Mr. Irek Kozicki for assisting me in metallurgical sample preparation. I would also like to thank Ms. Jane Moodie for language help and assistance on my writing which helped me a lot to improve my academic writing skills.

I would like to thank my colleagues who have supported and helped me throughout my PhD. I would also like to thank my relatives and friends for their encouragements and support. I should also thank Mr. Perayirampillai Thanikasalam and Dr. Selvasothy Sellathurai for their kindness blessings to pursue and succeed in my project. Finally I would like to thank my parents for their encouragement and never ending love in my life which bring me to succeed in this level of achievement.

List of Publications

- Sapanathan T, Khoddam S, Zahiri SH. Spiral Extrusion of Aluminum/Copper Composite for Future Manufacturing of Hybrid Rods: A Study of Bond Strength and Interfacial Characteristics. Journal of Alloys and Compounds. 2013; 571:85-92.

- Sapanathan T, Khoddam S, Zahiri SH, Zarei-Hanzaki A. Strength changes and bonded interface investigations in a spiral extruded aluminum/copper composite. Journal of Materials & Design. 2014; 57:306-14.

- Sapanathan T, Ibrahim R, Khoddam S, Zahiri SH. Shear blanking test of a mechanically bonded aluminum/copper composite using experimental and numerical methods. Journal of Materials science and Engineering A. 2015; 623:153-64

- Raymond S, Sapanathan T, Tim F, Ibrahim R, Nairn J, Lemiale V, Khoddam S. Investigation of Dynamic behaviour in the core material of a spiral extruded composite using a meshfree technique, *submitted to* Computing in Science & Engineering in May 2014

- Sapanathan T, Ibrahim R, Khoddam S, Zahiri SH., Numerical modeling to determine test conditions of shear blanking test for a hybrid material, Presented in ICMAE 2014 – Madrid, Spain and published in Advanced Materials Research (ISBN 13:978-3-03835-223-5), 2014, pp. 125-129

Copyright Notice 1

Copyright Notice 2

Table of Contents

List of Tables

List of Figures

Chapter 1:
Introduction

Chapter 1: Introduction

1.1 Background

It is hard to think of an electrical appliance without the use of copper. Copper is heavily used in electronics, electrical motor windings, large and small scale transformers, electric cables and connecting bus bars. Early days copper was heavily used in many other applications such as cooking utensils, water pipe lines, taps, and gas pipelines. However, due to the price of copper soars to its all-time high in recent years, copper is not preferred by manufacturers to be used in all sorts of applications where alternate materials are available.

On the other hand, it is also the peak of copper production than never before. The advanced technologies and resources, and increasing demand, high cost of copper are those underlying reasons for the heavy production of copper by mining industries. However, it is always true that the resources in the earth are finite which requires supplying sustainable alternatives for a long term supply of copper. However, due to aforementioned reasons, the need of copper cannot be ignored.

But, advancement in modern technology allows formulating alternate solution to the high demand of copper where a new material or a combination of more than one material could solve the issue of demanding supply for copper. Due to the increasingly high demand for competitive materials, hybrid material fabrication has received growing interest in the last decade. These materials are sought after since they are able to deliver more than one desired property [1, 2] while minimizing the downsides of conventional materials.

Joining process could be an attractive way to fabricate composite material such as copper and aluminum, which can reduce the material cost significantly. However efficient fabrication process to join dissimilar materials are limited. Therefore in this research two novel techniques were proposed to fabricate copper clad aluminum hybrid structures.

In the last decade “architecture hybrid materials” also became an attractive paradigm of material designed with improved specific characteristics, which enables to manufacture new pool hybrid materials. Bimetallic hybrid metals can be fabricated using various techniques by joining two materials in different orientations. In the past hybrid metals were formulated using metal forming and metal

joining processes. Modern metal forming techniques such as Severe Plastic Deformation (SPD) processes, which are typically used to process single materials, have been recently applied to fabricate “architectured hybrid materials”. SPD processes significantly improve material properties and become potential manufacturing methods to produce bulk ultra-fine grained materials [3]. The combination of the capabilty of producing bulk ultra-fine grained material and “inner architectured metal-based composites” introduces a new paradigm of materials design using these SPD processes [4, 5]. Formation of the ultra-fine grained micro-structure in such hybrid materials contribute to the ultra-high strength of these new advanced materials (“architectured hybrid materials”).

Therefore, fabrication processes of new hybrid materials are essential to fulfil the demanding need for new materials. Severe plastic deformation processes have a synergistic effect in the fabrication of the hybrid materials within the modern pool of advanced materials by improving the properties of fabricated materials and fulfilling the component requirements. Therefore in order to fabricate such “architectured hybrid materials”, Axi - Symmetric Forward Spiral Composite Extrusion (AFSCE) process and Confined High pressure Torsion (CHPT) processes were proposed and the fabricated composite samples were investigated using various mechanical and metallurgical characterization techniques.

1.2 Aims and approach

There is a growing interest in hybrid materials for many current industrial applications such as aerospace industry, chemical/petroleum processing plants, and medical equipment where the properties of one material alone are inadequate to fulfill particular requirements [2].In order to fabricate a bimetallic hybrid metal, an effective bond at the interface is required. An effective bonding can be produced using various methods such as cold welding, diffusion welding, explosive welding and friction stir welding. In general, those joining processes are considered as secondary manufacturing methods which have their own advantage and disadvantage. In general, the joint at the interface occurs due to a diffusion bonding mechanism or a mechanical interlocking mechanism. In a diffusive bonding, intermetallic compounds (IMCs), oxides and carbides may present at the interface. In order to create an effective bonding at the interface, various process parameters are required such as pressure, elevated temperature, holding time and shear vibration, which varies with a particular joining technique.

Here, in this project, severe plastic deformation (SPD) processes are proposed to fabricate hybrid metals with an ultimate aim of obtaining an effective bonding with ultra-high strength in processed materials.

Therefore, this project was investigated for two novel axi-symmetric hybrid metal fabrication processes. The newly introduced fabrication processes are called Axi-Symmetric Forward Spiral Composite Extrusion (AFSCE) process and Confined High pressure Torsion (CHPT) process. Both of these processes are using a combination of shear deformation and hydrostatic pressure for the fabrication of hybrid metal. These processes allow the fabrication of coaxial bimetallic composites which are difficult to be fabricated using convectional joining processes. These two novel processing techniques also produce the final product with near-zero change in diameter. More importantly, these two processes are performed in single step, which does required additional heat treatment stages. Therefore, these processes are more efficient in terms of cost and time.

It was considered to fabricate core-clad hybrid rods using these axi-symmetric hybrid metal fabrication processes. Firstly, the Axi-symmetric Forward Spiral Composite Extrusion (AFSCE) process was investigated for a solid metal to metal joining. In this process the helical grooves facilitate the material to rotate which induce the tangential shear deformation perpendicular to the normal extrusion direction. The first part of this project was conducted to identify the process parameters to produce an effective hybrid metal bonding. It was aimed to produce a hybrid metal bonding using AFSCE process with a good bonding strength. A case study of copper clad aluminum rod was successfully fabricated at an elevated temperature condition of 300°C and with a back pressure of 200MPa. The bond strength investigations of the fabricated samples were carried out using a specially designed dedicated blanking test (DBT) rig which was designed with the assistance of finite element simulations. The dedicated blanking test was designed for the requirement to cause to the failure at the interface to assess the effectiveness of the bonding.

Based on initial assessments using an optical microscope and by a physical examination of the split composite samples, a bonding was confirmed. The mechanism of the bond formation, nature of the interface and mechanism of material deformation during the process were further investigated using advanced techniques which include Scanning Electron Microscope (SEM), Energy dispersive X-ray spectroscopy (EDX) analyses, X-ray diffraction (XRD) analyses, fractography of the fractured interface analyses, Focused Ion Beam (FIB) and Electron Backscatter Diffraction (EBSD) analyses and Micro hardness tests. In addition to this, two extreme cases of proposed velocity field were considered for fully sticking and fully sliding conditions respectively, to develop an analytical solution which was used to calculate strain components of the processed samples using bimetallic co-extrusion.

After that, Confined High Pressure Torsion (CHPT) process was also investigated for a fabrication of powder – solid hybrid material. The CHPT is a modified version of high pressure torsion (HPT) process, performed on a solid or powdered material using concurrent application of hydrostatic pressure and shear stress using a rotating anvil. In this project, a case study of aluminum powder filled inside a copper ring was employed to fabricate a powder solid hybrid material using the CHPT process. The composite sample fabrication has potential to produce an aluminum region with a higher density and the lowest amount of porosity. The porosity elimination on the aluminum powder is one of the key features of investigation because of the aluminum powder experiences a multi-directional compaction that could help the porosity elimination of the powder region. Porosity and strength of compacted aluminum were measured using micro-shear punch tests and density measurements.

Prior to the aluminum/copper (Al/Cu) clad composite sample fabrication using the CHPT process, the CHPT process was also investigated for aluminum powder only which aimed to achieve high strength aluminum compacted samples at room temperature. Initial experimental studies of the CHPT processed using the aluminum powder samples were characterized using grain size measurements, micro-shear punch tests and density measurements and the results were compared with 99.999% pure bulk aluminum and the aluminum alloy AA5005-H34. After that, the effect of the hydrostatic pressure on the fabrication of Al/Cu clad composite samples were also investigated, by applying various amount of pressure to the composite samples without torsional straining, which facilitate a multi-dimensional compression in the aluminum powder region of the Al/Cu clad composite samples.

In both of these processes, the fabrication of axi-symmetric hybrid samples using shear deformation and normal pressure was established. In the AFSCE process, elevated temperature condition with applied backpressure was used to fabricate copper clad aluminum rods using both bulk materials. In addition to it, the analytical and experimental framework of these processes was utilized to understand the AFSCE process, hybrid bond strength, the nature of the bonded interface and the bonding mechanism. In the CHPT process, powdered aluminum filled inside a copper ring configuration was used to fabricate copper clad aluminum discs. CHPT processed samples were investigated to determine the effective compaction for the compacted powder region in the samples.

1.3 Thesis structure

Firstly, a comprehensive literature review will be presented in chapter two which included details of metal forming processes including severe plastic (SPD) processes and metal joining processes. The chapter two also includes the metal cladding and powder metal processing as this project involve SPD process on both bulk and powder materials to produce clad materials. In addition to is, this chapter also delves with the merits and drawbacks in the existing core clad bimetals fabrication methods and finally summaries the gaps in the existing research work in this area.

After that, the proposed AFSCE process is presented in chapter three, which explains the key features, experimental requirements and implementation of the process. Implementation of the process to fabricate hybrid material was explained using a case study of a copper clad aluminum fabrication. After that, the chapter three explains the detail of macroscopic and initial microscopic investigations using optical microscopy and scanning electron microscopy techniques. This chapter also includes the derivation of strain components of the processed samples for two extreme boundary conditions of the AFSCE process. In addition to this, bonding shear strength measurements using a dedicated blanking test (DBT) rig and justification was also included in chapter 3.

Chapter four presents the detail investigation of the bonded interface using various advanced delegate techniques. In order to avoid the artifacts of standard sample preparation during grinding and polishing processes, a focused ion beam technique was utilized to investigate the interface of the Al/Cu clad sample. A combination of FIB, SEM, and EXD were used to investigate the interfacial diffusion and formation of intermetallic at the interface of the processed samples is also explained in this chapter. After that, micro-hardness results along the radial direction of the transverse cross section of the sample in the parent materials are presented in this chapter. The micro-hardness results indicate a special cup shape behavior, which was explained using kinematic descriptions. Further verification for the formation of intermetallic compounds (IMCs) using was performed using X-ray spectroscopy (XRD), is also included in this chapter. The analyses of EBSD and texture are used to correlate with the strain energy accumulation in the material and micro-hardness results. This chapter also presents the finding of ultrafine grain formation in the copper region near the interface using the data obtained in the EBSD analyses.

The detail design and required parameters of the of the dedicated blanking test rig design is presented in chapter five, which incorporates a finite element analysis as well as the experimental procedure for design of the required test rig.

Chapter six introduces the second axi-symmetric hybrid material fabrication process, called confined high pressure torsion (CHPT) process. This explains the key features of the CHPT process and an application of the process to copper clad aluminum sample using a combination of bulk copper and aluminum powder material. The process is also investigated for aluminum powder samples and copper clad aluminum samples under multi-dimensional compression, are also presented in this chapter. This chapter also includes the density measurements; micro-structural observations, micro hardness results and micro shear punch test results for various cases of the CHPT process. These results are used to discuss the porosity and the shear strength for the aluminum region of compacted samples and compared with 99.999% pure bulk aluminum and the aluminum alloy AA5005-H34, are also included in this chapter. Microstructural changes at various locations of the CHPT processed aluminum powder sample is also presented in chapter 6.

Finally the chapter seven of this thesis that concludes the entire performed works and deliver some recommendations for further research in this area.

Chapter 2:
Literature review

Chapter 2: Literature review

2.1 Introduction

Hybrid materials are in a growing interest in current industrial applications; whereas property of one single material cannot fulfill with a number of requirements [1, 2]. Hybrid materials are formed as a combination of two or more component materials with different mechanical and chemical properties. Alternatively simple solution exists when one single material meet all the requirements [6]. They are classified based on their structure as composite, lattice, sandwich and segments. The hybrid materials are fabricated by combining metals, ceramics, polymers, elastomers and glasses. In this category, hybrid metals are a form of hybrid material which has two or more metallic component. Steel, cast iron, clad metals, bimetal strips and alloys are few examples of hybrid metal.

Hybrid metals can be classified into alloys and metallic composites. Alloys are made by using mixture of metallic solid solution composed of two or more elements. Metallic composite type hybrids are formed by metal joining processes or metal forming processes such as cladding of two metals. Bimetallic hybrid materials contain desired properties of the two metallic materials. For example these materials combine different properties such as light weight and high strength. Some of the earlier examples of these bimetals can be seen in automatic switches of Iron boxes. However, nowadays cladded materials are heavily used in many industries such as medical, aerospace, chemical industries and oil refineries. The manufacturing techniques of such composite materials are highly demanding and receiving a growing level of interest.

The production of hybrid materials is a cost effective way to produce materials with desired properties which increases the usage of such materials. For example, hybrid turbine router [7] and hybrid gas turbine blade [8] were invented because of the competitive advantages of hybrid materials. Aerospace companies prefer the fuel economy which can save a large amount of operational cost. In order to increase the fuel economy, it is necessary to increase the turbine operating temperature. But the temperatures vary throughout a turbine. Therefore specific parts of a turbine required to stand for a very high temperature of approximately 1500°C to 1800°C [8, 9]. The high temperature melting super alloys are expensive compared to the low temperature melting materials. Therefore, by studying the temperature variation in a single part, it is possible to manufacture a hybrid metal with a combination of

a high temperature and a low temperature melting materials. Therefore, hybrids metals are one of the economically viable solutions to manufacture effective gas turbine parts [7, 8].

In this current research, the main aim of the work is to fabricate hybrid metal as alternative to copper as discussed earlier in chapter 1. In general hybrid bimetal can be fabricated using various techniques using metal forming processes and metal joining processes. In this project, two severe plastic deformation (SPD) processes were considered to fabricate hybrid materials alternative to copper. An axi symmetric forward spiral composite extrusion (AFSCE) process and a confined high pressure torsion process were used to produce copper clad aluminum composite materials, are investigated in this project.

Firstly, literatures associated with the processes and similar forming methods are discussed in this chapter. After that, theories related to the techniques used in the project are also discussed. Reasons and fundamental advantages for considering these new processes (AFSCE and CHPT) are also presented in this chapter.

2.2 Metal forming processes

Metal forming processes can be defined to produce an intermediate shape or a final shape of metal part from a billet material. A few traditional metal forming processes are rolling, drawing, forging and extrusion. Metal forming processes mainly consist of specially made dies which facilitate materials to flow in desired shapes. The dies are made with high strength tooling materials to avoid wear and abrasion due to large amount of pressure and friction loads during forming processes. Metal forming processes can be primarily classified into bulk deformation processes and sheet metal forming processes. A bulk forming process generally involves significant plastic deformations and large shape changes. Forging, drawing, rolling and extrusion are some examples of bulk metal forming techniques. Bulk forming processes have a starting form of cylindrical bars, rectangular billets and metal slabs. The volume of the material remains constant while the surface area changes significantly in a bulk forming process. Bulk forming processes are economically viable to produce intermediate or final products with good mechanical properties [10, 11]. On the other hand, a sheet forming process mainly used to fabricate a sheet metal using a process such as deep drawing, rolling, bending and stamping techniques [12]. Final product of a sheet metal forming process is a sheet metal with constant thickness throughout the entire product.

These metal forming processes are performed in cold, hot and warm process temperatures [13, 14]. The elevated temperature working conditions are suitable to increase the formability of metal working conditions. However, high temperature forming can cause a significant change in mechanical properties metals due to micro-structural changes, annealing, recovery and recrystallization. Therefore, cold forming processes are mostly preferred over the hot forming processes [13]. Cold forming processes can also be aided by applying a small amount of heating which can facilitate the plastic deformation of the materials [13].

There are various governing parameters in metal forming processes such as metal flow, friction between die and material, heat transfer and heat generation [11, 15, 16]. Quantitative analyses of these parameters are important to design, control and optimize a metal forming process. Some of these parameters can be obtained by experimental methods while some other parameters such as relative velocity, friction effect and strain rate required both experimental and numerical modeling [17-19].

2.3 Metal joining processes

Various joining processes are used to join similar and dissimilar materials. Metallic material joining process can be performed by different processes such as Oxyfuel gas arc welding, solid state welding processes, brazing and soldering. The solid state welding process can be performed using various processing methods. Some examples of solid state welding processes are listed below:

- ***Forge welding*** – Forge welding is a very traditional welding method which is used to join two metals by applying gradual pressure or hammering the work pieces together at an elevated temperature.
- ***Cold welding*** – This process performed at room temperature by applying sufficient pressure to cause 30-50 percent plastic deformation, which cause the metallic bonding [13]. The cold welding process is performed using either dies or rollers which is more suitable for soft ductile material [13, 20]. However, bonding dissimilar metals at room temperature may form mutually soluble or brittle intermetallic compounds which could create a weak welded joint [20].
- ***Roll welding process*** – Two or more sheet metals or metals plates are bonded together using a rolling mill at either hot or cold temperature. Roll welding process performed at cold operating temperature can also considered as a cold welding process.

- ***Friction welding or Inertia welding*** – While one metal is rotating; the other metal is moved laterally and pressed together to create a bonding. The friction during the process produces the required amount of heat to bond the two metals together[13].
- ***Friction stir welding*** – A rotating probe produces the required friction heat which facilitates the bonding between two metals [13].
- ***Diffusion welding***- Atomic diffusion occurs at elevated temperature and high contact pressure with sufficient contact time of the two metals which facilitate this bonding process[21, 22]. It has been found to be a suitable welding method for dissimilar metals.
- ***Explosive welding*** –Two materials are closely placed to each other and the explosive material is placed on a surface of one of the materials. After that, explosive material was detonated to produce the required pressure and heat to perform welding of two materials.
- ***Ultrasonic welding-*** The ultrasonic welding is performed using high frequency (10,000 to 200,000 Hz) shear vibration on the surface of the metals [13].

2.4 Metal cladding process

Deposit of a material on a different material is generally known as coating. However, the term “coating” is only valid when a depositing material in a form of a liquid or gas [13]. The depositing material in solid form, the process called “cladding” [13]. Therefore, a fabrication of a composite material using roll bonding or explosive welding or extrusion processes can be considered as a cladding process [13]. As a result of a cladding process a formation of a laminating layer of a material over the parent material occurs which works together as a composite material and enhances the property of the parent material by adding properties such as corrosion resistance, wear resistance, electrical conductivity, thermal conductivity and improved appearance to the parent material.

Another research done by Chen et al. on the effect of laser cladding on fatigue strength of an alloy steel concludes that the laser cladding of the specimens improved the fatigue life of the parent metal by 2-5 times as compared with the un-cladded specimens [23]. However this research also demonstrates that defects such as voids in the cladding layer will affect the fatigue strength and cause a larger scatter in fatigue life of the parts. They had observed that the specimens without large defects were strengthened more notably [23].

2.5 Powder metal processing

On the other hand, the use of elementary powder as raw material instead of bulk metal in a process provides several advantages. Conventionally, powder consolidation can be done by several techniques, such as Die Compaction, Cold Isostatic Pressing (CIP) and Hot Isostatic Pressing (HIP). In powder metallurgy, the parts can easily be manufactured to near net shape of the final product which minimizes the material wastage during the additional machining stages. Typically, the waste produced in traditional processes, such as casting and press forming where bulk metal is used, often exceeds fifty percent of the starting form of the material [13]. Therefore, this advantage can become a key consideration when the process involved expensive or rare materials. Furthermore, the use of metal powder is also cost saving and enables wide variation in compositions and properties of green compact formed. Products with controlled porosity and complex shapes that cannot be machined economically can also be produced by powder process. In addition to this, the powder processing technique is well suitable for high strength materials such as titanium alloys because it minimize the machining requirement to deliver the final product.

However, the specimen produced by such techniques may become inhomogeneous, hence weaker in its mechanical properties because of the friction between the powder particles and the die wall [24]. Therefore, admixed lubricant is often used in these traditional techniques to increase the density and improve the mechanical properties of the produced green compact specimen [24]. In addition, CIP is often followed by vacuum sintering procedure due to its inability to fully eliminate the sealed-off pores of powders even at large isostatic pressure. Since HIP process typically involves high temperature, it may contaminate or oxidize the powder materials or cause grain growth at elevated temperatures. It is thus desirable to perform powder consolidation at room temperature to avoid heating damage caused by sintering process on green compact produced. Alternatively, high pressure torsion (HPT) process can also be used for powder consolidation as it satisfies the process requirements. The HPT process could also eliminate the step of additional sintering, to obtain a full density material with high strength.

2.5.1 Powder compaction stages and powder manufacturing

During the compaction stage, powder particles undergo three stages, as claimed by Seelig and Wulff [25, 26]. These stages usually happen at the same time, or overlap. In the first stage, the powder particles are rearranged or restacked [26]. Bridging of powder particles usually occurs in randomly arranged stack

or loose powder particles, is partially eliminated in this stage. In the second stage, powder particles undergo plastic deformation, depending on the ductility of the powder particles [26]. Due to the higher ductility of powder particles, particles usually experiences more extensive deformation as compared to brittle powder particles, such as ceramic powder. Lastly, smaller fragments would be formed as the powder particles, which are inherently brittle or have been embrittled through work hardening and fracture [27].

Mechanical properties of the green compact are also dependent on several characteristics of the starting form of powder particles, such as purity, particle size, distribution, particle shape, and surface texture [27]. These characteristics can affect the mechanical interlocking mechanism between powder particles. They also affect the apparent density and tap density of the green compact [27]. As a result, mechanical properties of the produced green compact, such as green strength and fracture resistance, are also affected. Powder particles can exist in several shapes, such as spherical, irregular, or porous powder particles [27]. Spherical powder particles have the highest apparent density among all, and bridging and arching are least likely to occur during compaction of these powder [27]. However, the size of powder particles also affects the apparent density, where it decreases with decreasing particle size due to inter-particle friction that is caused by the increase in surface area. With higher apparent density, the resulting compression ratio of the powder would decrease. In addition, there are several types of powder manufacturing processes, such as gas atomization and mechanical alloying, where gas atomization processes typical produce spherical metal powders [27].

2.6 Metal fabrication processes

2.6.1. Bulk metal forming processes

The bulk metal forming operations mainly use significant shape change by deformation in metals whose initial form is bulk rather than sheet. This thesis mainly consists of processes using bulk metals and powder material. Therefore it is important to cover the basics of the bulk metal forming in this chapter. These bulk forming processes are performed to cause plastic flow in the metals to deform into desired shape by applying sufficient stress to the materials. Some bulk forming processes produce the metals parts with almost near net shape of the final desired outcome, which is also an advantage of this bulk forming process. The basic bulk deformation technique can be divided into four processes such as forging, drawing rolling and extrusion.

2.6.1.1 Forging process

Forging is a traditional metal forming process by applying compressible force to a work piece between two dies. This is an oldest metal forming technique dated back in 5000 B C [13, 14]. An example of a die forging method is shown in Fig 2-1a. A forging process can produce metallic parts such as aircraft structural components, gears, engine crankshafts and connecting rods. Forging can be performed either in cold or hot temperatures. The method of delivering force in a forging process could be either in a form of a sudden impact force or a gradual pressure force. Cold forging has the advantage of increase strength due to work hardening and less energy requirement during the process. Hot forging is a very common forging method which increases the ductility of the work piece and cause significant plastic deformation to the metal work piece.

2.6. 1.2 Rolling process

Rolling is a form of drawing process, using compressive force to deform metals caused by the rotating rollers in opposing direction. A schematic diagram of a rolling process is shown in Fig 2-1b. This exerted compressive force squeezes the work piece trough the rollers to produce the final product. The force required for this process is applied either by work piece transport or power driven the rollers. Slab or plate and 'I' beam sections are commonly produced by using the rolling process. The rolling process is also heavily used in production of sheet metals.

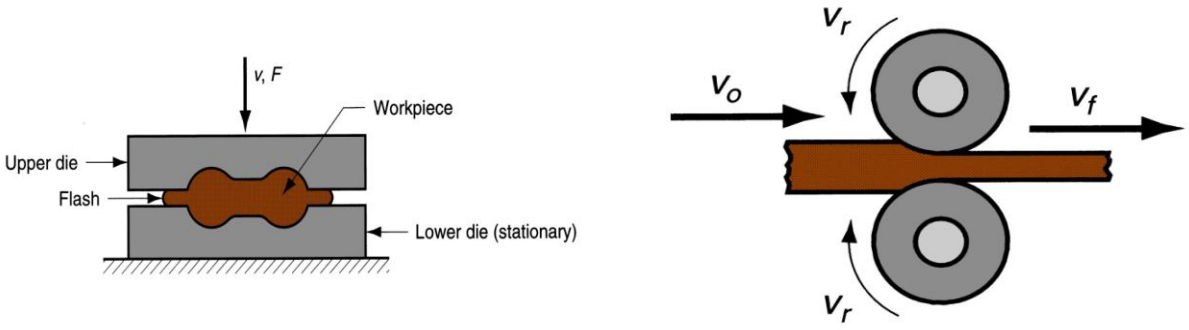

(a) (b)

Fig.2-1 (a) Schematic diagram of an impression-die forging process (b) Schematic diagram of a rolling process [14]

2. 6.1.3 Drawing process

The drawing process is used to reduce a diameter of wire or bar by applying a force on the exit side of the die. A schematic diagram of a drawing process is shown in Fig 2-2a. A combination of tensile force

and a compressive force cause the plastic flow of the work piece in a drawing process. Drawing can be performed either using rollers or dies. Drawing process using rollers are discussed in section 2.6.1.2. Drawing process using dies commonly produces solid parts and hollow sections. Solid drawing with dies can be further classified into wire drawing or sheet drawing which depend on the final product of the drawing process. The reduction in area during a drawing process is approximately 20 to 50 percent. Drawing process also has sub categories as bar drawing and wire drawing. Bar drawing process commonly uses single pass to create large size bars and rods. But wire drawing process produces small size wires using multiple passes of the material.

2.6.1.4. Extrusion process

Extrusion process is similar to a die-drawing process, where the work piece squeezed though a die opening by forcing the at the entrance side of the die. Dies in both drawing and extrusion have a common form of nozzle or chamfer like feature. In general, die openings are smaller to drawing die compared with extrusion die [28]. The extrusion process and drawing process can be used to achieve very good surface quality of the final product because of forced action on all the surfaces [28].

An extrusion process mainly consists of a die, container and punch or ram components. An extrusion process can be primarily classified as a direct or an indirect extrusion process. Direct extrusion is also known as forward extrusion. An example of a forward extrusion process is shown in Fig 2-2b. The direct extrusion process produces solid, hollow or semi hollow uniform cross sections. Indirect extrusion is also known as backward extrusion or reverse extrusion. An indirect extrusion process produces uniform solid and hollow cross sections are shown in Fig 2-3a and 2-3b respectively.

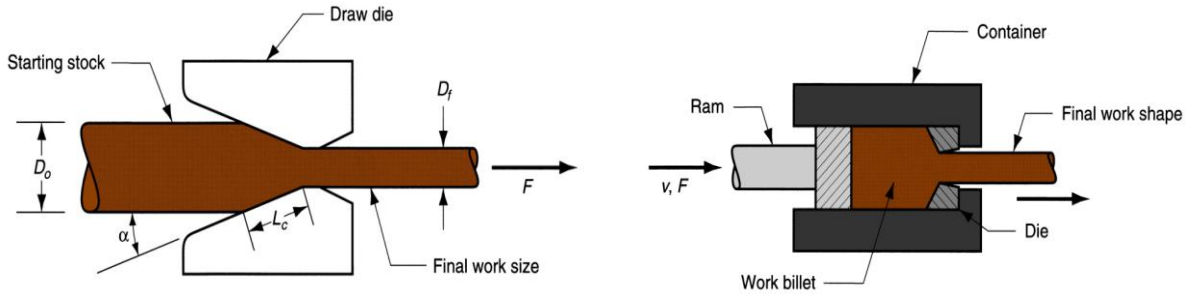

(a) (b)

Fig.2-2 (a) Schematic diagram of a drawing process (b) Schematic diagram of a forward extrusion process [14]

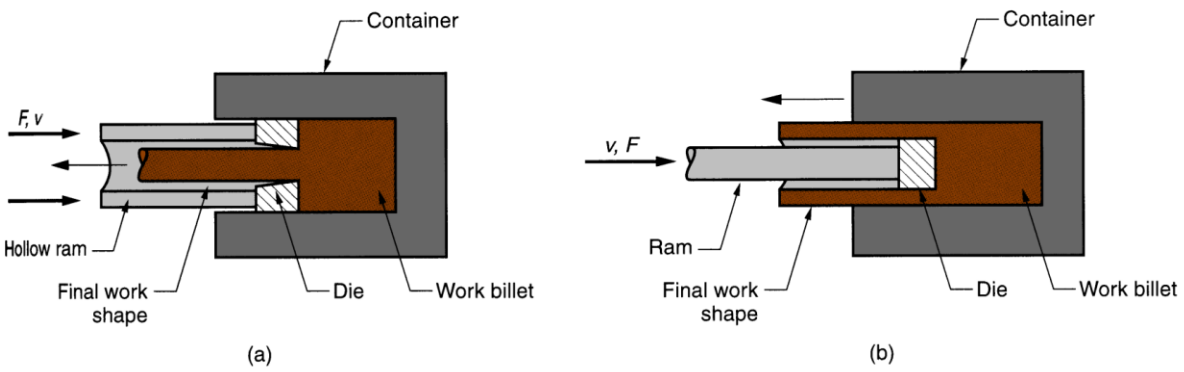

Fig.2-3 Schematic diagram examples of indirect extrusion processes (a) indirect extrusion produces a product with solid cross section and (b) indirect extrusion produces a product with hollow cross section [14]

Extrusion processes is also classified based on tool movement and their final product geometry which produce either solid or hollow components. Extrusion processes are also categorized into hot extrusion or cold extrusion based on their operating temperatures. A cold extrusion process is an energy efficient method compare to a hot extrusion process. The cold extrusion process also produces high strength material because of the high value of strain hardening (work hardening) index of metals at low operating temperatures [14]. On the other hand, the hot extrusion process facilitates significant size reduction and creates complex shapes because the metals can easily deform at high temperature. In contrary to the cold extrusion, the hot extrusion reduces the strength and increases the ductility of the materials.

In order to maintain a constant temperature during an extrusion process, hot extrusion are generally performed at high speed (fast process) compared to cold extrusion in either direct or indirect mode [13]. Ram speed, temperature, punch pressure can be monitored using various sensors during the process.

In addition to these fundamental extrusion methods, there are a number of relatively modem extrusions methods were introduced due to their special advantages over the existing methods. Hydrostatic extrusion, equal channel angular pressing / equal channel angular extrusion (ECAP/ECAE) process, continuous extrusion, multi pass extrusion, and Axi-symmetric Forward Spiral Extrusion (AFSE) are few examples of such extrusion processes. The ECAE and AFSE processes are discussed in detail in Section 2.6.2. The continuous extrusion is an extended modern form of extrusion technique which uses infinite feedstock and produces a continuous product [29] while the multi pass methods are commonly used in severe plastic deformation methods to further enhance the material properties.

Hydrostatic extrusion is mainly performed in cold condition, where the work piece surrounded by high-pressure fluid which exerts the required force to extrude a material [13]. This extrusion process is a

more efficient method in terms of causing plastic flow of the material. However, there are issues associate with fluid handling during the high pressure operations at a range between 900 to 1700 MPa, which cause leakages and blowout scenarios during an ejection process of the material [13]. It is also impossible to perform high temperature extrusions using this technique because of the fluid can act as a heat sink at high temperatures [13]. Therefore, this process has more disadvantages than its own advantages.

2.6.2 Severe plastic deformation processes

SPD processes are able to improve the mechanical properties of the materials through an inexpensively viable work hardening mechanism. The SPD processes mainly impose high shear deformation with the presence of pressure to deform materials at relatively low temperature. Severe Plastic Deformation (SPD) processes are considered mainly to enhance the material property using various techniques which can induce large amount of plastic flow within a sample while retaining its original shape.

In general, SPD processes increase the number of dislocations to accommodate the strain energy due to the plastic deformation [11]. The dislocation density in an annealed metal (without stored residual stresses) is about 10^4 to 10^6 dislocations per square millimeter while a metal processed using an SPD process contains about 10^{10} dislocations per square millimeter [11]. Although, most of the consumed energy of the material is converted into friction heat loss, approximately, 10% of the energy through deformation process is stored in the lattice as an increase in the internal energy. The energy accommodation in the material increases with the plastic strain up to a limiting saturation value corresponding to the strain energy. The saturation limit increases with decreasing the temperature of deformation. Hence, performing the deformation process at room temperature can maximize the increase of internal energy through large amount of work hardening. The major part of the stored energy is utilized in the form of creation and interaction of dislocations while small fraction of energy is stored in vacancies formation, stacking faults and twins [16].

The SPD processes very commonly known for grain refinement application which increase the strength of the materials while reduce the ductility of the materials [30, 31]. This phenomenon can also be explained using the length of the grain boundary of the material. That is, the SPD processes create new grains that increase the number of grain boundaries, which is responsible for the moment of materials in a lattice. More grain boundaries in a material can cause a lot of hindrance to the grain moment which required a large amount of force to deform the material. Therefore the yield strength of the processed

material can increases on the expense of the ductility by applying SPD processes. The general relationship of yield strength versus grain size can be explained using the phenomenon of grain boundary strengthening or Hall-patch strengthening.

The Hall-patch strengthening equation was derived based on the work of Hall [32-34] and Patch [35-37]. The Hall-Patch equation is in Eq.2-1 [38];

$$\sigma_y = \sigma_o + \frac{K_y}{d} \qquad \text{Eq. 2-1}$$

Where, σ_y, σ_o, K_y, d, are respectively the yield stress, friction stress of a materials which is the stress resulting from the movement of the dislocations, the strengthening coefficient of the material, and the average grain diameter. The friction stress is also known as the resistance of the lattice to dislocation motion.

However, certain materials showed a contradicting results of increase in both yield strength and ductility after SPD processes [39-41]. Formation of nanocrystalline grains in such materials increases the yield strength and improves ductility of the materials. An example of ECAP processed copper is shown in Fig. 2-4, which shows increase in both yield strength and ductility after 16 passes of the material in the SPD process.

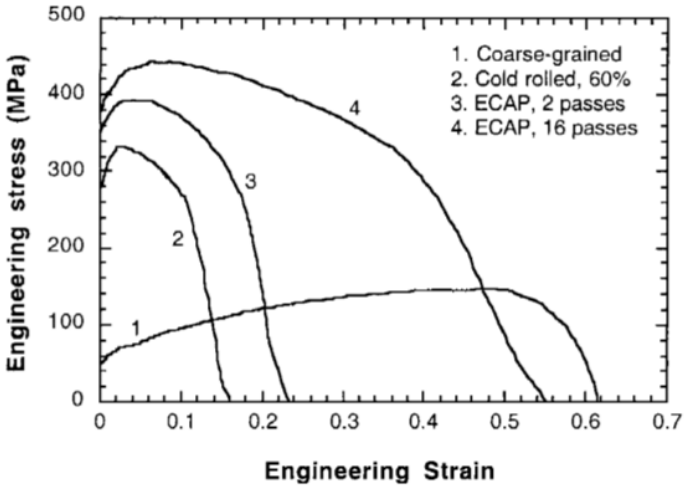

Fig.2-4 Tensile test curve for copper at 22° as an example of ultrafine grain formation and increase in both strength and ductility from curve 3 to 4 in an equal channel angular pressing (ECAP) process [39]

In recent years, growing interest has been shown in the area of material processing technology for the capability of manufacturing bulk ultrafine materials and nanocrystalline grained materials using SPD techniques [3, 42-46]. According to Valiev et al. [46], a "true" UFG can be defined as having a size of less than 1 μm and more than 70% high angle grain boundaries with a misorientation angle of greater than 15°. SPD processes can produce submicron grains (grains < 1μm) at temperatures lower than 0.4Tm and nanocrystalline grains at temperatures below 0.2Tm [47]. However, a large hydrostatic pressure is needed to successfully produce nanocrystalline grains in most metals when the operating temperature is below 0.2Tm [47].

Recently, researchers developed new SPD techniques for its exceptional advantages of improving material properties [31, 48]. These SPD techniques are also well known to produce nanostructured materials [49, 50]. Commonly known SPD techniques are high pressure torsion (HPT) and equal channel angel extrusion (ECAE) [51], multi-directional forging (MDF), sandglass extrusion (SE), repetitive corrugation and straightening (RCS), twist extrusion (TE), constrained groove pressing (CGP), accumulated roll-bonding (ARB) additive roll bonding (ARB), forward or direct extrusion (FE/DE). Techniques, that are used in most of the fabrication industries include HPT and ECAE, were developed during the 1980s by V. M. Segal are considered one of the earliest SPD processes invented during the 19th century [51].

2.6.2.1 Equal Channel Angular Extrusion (ECAE)/ Equal channel angular pressing (ECAP) process

ECAE process is a well-known as a severe plastic deformation (SPD) process, produces ultra-fine grained materials. It has the modified extended versions in the names of equal channel multi-angular pressing (ECMAP) [52] , rotary- die ECAP [53], cross-ECAP [54], T-shaped ECAP[55, 56], multi-pass ECAP [57-59], torsional- equal channel angular pressing (T-ECAP) [60], incremental ECAP (I-ECAP)[61]. The fabrication process of the material by ECAE involves forcing the material to flow through a die with an elevated angular channel that allows the deformation of the material to produce high shear strain when forced through the angular channel [51, 62, 63]. This process allows the material to generate significant plastic deformation while maintaining the cross sectional area of the material throughout the process. Fig 2-5 shows a work piece, which was extruded through an angular channel with φ angle [64]. It is also possible to perform this ECAE process at an elevated temperature. In addition to this, it can be controlled by various ram speeds and a backpressure unit. Recently the ECAE process was also implemented for powder materials with applied hydrostatic pressure [65].

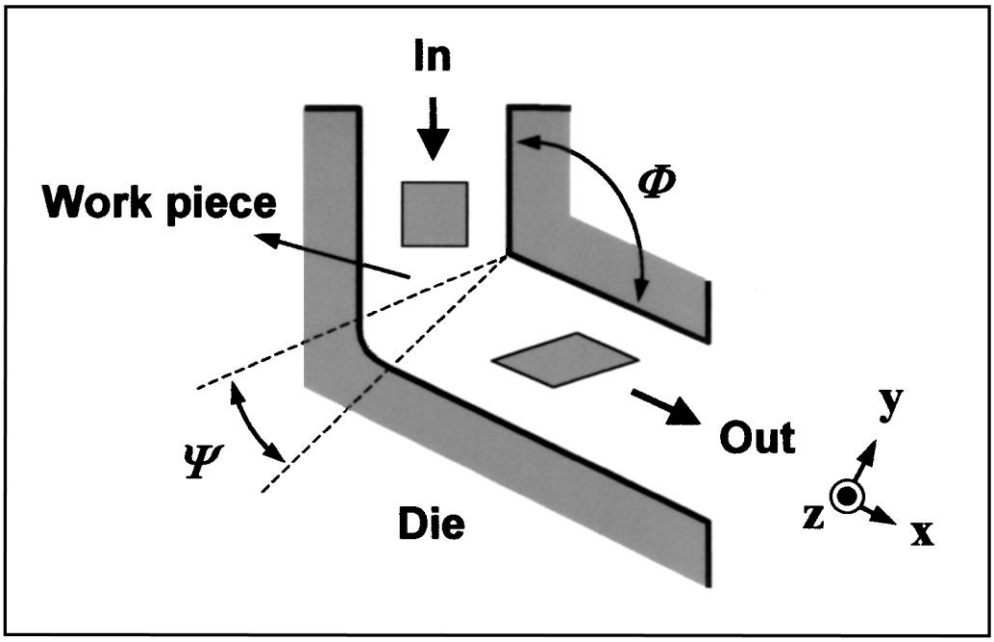

Fig. 2-5 A schematic diagram of the ECAE/ECAP process [64]

2.6.2.2 Twist extrusion (TE)

Varyukhin and Baygelzimer are the first to investigate an another SPD process called “Twist Extrusion” (TE) which was claimed as a continuous process and caused by an angular twist along the axis of extrusion [66-69]. A schematic diagram of a TE is shown in Fig 2-6. In this process the original specimen cross section was maintained after a twisting deformation in the material.

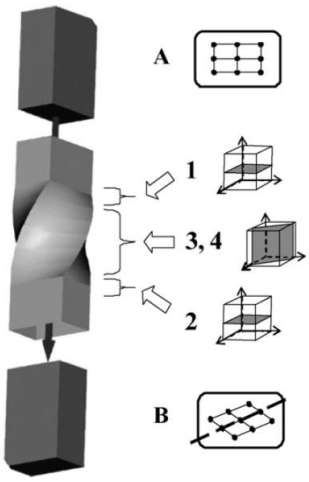

Fig. 2-6 A schematic diagram of the Twist Extrusion (TE) process [68]

In the TE process, the material has to go through a single twisting angle which required a much higher force. As the extrusion and twist happen at the same time which also requires large amount of energy to perform this process. In addition to this, TE is only suitable for rectangular specimens.

2.6.2.3 High Pressure torsion process (HPT)

High pressure torsion (HPT) is a well-known SPD process initially investigated by Bridgman [70]. This process induces large strain deformation which introduces large number of dislocation density and consequently increased strength into the new ultra-fine grain (UFG) material. The prospect and potential of HPT has intrigued by various researchers to understand the change in bulk and powder material properties on the HPT processed samples [71-76]. Zhilyaev & Langdon [71] explained the HPT process and its parameters while other researchers investigated the homogeneous deformation during the HPT process [72-74]. A schematic diagram of the HPT process is shown in Fig. 2-7. In the HPT process, material experiences large strain deformation when it is pressed in a die with high amount of pressure and is subjected to torsional straining. Although, extensive research has also been carried out on grain refinements occurs in such high pressure and shear deformation conditions, the understanding of the stress development in specific locations within the material is still somewhat unknown.

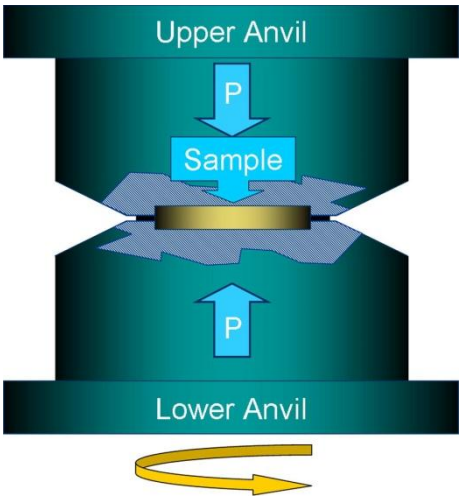

Fig. 2-7 A schematic diagram of the High Pressure Torsion (HPT) process [75]

A perfect application of HPT at the exact center of the sample would result in consequently a UFG material with its extent of refinement increasing with radius. The theoretical prediction suggests that a

linear or consistent strain/work hardening response would occur from the center of the sample, however many literature reviews have showed otherwise. For an example of the average hardness distribution for HPT processed aluminum with 10% iron samples of various numbers of revolutions are shown in Fig 2-8 against the distance from the center [77].

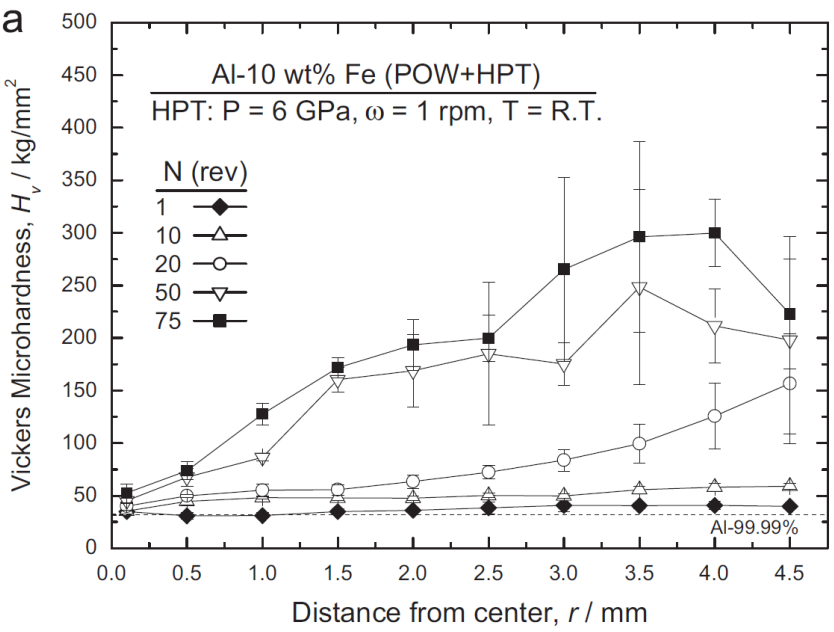

Fig. 2-8 Vickers micro-hardness against distance from center [77]

In addition to this, Cubero-Sesin et al. experimentally and numerically studied the variation in the Vickers micro-hardness distributions on both top and bottom surface of the HPT processed samples [77]. The numerical results clearly show the non-uniformity in the hardness distribution between the top and bottom surface and localized hardening patterns in the HPT processed samples. The numerical simulation results of non-uniform distribution of the micro-hardness are shown in Fig 2-9.

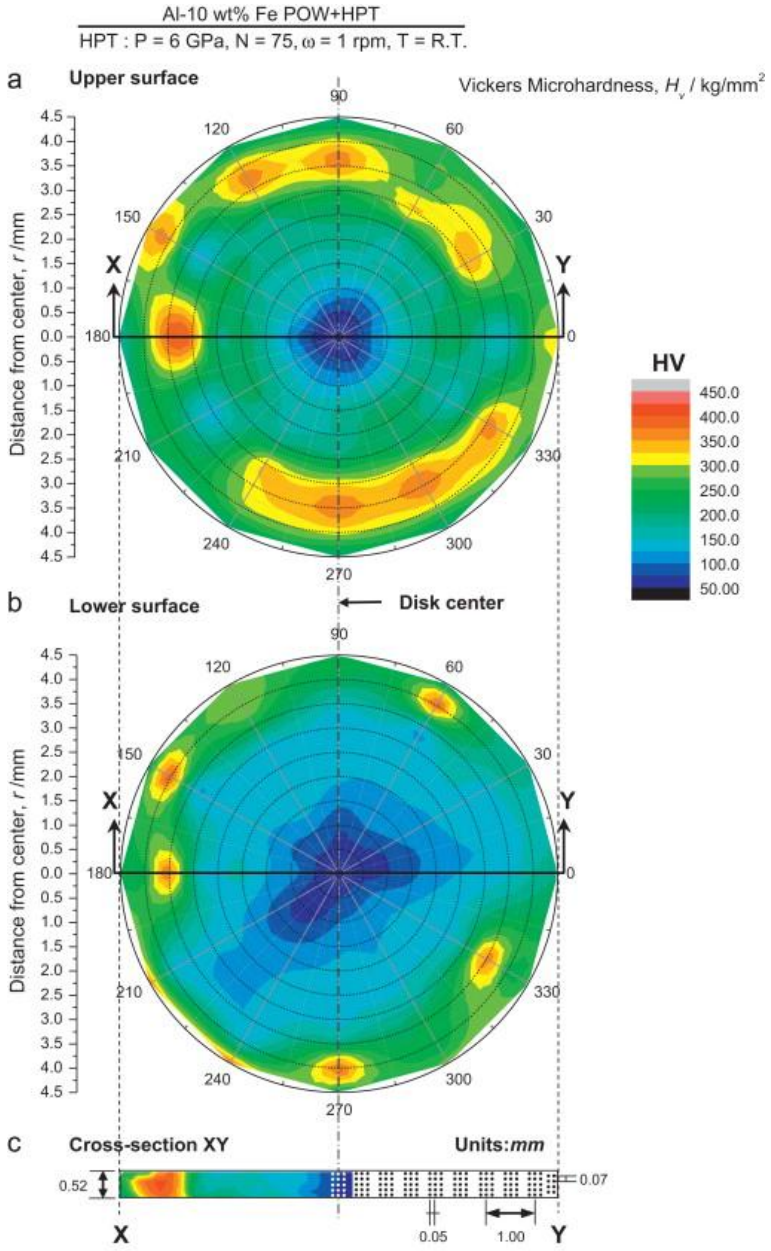

Fig. 2-9 Vickers micro-hardness distribution of disk processed for 75 revolutions using HPT process (a)top surface (b)bottom surface and (c) cross-section [77]

In addition to this, in terms of homogeneity of the processed sample, formation of a “dead metal zone” became an issue in the samples processed under very high pressure [78]. The formation of “dead metal zone” was determined where the effective strain and strain rate development decrease to zero at the surface corner of the disk due to the vertical wall constraint under high pressure [78]. Therefore, this region experiences a stagnant region and no metal flow occurs under high pressure [78]. A schematic

diagram shows the location of the “dead metal zone” shown in Fig 2-10c and finite element simulation results of the HPT process under high pressure shown in Fig 2-10a and 10b

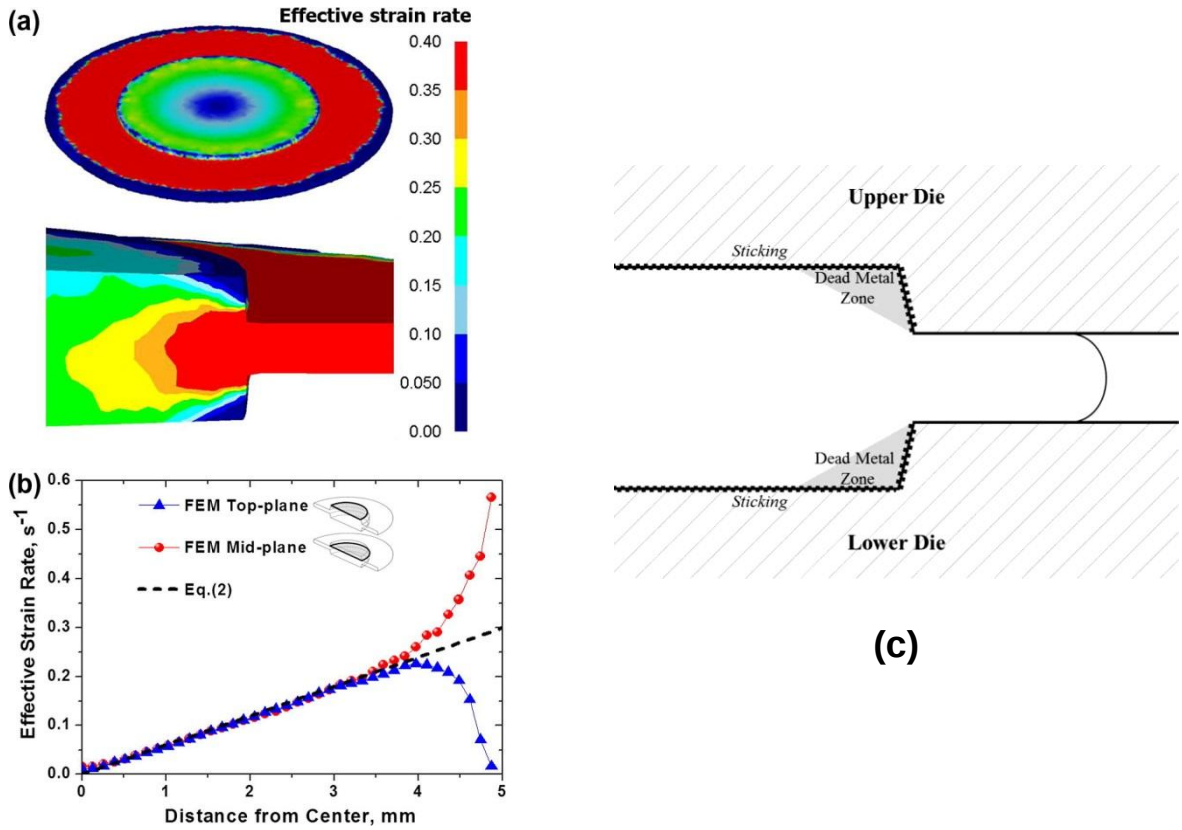

Fig. 2-10 (a) Distribution of effective strain rate during HPT process, (b) path plots of the effective strain rate from the center to the edge on the top plane and the mid-plane of the HPT processed sample shows the effect of dead metal zone and (c) A schematic diagram shows the “dead metal zone” in the HPT process [78].

Moreover, the HPT process is a very precise process that requires the perfect alignment and precision to ensure that the application of torque is transferred uniformly throughout the sample. The homogeneity of grain refinement within the sample is severely compromised as a result of poor processing. Shear voids, uneven flash-out of material from dies and inconsistent surface profile after HPT are signs of uneven application of torque. It is clear that the presence of these aforementioned defects can affect the homogeneity of the sample and by recognizing these defects in the HPT processed samples, researchers developed the understanding of the homogeneity without disrupting the samples integrity with testing.

Huang et al. investigated the pronounced impact of misalignments of anvils on the material flows pattern during HPT [79]. Three different degrees of misalignment from the origin were studied for

25microns, 100 microns and 200 microns in order to understand the impact misalignment on the flow of material [79]. Schematic diagrams of an aligned anvil setup and a misaligned anvil setup are respectively shown in Fig 2-11a and 11b.

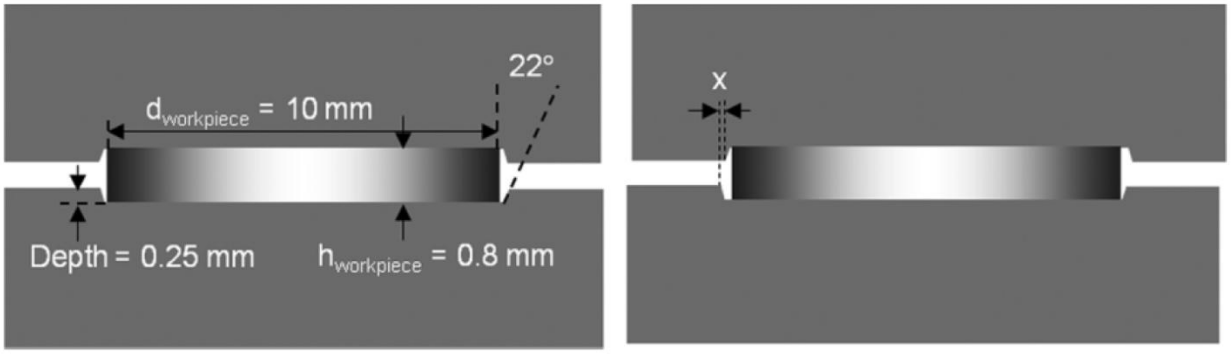

(a) (b)

Fig. 2-11 Schematic diagrams of (a) an aligned anvil setup and (b) a misaligned anvil with a small misalignment of x in HPT [79].

An example flow pattern results obtained using Stereoscopic imaging technique for various number of revolutions of a material after an HPT process for 100µm are shown in Fig 2-12. The double-swirls flow pattern formations are marked with dashed white arrows in Fig 2-12. It is not the aim of the researchers to define how the 'double-swirl' affects the grain refinement and mechanical properties of the sample but to rather use the prominence of a double swirl as an indicator of anvil misalignment and consequently poor quality of sample in regards to material homogeneity. The nature of this double swirl was quite consistent and appeared quite distinctly at low revolutions. However, the double swirl began to shrink as the revolutions reached 16. The disappearance of the double swirl at high revolutions could be potentially due to SPD reaching a point where dislocation densities and shear lines stack up causing the swirls to condense to eventually what appears as an almost linear flow pattern through the center of the sample [79].

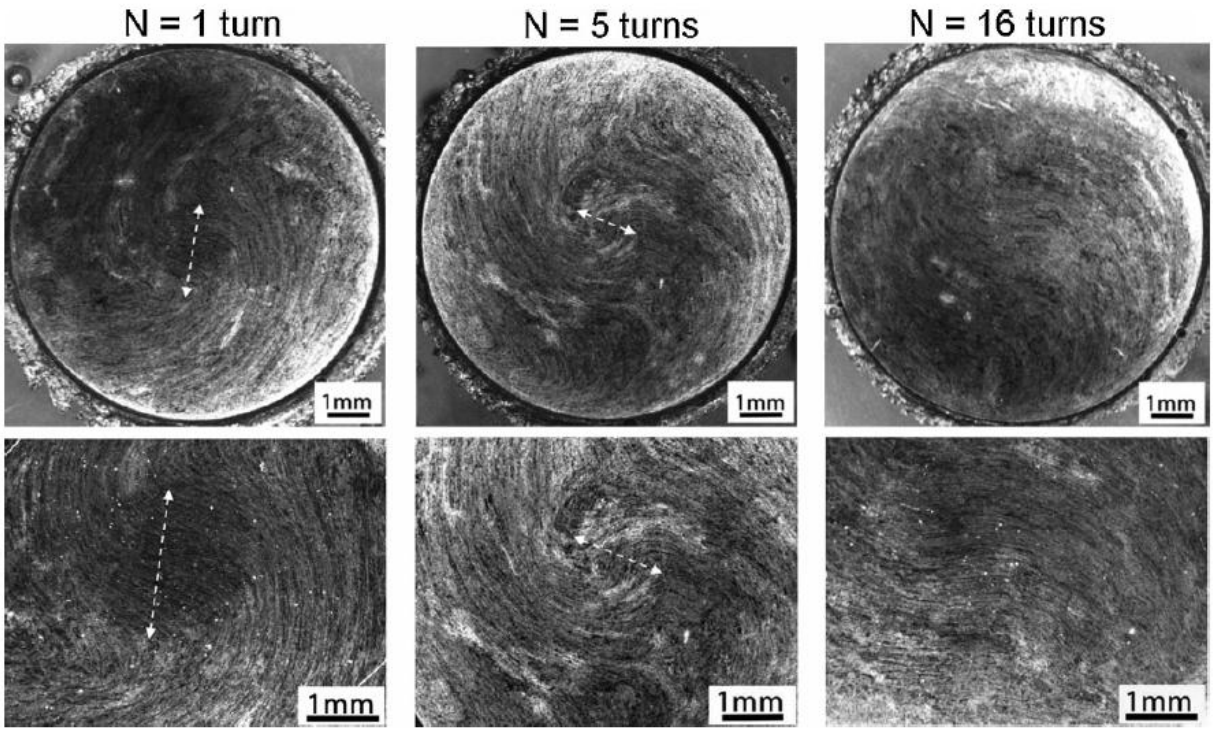

Fig. 2-12 Material flow patterns of top surfaces of discs processed using HPT with an anvil misalignment of 100 µm with 1, 5, and 16 turns revolutions using stereoscopic imaging technique, second row shows the enlarged image of the center region of the samples from first row respectively [79].

In addition to this, local shear vortices after processing were also appeared near the periphery of the processed samples from misaligned anvil setup [79]. Formation of voids were evident as a build up of shear concentrations and were clearly visible courtesy to the electro-etching which showed high levels of deformation from the different phase layers indicating high shear rates in order for these phases to flow in this way [79]. The researchers also identified that the voids were more clearly visible and pronounced when the misalignment increased from 100µm to 200µm. These voids in the material can significantly varying the homogeneity of the processed material and which could lead to brittle behaviour and impede slip of other planes propagating uniformly thought the material leading to further disruptions in the refinement of the grains under HPT.

Moreover, Huang et al. also investigated the significance of the material outflow (flash-out) during an HPT process with various alignments [79]. A standard alignment could cause the material outflow in a non-uniform fashion which leads to an asymmetry in the final processed sample. The asymmetry is clearly visible in Fig 2-13a and 13b on the left side and the right side of the processed material in the

horizontal direction. This asymmetric material flow can definitely lead to a processed material with heterogamous material properties.

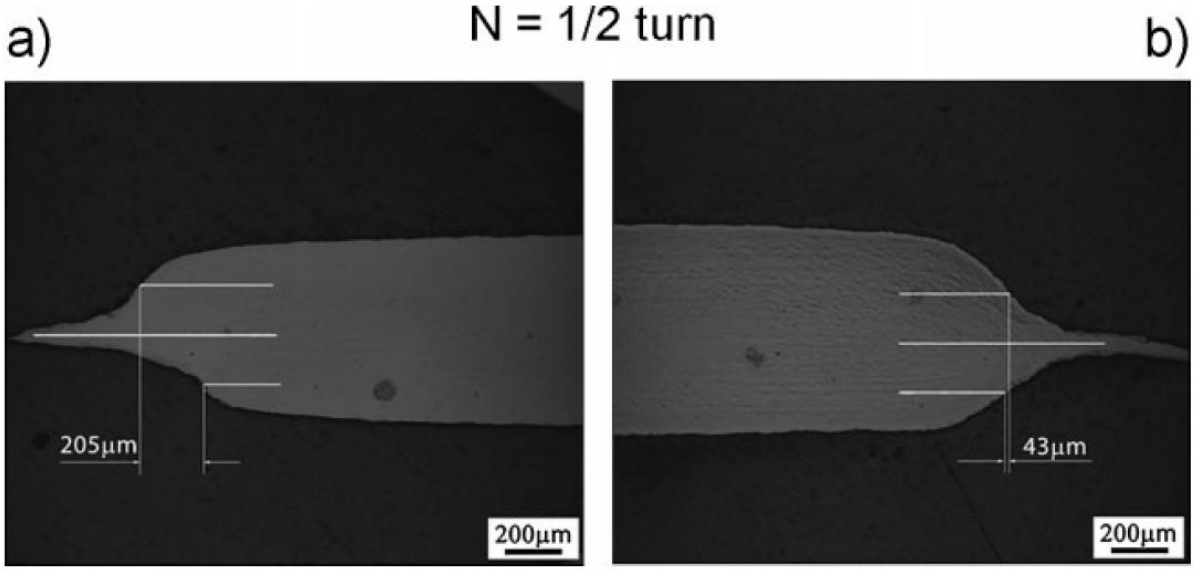

Fig. 2-13 Material outflow at the periphery of the disc processed with an anvil alignment of less than 25 µm for a ½ revolution HPT processing (a) left side of the processed material (b) right side of the processed material [79].

The results in Fig 2-13 clearly indicate the required precession of a perfectly aligned setup to obtain a sample with uniform mechanical property using an HPT process. The HPT process also has limitations in terms of the sample size and shape and is currently confined to the performance of the machines to supply the required pressure and the rotational nature allows only for circular samples to be processed. However, a modified/extended version of the HPT process without these issues can produce materials with significantly increased mechanical properties because of the occurrence of grain refinement in bulk samples.

2.6.2.4 Axi-symmetric Forward spiral extrusion (AFSE)

Axi-symmetric Forward spiral extrusion (AFSE) is also classified as an SPD process to improve the material property by refining the grain size [31]. The AFSE process is a novel processing technique uses a die which contains small spiral grooves along the axis of extrusion [80]. A kinematic concept of strain accumulation during an AFSE process was investigated with a linear velocity field assumption [80].

In this process, force is applied as a punch force in the direction of extrusion. A schematic diagram of the AFSE process and the specially engraved die are respectively shown in Fig 2-14a and 14b. The die has a

0.15mm radius chamfer section at the entrance, which causes the reduction in cross section of the billet material. These spiral grooves facilitate the rotation of the billet about the z-axis which causes the shear deformation of the material [81].

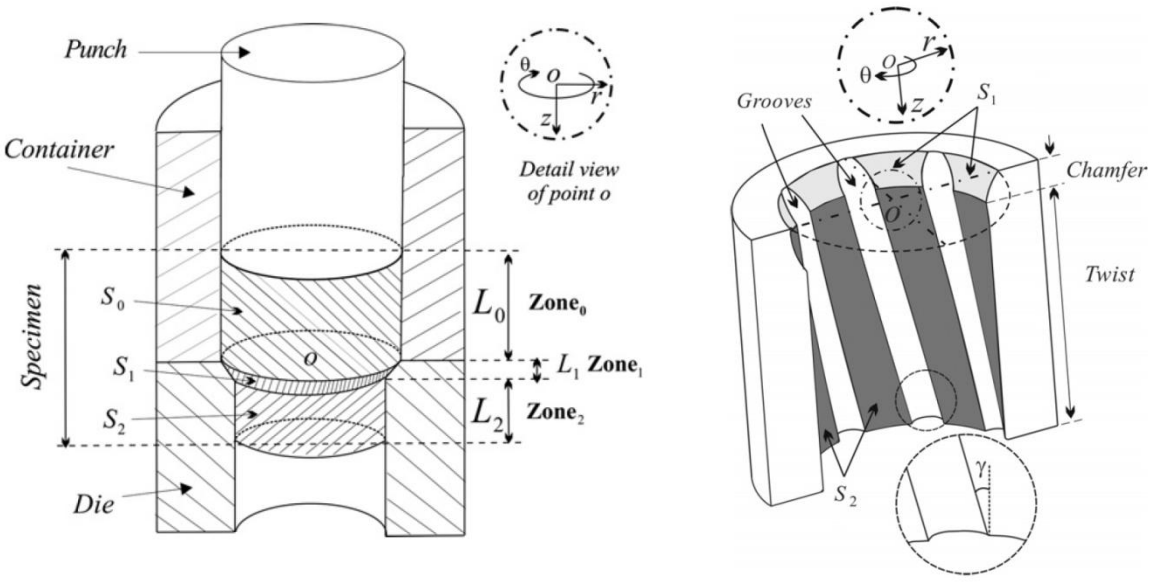

Fig 2-14 (a) A schematic diagram of the AFSE process and (b) The die used in the AFSE process showing different zones (zone$_o$ – container, zone$_1$ – Chamfer zone, zone$_2$ – Twist section, according to the zones in Fig 2-6a) [81]

In addition to this, backpressure is an optional parameter controlling the metal flow. The backpressure provides resistance to the moving material along the direction of extrusion. The backpressure increases the hydro static pressure of the sample and creates the material flow in a controlled manner. Therefore, it creates high frictional shear along the wall due to the increased contact pressure.

The AFSE process also has its own extended versions, as such variable lead axi-symmetric forward spiral extrusion (VLAFSE) [82, 83] and multi-pass AFSE [84]. These extended versions of the AFSE process show significant improvements in grain refinement on the processed materials.

In addition to the kinematic, experimental and upper bound analysis of this process, Finite Element (FE) simulations using Abaqus explicit algorithm was conducted by Farhoumand et.al [85, 86] , to investigate the plastic strain distribution and subsequent mechanical property changes in the AFSE processed material. Equivalent plastic strain distribution across the circular cross section of the AFSE processed sample after a single pass is shown in Fig 2-15a where the helix angle of the die is 23°. Various helix

angles were also numerically investigated for the AFSE process and an example of 70° helix angle is also shown in Fig 2-15b [86]. These results showed that the AFSE process with higher helix angle die develops a large plastic strain in the processed material compared to the process with lower helix angle die.

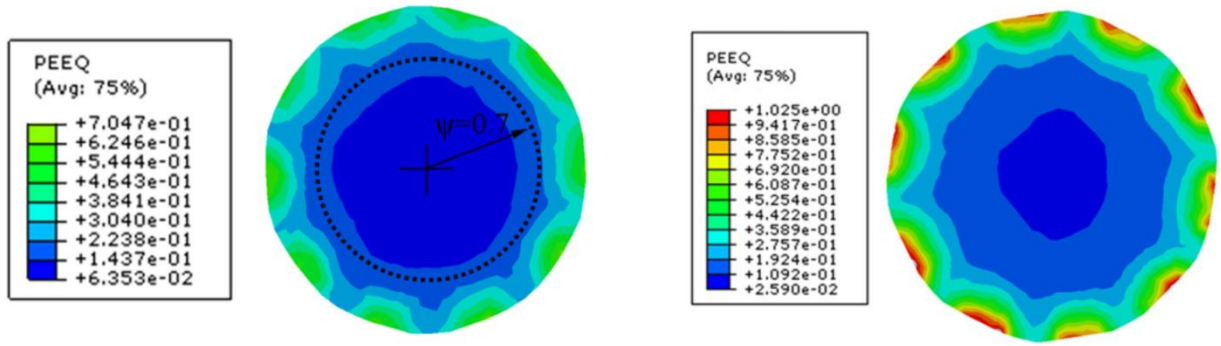

(a) (b)

Fig. 2-15 Equivalent plastic strain distribution (PEEQ) on the circular cross section of the AFSE processed sample with (a) 23° helix angle (b) 70° helix angle [86]

The strain development in the AFSE process and VLAFSE process were also numerically compared for both processes [83]. The Equivalent plastic strain (PEEQ) distribution on the longitudinal section of the material for the AFSE and VLAFSE processes are respectively shown in Fig 2-16a and 16b. In both cases the unsteady material flow region (ZONE I) and the steady flow (fully developed) region (ZONE II) are marked in Fig. 2-16. [83]. These results signify that the VLAFSE continuously accumulate the plastic strain in the "ZONE II" region while the AFSE primarily have a rigid body rotation inside the die in the grooves section.

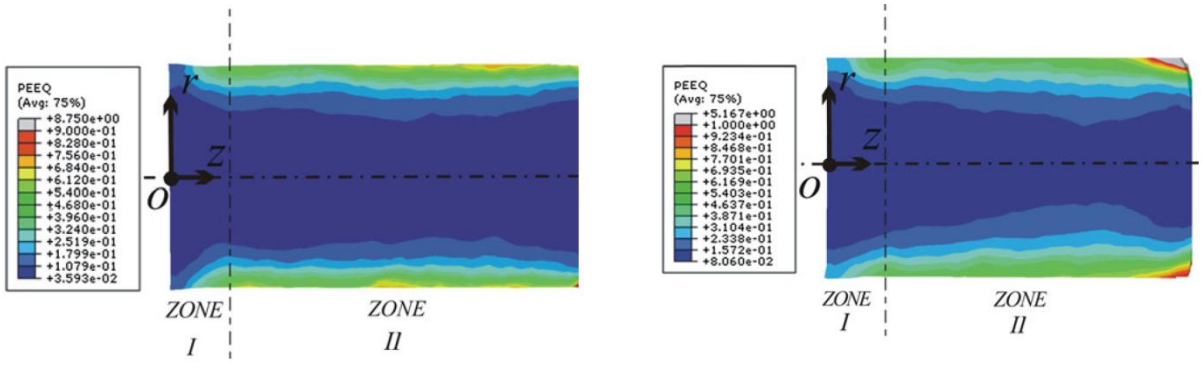

(a) (b)

Fig. 2-16 Equivalent plastic strain distribution (PEEQ) on the longitudinal cross section of the (a) AFSE processed sample (b) VLAFSE processed sample [83].

2.5.2 Powder processing using high pressure torsion process

In contrast to hot powder processing techniques, there are also benefits in performing the powder processing at room temperature such as no oxidation occurs during the compaction process and can achieve enhanced mechanical properties due to severe cold working at room temperature which is below the re-crystallization temperature of those materials. Numerous investigations on the influences of mechanical and microstructural properties for many materials using SPD processes are discussed in Section 2.6.2. The details of the HPT process are also presented in Section 2.6.2.3. A summary of aluminum and aluminum alloy powders processed using the HPT process is shown in Table 2-1.

Table 2-1: A summary of aluminum and aluminum alloy powders processed using the HPT process

Source / Details	Kanego et al. [87]		Botta et al. [88]		Yavari et al. [89]	Bachmaier et al. [90]	Lee et al. [91]	Tokunaga et al. [92]	
	Case 1	Case 2	Case 1	Case 2				Case 1	Case 2
Purity (%)	Al with 5% of (Mg)	Al with 20% Mg	$Al_{90}Fe_7Z_3$	$Al_{84}Y_3Ni_8Co_4Zr_1$+ SiC	$Al_{90}Fe_5Nd_5$ (90 at. % Al powder)	99.5% purity of Al powder	Al-7.5%Mg	99.99% purity Al powder with 5% mass of fullerenes	99.99% purity of Al powder only
powder size (µm)	75 in diameter (spherical form)	75 in diameter (spherical form)	5-20 (mechanical alloying)	5-20 (spherical form)	25 or less in diameter (spherical form)	Mean particle size of 90 & 1.3	N/A	N/A	N/A
Initial dimensions of sample (mm) D – diameter T - thickness	D=10 T=0.25	D =10 T=0.25	N/A	N/A	D=10 T=0.3	D=8 T=0.8	N/A	D=10 T=0.25	D =10 T=0.25
Amount of pressure used at room temperature (GPa)	2.5	6	5	5	5	4	6	2.5 (does not damage the structure of fullerenes)	2.5
Number of rotation with rotation speed in rpm (rotation per minutes)	40	60	5 rotations with 1 rpm	5 rotations with 1 rpm	N/A	25 rotations with 0.2 rpm	5	15 rotations with 1 rpm	15 rotation With 1 rpm

Final dimensions of sample (mm) D – diameter T - thickness	D=10 T=0.7	D =10 T=0.7mm	D = 7 T=0.3	D = 7 T=0.3	N/A	N/A	D =10 T=0.5	N/A	N/A
Grain size after compaction (nm)	80nm	45 nm	N/A	N/A	N/A	1) 145 nm for 90 µm particles 2)104 nm for 1.3 µm particles	19 nm (+/-2nm)	80 nm	500 nm
Micro-hardness (Hv) or yield strength (MPa)	202 Hv	288 Hv	3580 MPa (+/- 150 MPa)	4600 MPa (+/- 100 MPa)	3100 MPa (+/- 50 MPa)	1) 880 MPa for 90 µm particles 2) 1300 MPa for 1.3 µm particles	3400 MPa at center, 3800 MPa at 5mm from the center	382.5 MPa at center, 1157 MPa at 3mm from the center	Slightly higher than 382.5 MPa at center, increase with distance was smaller
Other comments	Increase of final sample thickness due to the amount of mixed powder added to prevent upper and lower anvils from contacting damage and wear		N/A	N/A	N/A	N/A	N/A	N/A	

The Table 2-1 showed a summary of single powder material processing using HPT process. This research did not consider composite material fabrication. Number of applied rotation cycle to the process are between 5-60. This higher number of required revolution also requires high energy consumption to process the material. In addition to this, these HPT process has large amount of flash out of material and required a rig with precision alignment (alignment between punch and die) to process the material. After the process, there was a lack of understanding in the particle morphology in those research works. Investigation on the heterogeneity of processed sample was not clearly investigated in those processes.

2.6 Bimetals joining processes and occurrence of diffusion at the interfaces

Diffusion welding (DFW) process is a solid state joining process performed at elevated temperatures. The bonding between metals occurs due to the diffusion interface. The diffusion bonding process is mainly suitable for joining dissimilar metals. Highly reactive metals such as titanium, beryllium, zirconium and other composite metals are joined using diffusion bonding [20]. Many military aircraft are

using diffusion bonded parts including fuselages frames, outboard and inboard actuator fittings, bulkhead, main landing gear trunnion and nacelle frames which are made of titanium and super alloys, which reduces the manufacturing costs and the required amount of rare materials [20].

The diffusion welding process requires high temperature, pressure and sufficient contact time to perform a successful bonding. Surface finish with low roughness and clean contact surface without any contamination are also required to facilitate a diffusion bonding. Smooth surface finish brings the surfaces close together. Therefore, the joining surfaces can easily become in contact which facilitates the diffusion bonding. In addition to this, contamination of any other chemicals or grease or water vapor or trapped air can cause unfavorable results in a diffusion bonding.

In recent years, new metal joining techniques and their applications were increased in aerospace, chemical processing plants and structural applications. Shang et al joined 6061 Al alloy with AZ31B Mg alloy by using cold metal transfer welding with pure copper (HS201) as the filler metal [93]. Recently researchers joined aluminum with steel using friction welding [94]. H90 steel clad H90 strip has better properties compared to brass for making bullet jackets because of its low cost and better ballistic properties [95]. Another research was demonstrated a technique to perform cold diffusion welding of gold nanowires without defects [96, 97]. Shi & Zhang designed a copper clad aluminum wire for winding alternator of a vehicle application [98]. In recent years, researchers developed new efficient joining methods to join dissimilar materials to obtain materials with specific combined properties.

A three ply clad sheet of copper, aluminum and stainless steel was fabricated using hot rolling process at 350°C [99]. After the fabrication of the 3ply clad sheet, they annealed the samples at 100°C, 200°C, 300°C and 400°C and investigated the mechanical properties of the sample and interfacial properties [99]. Tensile test was utilized for the 3 ply sheet metal to study the strength of the fabricated material. In addition to this, Al_2Cu, a copper aluminum intermetallic compound (IMC) was formed at the interface of the 400°C annealed sample using Scanning Electron Microscopy (SEM) imaging technique [99]. This study confirmed that the Al_2Cu was brittle and causes fracture during the Vickers hardness test and reduced the ductility of the material [99].

Metal forming techniques such as forward extrusion, ECAE and hydrostatic extrusion were also used to create a bonding which involves diffusion mechanism at the interface. Nilsson invented the copper clad aluminum rod using hydrostatic extrusion process in 1973 [100]. Another research was performed to investigate a composite metal extrusion using hydrostatic extrusion process [101]. This study was aimed

to fabricate hard core with soft sleeve material as an alternative method for coating. It was expected that the hard core would not undergo a significant shape change or deformation in the project. Various core failures with different extrusion ratios and the failure mode as either necking under tension at the exit or irregular non-steady deformation of the core material were also investigated by assuming a proportional material flow behavior when deriving the mathematical formulas [101]. According to Osakada et al. core and sleeve must experience the same amount of reduction which is same as an extrusion ratio [101]. Afterward, Ahmed also investigated copper clad aluminum fabrication process parameters such as die design, extrusion ratio, extrusion velocity, extrusion pressure and percentage of copper for an axi-symmetric hydrostatic extrusion [102]. Ahmed developed analytical solutions to calculate the required hydrostatic pressure at various extrusion ratios for 15% copper clad aluminum hybrid rods [102].

Plastic flow behavior for a co-extrusion of two metals for a number of combinations were also investigated [103]. In the study, the researcher quantified the total plastic strain of the combined material and the individual plastic strain of each material [103]. In order to understand the plastic flow, micro structural properties of the co-extruded materials were investigated [103]. This research work outlined that the material flow of a composite rod depends on individual deduction ratios of the core and sleeve. Therefore, the researcher mentioned that, considering the global extrusion ratio for the deduction ratios of the core and clad materials was not suitable. In addition to this, further research was carried out to investigate the plastic zone and dead zone in a simultaneous extrusion process for non-propositional and propositional flow [104]. It was claimed different velocity distribution at the die entrance, which would lead to different extrusion ratios on core and sleeve in that paper [104]. In addition to this, the researcher also mentioned that the extrusion ratios depend on the interfacial bonding between the materials [104]. However, the research was not considered the effect on the core sleeve extrusion ratios on the formation of bimetallic bonding.

An industrial scale experiment of fabricating copper clad aluminum composite using hot hydrostatic extrusion process were conducted at 320°C temperature on a horizontal hydrostatic extruder with 1.5MN capacity [105]. The process parameters such as stroke versus pressure using different extrusion die angles of 30°, 45° and 60° for three different extrusion ratios (8.5,19 and 49) were investigated [105]. The researchers also investigated the bonding using Scanning Electron Microscopy (SEM) and Energy-dispersive X-ray spectroscopy (EDX) analysis [105]. From their study, they optimized that the extrusion ratio of 19 with the die angle of 45° is more suitable for fabricating Al/Cu bimetallic composite rod using

hydrostatic extrusion process [105]. However, hydrostatic extrusion process is a costly process and having difficulties to operate due to the fluidic environment as discussed in detail in Section 2.6.1.4.

Al/Cu clad rods were also fabricated using indirect extrusion and drawing process [106]. Researchers firstly investigated the bonding strength of the copper clad aluminum interface. In their research they found 573K to 623K with an extrusion ratio of 21.39 was optimized as a best extrusion condition [106]. In addition to this, above 623K they observed copper sleeve fracture during the extrusion [106]. In their experiments below 523K the bonding strength was approximately 10MPa on an initial copper thickness of 6mm with an extrusion ratio of 6.68 [106]. However, at the same extrusion ratio of 6.98 with a temperature of 623K they observed diffusion with diffusion layer thickness of (DLT) of 1.6µm while the bonding strength of the fabricated sample was approximately 60MPa [106]. They also claimed the DLT and the bonding strength were increased respectively to 1.8µm and 65MPa at a given extrusion ratio of 21.39 [106]. The DLT and the bonding strength were also respectively increased to 3µm and 75MPa after annealing the sample at 573K [106]. However, they failed to mention the method of the bonding strength test and DLT measurement.

A new method was proposed to fabricate bimetallic rod using ECAE process [107]. An extrusion of aluminum/copper clad rod was conducted using ECAE process at 350°C and tested the bonding strength as extruded using a blanking sample with a thickness of 5mm [107]. The samples were also tested after annealing it for 300° for an hour and found the annealing process increased the bonding strength. The paper also claimed that multiple passes through the ECAE die would have increased the bonding strength of the joint [107]. In those experiments the annealing process required additional processing time and processing setup.

Furthermore, another investigation was carried out to examine the diffusion bonding of copper clad aluminum rod using ECAE process [108]. Temperature was varied from 100°C to 225°C by 25°C and the holding time for 20,40, 60, 80 and 100 minutes at each of the temperature and studied the shear strength of the bonding [108]. A good bonding was reported during 200°C with a holding time of 60 to 80 minutes [108]. It was also found that, the bonding strength adversely affected by increasing the temperature to above 120°C, due to formation of brittle intermetallic compound in a vacuum free processing environment [108].

Another study reported that Aluminum welded with copper in cold condition using ECAE process [109]. Bonding strength of the Al/Cu clad sample was found to be 33MPa using a blanking test, as compared to

be same as aluminum yield strength [109]. Although the experiment was performed in cold condition, the bonding strength was tested after annealing the final product for 250°C for one hour [109]. However, the role or contribution of the annealing in the bonding strength was not clear in their process.

In addition to the experimental investigations, many other researchers investigated the analytical frame work of bimetallic extrusion processes. Hartley was first developed an upper bound solution for composite rod extrusion process [110]. In the theoretical formulation, Hartley assumed the process as a piecewise homogeneous process [110]. However, a homogeneous material flow is impossible in a non-proportional bimetallic forming process with different material [103]. Metal flow of bimetallic extrusion was characterized for a soft sleeve with a hard core and a hard sleeve with a soft core effect by Tokuno & Ikeda using analytical and experimental studies [111]. Tokuno & Ikeda formulated the velocity field when the material flow plane not remained in parallel [111]. Their analytical formula was formulated based on a velocity field assumption on an extrusion process.

Some other researchers investigated a core fracture behavior and a sleeve fracture behavior using a velocity field analysis in various composite extrusion processes [112, 113]. Another study reported the formulation of axi-symmetric bimetallic tube extrusion using slab method [114]. Another theoretical study of a bimetallic rod in a double reduction die with two extrusion ratios was investigated using "FORGE2" commercial software [115]. In addition to this, a generalized spherical velocity filed was developed for a bimetallic extrusion [116]. However, there is no complete theoretical stress analysis solution exist for a solid bimetallic extrusion. Furthermore, all these theoretical analysis are different from an AFSE of a bimetallic rod.

A parametric optimization study of bimetallic rod extrusion was conducted for aluminum alloy2014 (core) and aluminum alloy6063 (sleeve) [117]. In order to optimize the extrusion length of the bimetallic rod the researchers used a physical modeling and a numerical modeling using "Deform^{TM} 3D" software package [117]. In their study, they varied the lengths of the core and sleeve and optimize the best sample length by comparing the free end of the extruded samples [117]. However, in this AFSE extrusion core and sleeve at the free end are held together by the backpressure. Therefore relative movement of core and sleeve at the free end does not happen in AFSE with backpressure process.

A numerical study was conducted using LS-DYNA commercial package for a bimetallic extrusion of composite aluminum/copper clad rods [118]. It was investigated the force-displacement, radial strain and interfacial strength [118]. The results showed that the radial strain is uniform in a bimetal extrusion.

In addition to this, Rhee et al. performed bimetallic extrusion with extrusion ratios of 8.5,19 and 49, while Kwon et al. considered forward extrusion with an extrusion ratio of 6.98 to 21.39 [105, 106]. However, according to Sliwa it is not suitable to consider global extrusion ratio to core sleeve material ratios [103]. Therefore in order to fabricate certain core to sleeve ration there is no simple prediction exist. In addition to this, higher extrusion ratio required high amount of energy to run the process. Moreover, the hydrostatic extrusion and the forward extrusions are homogeneous processes.

The ECAE process was considered to fabricate composite aluminum/copper clad rods [107-109]. In the ECAE process extrusion ratio is almost zero. ECAE process is also a homogeneous deformation process. But in the AFSE, additional torsion component causes additional shear deformation to the material and makes the process heterogeneous.

2.7 Summary

It has shown in this chapter the significance of fabrication processes used in the manufacturing of hybrid materials using various metal forming and metal joining processes such as extrusion, drawing, and diffusion welding. In term of hybrid metal fabrication, cladded rods and tubes have many applications in electrical applications and chemical processing industries. Cladded hybrids have been fabricated using traditional processes, such as extrusion, drawing, hydrostatic extrusion process in the past. However, these processes have complications because of the high extrusion ratios and do not have control on the final dimension of the core material. Moreover the hydrostatic extrusion process is an expensive process and crate venerable operating environment because of the fluid use in the application. In addition, the interface of composite materials in the fluidic environment can easily contaminated in a hydro static extrusion and it is difficult to perform the process at elevated temperatures. Moreover, some researchers fabricated the clad composite which requires multiple passes in a drawing process.

On the other hand, severe plastic deformation (SPD) processes are become attractive alternatives to traditional processes to fabricate hybrid materials and they also add additional exceptional high strength to the processed materials. In this way, equal channel angular extrusion (ECAE) process was recently investigated for cladded hybrid material fabrications, however they involve multiple steps. In this case, ECAE required either a room temperature extrusion step followed by an additional post heating step or an elevated temperature extrusion followed by a long holding time to create an effective bonding. In

addition to this, ECAE process produces a homogeneous product; however it requires route changes to produce an equiaxed grain structure and is limited to produce parts in batch mode only.

In addition to this, the existing manufacturing techniques produces samples with defects such as sleeve fracture, core fracture and non-uniform core diameter. Moreover longitudinal slippage (relative motion between core and clad in the longitudinal direction) may play a destructive role in bond formation at the interface of those materials fabricated in the existing processes.

In order to resolve these manufacturing difficulties and obtain a high quality bonding, an axi-symmetric forward spiral composite extrusion process (AFSCE) was proposed to fabricate cladded hybrid materials as discussed in this thesis. This process is an extended version of the AFSE process discussed earlier in this chapter, which was used primarily for grain refinement in single materials. This manufacturing process is proposed because it has a better dimensional control and near zero shape change effect of the fabricated samples. Also, this process does not required additional step (heat treatment or holding under pressure for long time) to manufacture a hybrid material.

Therefore, the AFSCE process was investigated for a case study of copper clad aluminum fabrication which showed a successful bonding and ultrafine grain formation as presented in this thesis. In addition bond strength of the composite was determined using a specially designed dedicated blanking test which is also presented in the thesis. The average bond shear strength of the copper clad aluminum fabricated using AFSCE process was found to be 50.5MPa, which is higher than the shear yield strength of the pure bulk aluminum used in this study, which demonstrates a good potential of this process to be used in industrial applications to manufacture hybrid rods with energy and material savings. The design detail of the dedicated blanking test is also included in the thesis.

In addition to this, confined high pressure torsion process (CHPT), was also investigated to fabricate axi-symmetric hybrid material and presented in this thesis. This process is beneficial and having potential applications compared to the traditional high pressure torsion process, because this process minimize the issues of dead zone and misalignment of anvils in an HPT process. In addition to this, the CHPT process can be used to fabricate net-shape composite materials, where the process does not have any flashout during the processing which eliminates the additional machining of the components. This CHPT process was investigated for fabrication of aluminum powder and copper clad aluminum samples. The results shows the CHPT process having a potential application and eliminate the need for sintering in traditional powder material processing to obtain a high quality fabrication also documented in the thesis.

In summary, this thesis contains valuable information of two novel axi-symmetric hybrid material fabrication processes, which eliminate the drawbacks in the existing hybrid metal manufacturing techniques and produce materials with enhanced properties which are highly desired in modern engineering applications.

Chapter 3:
Hybrid metal fabrication using Axi-symmetric forward Spiral Composite Extrusion (AFSCE)

Chapter 3: Hybrid metal fabrication using Axi-symmetric forward Spiral Composite Extrusion (AFSCE)

3.1 Introduction

Hybrid metals are fabricated using mechanical joining process. This mechanical joining process also known as welding process is generally performed at high temperatures and offers only a limited number of shapes. In particular, a conventional mechanical welding technique is not convenient for long axi-symmetric shapes because of the difficulties in developing radial pressure at the interface of the sample in a continuous fashion. For this aforementioned reason extrusion become an attractive alternative to fabricate bimetallic composite rods. There are various extrusion processes such as hydro static extrusion, equal channel angular extrusion or other continuous forward extrusion processes were considered in the past. Nilsson in 1973 [100] introduced a technique to manufacture Al/Cu composite rods using hydrostatic extrusion process. Kwon et al. [106] fabricated Al/Cu composite rods using an indirect extrusion and drawing process in that bond strength of the copper clad aluminum interface was investigated. They found that the optimum extrusion condition for the process was 350°C with an extrusion ratio of 21.39 [106]. Rhee et al. studied the fabrication of hybrid Al/Cu composite composites at 320°C using horizontal hydrostatic extrusion with the extrusion ratios of 8.5,19 and 49. A creation of successful mechanical bonding under an extrusion processes requires large extrusion ratio. Applying large extrusion ratios are expensive because of the high pressure requirement and the expensive high strength tool designs. A large extrusion ratio also requires high energy and may not produce uniform core diameter because of the significant change in core clad diameter.

In recent years, severe plastic deformation (SPD) processes (see for example Segal [51]) have also been considered as alternatives to reduce the mechanical bonding temperature by leveraging the synergy between high pressure and shear deformation. For example, composite Al/Cu composite rods have been successfully fabricated using the Equal Channel Angular Pressing (ECAP) process [107-109]. The bonding mechanism in ECAP is governed by presence of the shear and high pressure simultaneously at the interface of aluminum and copper.

The ECAP process produces a homogeneous product which needs route changes to produce an equiaxed grain structure and is limited to produce parts in batch mode only. In a recent research copper - aluminum composite samples were produced by ECAP at “room temperature” following a 250°C annealing for one hour to increase the ductility and to relieve the residual stresses [109]. Their sample showed a good bond strength [109]. However, the role and contribution of the high annealing temperature in the bonding is not clear. In another study, bonding strength was investigated for Al/Cu composite samples which were fabricated using the ECAP process [108]. The temperature was varied from 100°C to 225°C in steps of 25°C and used the holding times of 20, 40, 60, 80 and 100 minutes for each of the temperatures [108]. Measuring the bonding shear strength, the researchers found an optimum shear bonding strength of 34.9 MPa can be obtained when the specimen was processed at 200°C with a holding time of 60-80 minutes [108]. Thus, in order to obtain a strong bonding strength, the ECAP process required either a room temperature extrusion followed by an additional post heating step or an elevated temperature extrusion followed by a long holding time.

In order to reduce these limitations we propose a method, axi-symmetric forward spiral composite extrusion (AFSCE), to fabricate bimetallic rods in a single step. In the current study, the AFSCE technique will be applied to a specific case to fabricate composite Al/Cu composite rods.

3.1.1 Key features of the novel AFSCE process

The axi-symmetric forward spiral extrusion (AFSE) process is a recently proposed severe plastic deformation technique [80]. This process was initially proposed to extrude single materials with the aim to achieve refined grain size at room temperature. The process also having its multi-pass process capability to further reduce the material’s grain sizes [84]. A modified version of the AFSE with variable pitch die also allow further deformation during the extrusion process which is known as Variable Lead Axi-symmetric Forward Spiral Extrusion (VLAFSE) process [82, 83]. The small spiral grooves along the axis of the extrusion die allow a unique “near zero shape change” extrusion, which develops a combination of a compressive and shear forces in the material. It was classified as near zero shape change because the initial billet diameter and the extrusion die diameter are almost in same dimension. In these experiments, 13mm initial billet diameter was reduced to 12.7mm final diameter after the extrusion. The die has a small chamfer section at the entrance, which causes the reduction in cross section of the billet material. The spiral grooves facilitate the material to rotate about the extrusion longitudinal

(extrusion) axis, which in contrast to an ECAP process eliminate the need for the route change in the processing material.

The bonding in this process is governed by developing shear deformation and high pressure at the Al/Cu interface at an elevated temperature. In this chapter, kinematic considerations and shear deformation in the hybrid samples will be discussed first. The discussion is assumed to be independent of the materials chosen for hybrid fabrication. This will be followed by an experimental case study of the technique by the fabrication of hybrid Al/Cu samples using the AFSCE process at 300°C with an applied backpressure of 200Mpa. Bond strength is determined experimentally by measuring the shear strength at the interface using a dedicated blanking test (DBT). The DBT results show that for the conditions of this study AFSCE has successfully produced a hybrid metal bonding between copper and aluminum.

3.1.2 Fundamental concepts of AFSCE process

Implementation, kinematics and stress development during the AFSCE process were discussed in this section to understand the basics of the extrusion process. Main aim of this section is to investigate the basic theories and possibilities of axi-symmetric hybrid material fabrication using the AFSCE process. Therefore the detail of the process is introduced in this section with basic kinematics and stress development analysis, which brings the overview and nature of the process and suggests the possibility of processing a successful fabrication of axi-symmetric hybrid material using this AFSCE process.

3.1.2.1 Implementation of the AFSCE process

Details of AFSE process for extrusion of single solid materials can be found in Khoddam et al. [80, 81]. The AFSE process was investigated for cold forming of one single material which has the capability to accommodate high temperature process conditions. Fig. 3-1a shows a 3 dimensional view of the AFSCE die assembly used here to fabricate a hybrid bimetallic sample by extrusion.

The schematic diagram of the longitudinal section of the assembly configuration shown in Fig. 3-1b, illustrates the AFSCE die with the punch at a position at the beginning of the extrusion process. The die (part 3) is shown in the middle of the assembly which is utilized by including a container (part1). A back pressure punch (part 6) is also placed in opposite direction of the extrusion to develop a large hydrostatic pressure and is guided by part 5. A heating jacket (part 7) facilitates the heat transfer from heating cartridges (part 8) and encloses the multilayer die assembly. Backpressure is applied by using a

hydraulic system. To protect the punch and die grooves from colliding, a step punch was used to apply the backpressure from the beginning of the process. A composite sandwich type bi-metallic sample is fitted by sliding fit (shown in Fig. 3 - 4b). In order to avoid longitudinal slipping of the two metals during the process and to prevent the un-wanted side extrusion/flash out of materials through the clearances (punch - die clearance and backpressure punch - die clearance), small steel disks were placed on the top and bottom of each sample. A dummy sample was also placed on top of the main sample (shown in Fig 3-1b) inside the container to protect punch and die during the extrusion.

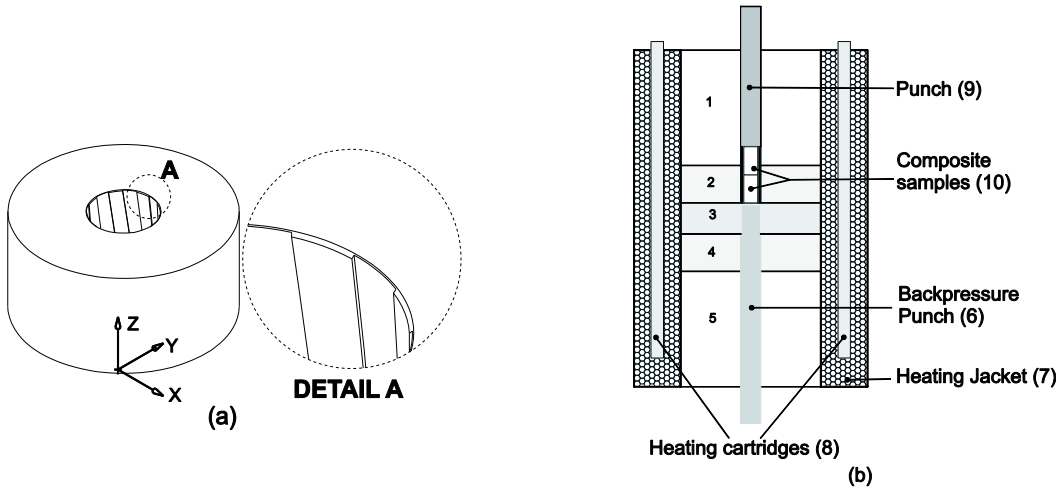

Fig.3 - 1. (a) Schematic diagram presentation of the AFSE die and (b) The AFSE die set with heating unit assembly, 1 and 5 punch guides, 2 and 4 containers and 3 is the AFSE die.

The main aim of the above design was to facilitate diffusion of atoms at elevated temperature and pressures [22]. Introduction of back pressure proved to be an effective way to increase the pressure at the interface of the two metals. In the current literature, two possible mechanisms are mainly assumed responsible for bonding between dissimilar metals viz. mechanical interlocking and metallurgical bonding induced by proper diffusion under the feasible process parameters. The diffusion is enhanced at elevated temperatures with high pressure compensating for the required holding time for diffusion bonding to occur [13, 119]. The term “hybrid bonding” is used here when referring to the core-clad bonding established during the AFSCE. A case study of the formation of Al-Cu joined by the AFSCE will be presented later in which we will discuss the nature of its hybrid bonding.

While the focus of this current chapter is mostly experimental, due to the key role of shear deformation during the AFSCE, it will be useful to discuss the kinematic of the process briefly before presenting the experimental case study in the succeeding sections.

3.1.2.2 Kinematic Consideration of shear deformation in the AFSCE process

AFSCE's velocity field is a key to understand the developed shear strain in the AFSCE sample during the process. Neglecting radial and longitudinal deformation during the AFSCE, the tangential velocity component in the sample, excreted by the grooves, is the most important parameter describes the shear deformation. The description is complex due to the presence of contact at the two materials interface. This velocity is only known at two points, viz. at the specimen centre ($r = 0$) and at the die-clad interface ($r = r_0$). Velocity description is complex elsewhere due to the presence of contact at the core-clad interface. Due to inaccessibility of the material at the interface, it is not simple to understand the real contact condition at materials interface. Currently, the nature of the bonding mechanism and the corresponding boundary condition for the two materials in this process are unknown. However, only a range of possible scenarios can occur:

1. Fully sticking boundary condition
2. Fully sliding boundary condition
3. Partially sticking and partially sliding boundary condition

The kinematic interpretation of the velocity field of the two extreme cases which were either fully sticking or fully sliding conditions may be considered to allow a limit analysis to develop kinematic equations for AFSCE process. A schematic representation of the boundary conditions which relates to those two extreme cases is shown in Fig 3-2.

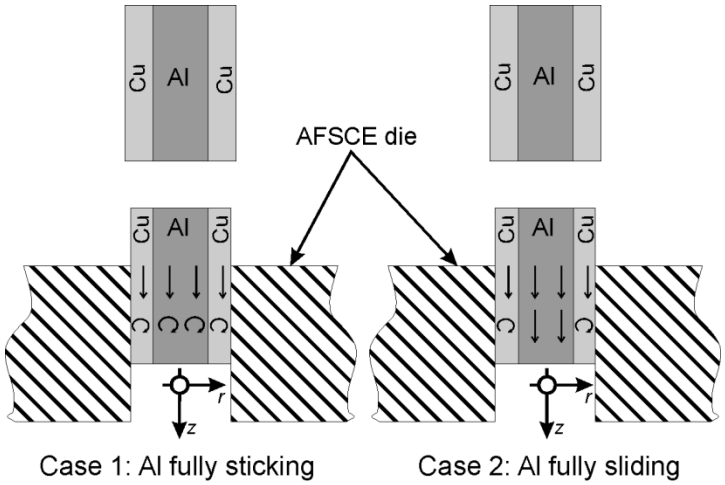

Fig 3- 2. Two extreme cases for the boundary conditions of core material (here aluminum shown as the core material and copper shown as the clad material)

These cases include velocity continuity or discontinuity at the interface of the materials which correspond to "fully sticking" and "fully sliding" conditions. The fully sticking condition (case 1), shown in Fig. 3-3a, occurs when the relative velocity between the two materials at the interface is zero which results in a continuous velocity field. Extending the continuity to the first derivatives of the tangential velocity will result in shearing stain continuity at the interface. The fully sliding condition (case 2), shown in Fig.3-3b, happens when the relative velocity, in the tangential direction, at the interface is maximum. This is when the inner core material remains rigid and only the outer layer deforms. Quadratic tangential velocity distribution for fully sticking and sliding conditions are shown in Fig.3-3a and 3-3b respectively. The parameters $\mathrm{r} = 0$, $\mathrm{r} = \mathrm{r_a}$ and $\mathrm{r} = \mathrm{r_O}$ represent center, materials interface and die interface points respectively in Fig. 3a and Fig.3b. Due to the axi symmetric nature of the process, these three points are sufficient to describe the velocity field in the composite sample cross section. The velocity field in the tangential direction based on the quadratic distribution assumption from Khoddam et al. [82] can be written as:

$$V_\theta = (r/r_O)^2 V_0 \tan\beta \qquad \text{Eq. 3-1}$$

where $0 \leq \beta \leq \gamma$ is instantaneous helix angle in the chamfer zone and γ is the helix angle for the die.

In both extreme cases, a uniform longitudinal flow can be assumed to satisfy the mass conservation. According to the mass conservation it can be proved the longitudinal component of the velocity field in all three zones is equal to the punch velocity which is independent of β [80].
Also, the radial component of velocity is negligible because of the near zero shape change along the radial direction

Based on an existing solution of AFSE [80], the induced shearing strains corresponding to each condition will be estimated here. However, one could speculate various cases of the interfacial shear strain in between these two extreme cases.

Based on the velocity field described by Eq. 3-1 and the solution presented in [82], at $\mathrm{r} = \mathrm{r_a}$, the effective strain can be estimated as:

$$\bar{\varepsilon}_a = \frac{r_a^2}{\sqrt{3}{r_O}^2}\tan\gamma \qquad \text{Eq. 3-2}$$

For the fully sticking condition, the effective strain at materials interface can be estimated using Eq. 3-2 which predicts the same strain for the core and clad material at $r = r_a$. For the case of fully sliding condition however, the effective strain in the core material is zero everywhere (rigid) while the same strain may be estimated at the material interface at $r = r_a$ in the clad material.

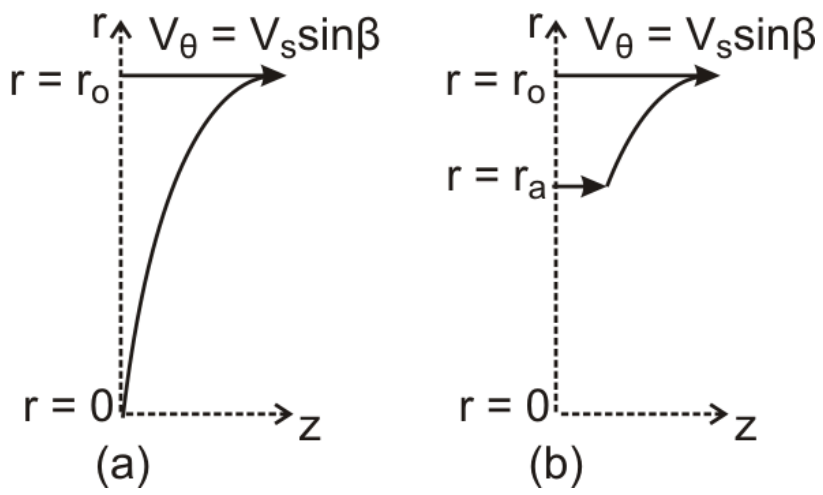

Fig 3- 3: velocity field of two extreme boundary condition cases (a) Fully sticking (b) fully sliding condition

Since shear deformation, pressure, temperature and holding time at the materials interface are important for the bi-metallic bonding, the shear deformation solutions discussed above will allow a limit analysis for a better understanding of the role of shear deformation on the bonding. One might postulate that the fully sliding condition to be harmful for the bonding since it could prevent an effective diffusion at the interface. This hypothesis can be rejected by noting that AFSCE is a "sequential process". The shear deformation described by Eq. 2 (a possible non-zero relative velocity) is only operational during the first sequence when the materials are passing through the chamfer zone [80]. The material deforms only inside the chamfer region where the instantaneous helix angle β can grow to the maximum helix groove angle γ and there will be no more strain accumulation in the groove section [80, 82]. During this step, both materials are passing through the grooved section experiencing a rigid body motion together. Under this condition, the relative velocity is zero while the high temperature and the high pressure are active. Therefore, the first short and transient step of materials extrusion inside the chamfer can play in the first step (a preparation role) for the subsequent second step where the bonding will be completed. In the second steps, the oxide layers at the materials interface have been broken due to the previous step of shear deformation to allow intimate contact in presence of high pressure, temperature and zero relative velocity.

3.1.2.3 Stress development in the sample during the AFSCE Process

The mechanism for matching of the flow stresses at the core-clad interface is a key to understanding the hybrid bonding at the core-clad interface during AFSCE. Estimating the flow stresses within the composite sample is an extremely difficult task due to the presence of two materials during the AFSCE process. It involves simultaneous solution by trial and error of non-linear stiffness equations and their boundary conditions for core and clad material. The solution should be followed by "stress recovery" based on an accurate constitutive description of core-clad, kinematic equations and equilibrium of the forces at die-clad and core-clad interfaces. Two extreme kinematic cases discussed in section 3.1.2.2 lead to different stress distributions in AFSCE samples. To identify which case governs at the core-clad interface, a full description of pressure/friction at the interface and knowledge of all process parameters such as temperature, holding time, microstructure and surface finish are needed. A numerical solution of the problem requires the development of a sophisticated model based on complex and detailed boundary conditions at the interface of the core-clad metals. Limited experimental observations at the interface can be performed to understand the deformation/stress distributions at the interface. Examples of potential observations include radial hardness distribution, grain size changes and texture distribution.

The preceding discussion explains the need for sufficient experimental data before a reliable (numerical) model for the problem can be established and solved.

In the current work, a case study of bonding between Al-Cu and a number of assessments of the bonding are carried out to allow a better understanding of the synergy between the process parameters and to pave the way to developing a numerical model of the process in the future.

The multi axial stress development in the AFSCE process has been noticed after careful investigation of the longitudinal cut section was studied. With the initial assumptions the strain components predicted to be as shown above in Eq. 2. However, the actual nature of the process experimentally was further investigated to understand the stress development in the AFSCE process. The plastic deformation, stress development and strain accumulation in the material are discussed using micro structural changes, interfacial investigations and micro hardness results in chapter 4.

3.2 Experimental work

3.2.1 Implementation of AFSCE experiments

3.2.1.1 Choice of materials

Steel/copper clad, steel/Aluminum clad and aluminum/copper clad composite materials have many industrial applications. Steel/copper clad composite is mainly used by wire industries; while steel/aluminum clad composite has main use in heat conduction such as in cooking utensils and heat sink application. Aluminum/copper clad composite hollow sections are also used as heat exchangers and composite solid sections are used in electrical wiring.

The AFSCE process was proposed to fabricate axi symmetric hybrid materials with shear and pressure loading conditions. With the initial plan steel and copper were chosen to fabricate composite steel/copper clad material as a case study with this AFSCE process. For this experiment pure copper C11000 (99.90% copper) and bright mild steel 1020 were chosen. Samples were made using turning and polishing with a good surface finish average value of 0.8 μm. Although machining the samples create a new surface in those materials, the material surfaces especially copper surfaces accumulated surface oxidation as they were kept in the environment prior to the experiment. Therefore, surface of the samples were carefully cleaned at the beginning of every experiments. Surface preparation before experiment was performed by a mechanical cleaning with fine grade emery paper then washed with distil water and wiped it to make it clean surface. Initially test was performed in room temperature with backpressure of 200MPa.

Samples were split across the axis of extrusion and examined for bonding. Copper with steel co-extrusion at room temperature, there was no bonding occurred. It was also clearly noticed that steel is a relatively high yield strength material, difficult to bond with copper at low temperature. In addition to this, diffusion bonding required 50 percent to 80 percent of the melting temperature to perform bonding. Therefore in this project, it was planned to apply a combination of hot condition and extrusion to formulate the bonding. However, high temperature of 50 to 80 percent melting point of steel is not achievable with the existing heating facilities. Therefore it was decided to switch to the materials with low yield strengths and low melting points. After careful consideration of the applications of hybrid material copper and aluminum were considered to investigate the AFSCE process.

3.2.1.2 Experimental method of the AFSCE process

The composite Al/Cu samples were extruded using the AFSCE process at 300°C and 200MPa back pressure. In order to improve the pressure at the interface, the confined pressure of the sample was increased by applying a back pressure to the process. In addition to this, back pressure prevents the aluminum flow in the longitudinal direction (z direction or extrusion direction). The reason for aluminum plastic deformation in the longitudinal direction is because of the lower flow stress of aluminum compared to copper. Further to this, the friction between die-wall and the specimen is much higher than the friction between copper and aluminum facilitating flow of core aluminum in the longitudinal direction. In addition to the back pressure, small steel disks were used to prevent the longitudinal slippage of the Al core from the cupper clad.

The die included eight helical grooves with a helix pitch of 305mm and 0.15mm depth. The AFSE die was 20mm in length with a helix rotation angle of ~23° with a root diameter of 13.0 mm. The flow of material inside the grooves was facilitated by a chamfer section of 0.15mm x 45° located at the die entrance.

Pure copper C11000 (99.90% copper) with pure aluminum rod was fabricated initially at room temperature. But the room temperature process gave similar results to that of steel/copper case study. However in aluminum/ copper composite extrusion, deformation was observed in both aluminum and copper. The aluminum cross section was changed to a slightly octagon shape due to the presence of eight grooves in the AFSCE die. Aluminum core cross section diameter also changed during the AFSCE process which confirmed the deformation in the Al core.

After that pure copper C11000 (99.90% copper) and pure cast aluminum were used in the AFSCE experiments at elevated temperature. As shown in Fig.3-4a and Fig.3-4b copper sleeve was made with an internal diameter of D and an external diameter of 13mm. Tolerances for the sample diameters were chosen as H7g6 (ISO 286-2). This ensures a low clearance slide fit tolerance between the aluminum core and the copper sleeve. The low clearance slide fit minimized trapped air between aluminum and copper which contributed to prevention of oxidation at the interface during the warm extrusion. Samples were machined and polished with average surface roughness Ra=0.8 µm. To further minimize formation of surface oxide layer, all sample surfaces were carefully cleaned mechanically with a fine grade emery

paper followed by washing with distilled water immediately prior to the experiments. Lubrication was not used in the experiments to avoid contamination of the bonding surfaces.

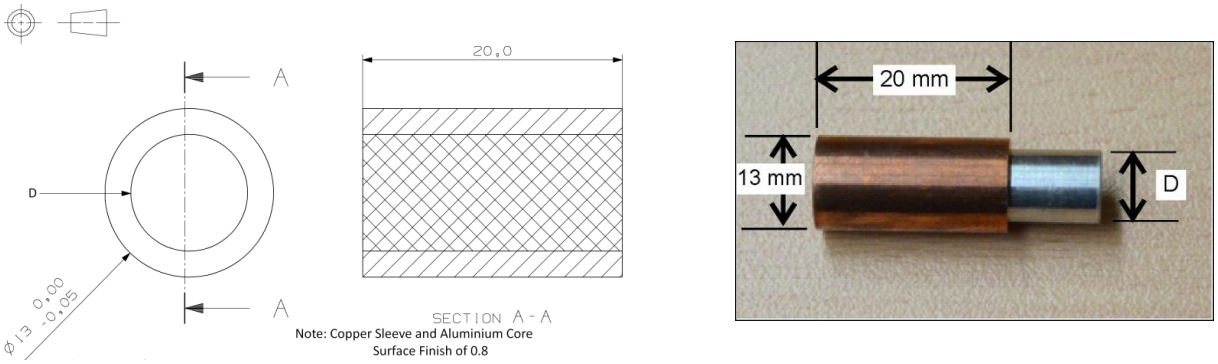

(a) (b)

Fig. 3 - 4: sample before processing (a) critical dimension of the composite sample (b) Composite sample with copper C11000 (99.90% Cu) clad and commercially pure cast aluminum core

To investigate the effective bond formation between copper and the aluminum samples, five different combinations of samples were produced by varying the inner diameter (D as shown in Fig. 3-4a), with 11.0mm, 10.5mm, 10.0mm, 9.5mm, and 9.0mm values. Samples were made to 20mm length with a clearance fit and can be easily assembled and disassembled by hand. The composite samples at the beginning of the extrusion were shown in Fig 3-4b.

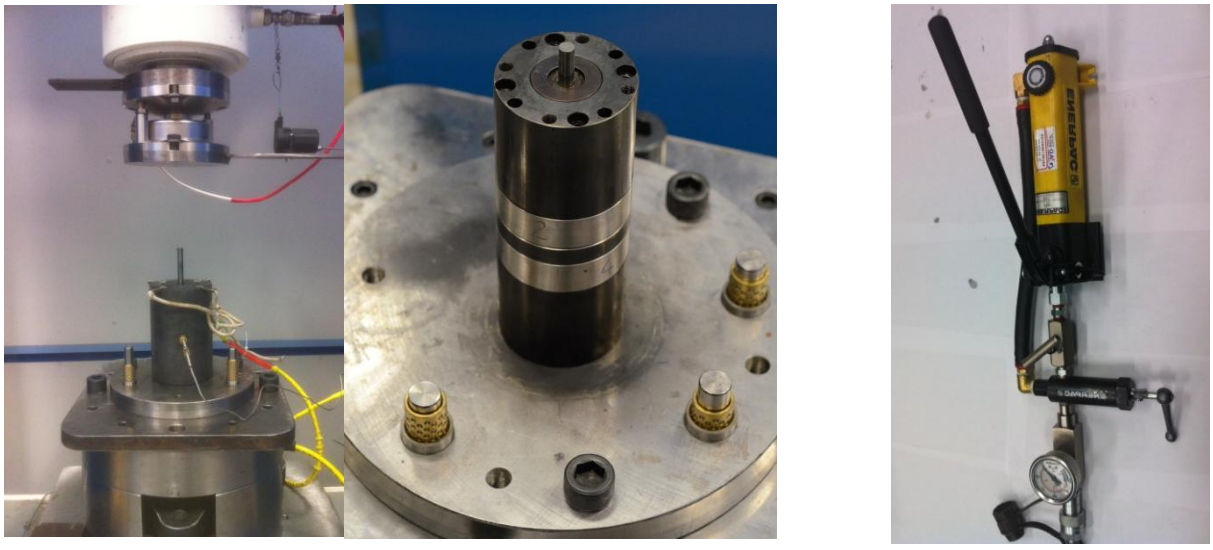

(a) (b) (c)

Fig 3-5 (a) AFCE process rig (b) The assembly of the AFSCE experimental setup (c) hand pump used for back pressure application.

The AFSCE extrusion process rig is as shown in Fig 3-5a. The actual assembly of the die container and the punch before placing the heating jacket is shown in Fig 3-5b. The extrusion force was applied using a hydraulic press with a capacity of 150 tons. Load cell monitors the applied pressure which was mounted to the ram as shown in Fig.3-5a. The load cell with a capacity of 50 tons was used in this experiment. However the experiments required the maximum force of up to 30 tons which is 60% capacity of the load cell. An electronic displacement gauge fitted to the ram to measure the displacement is also shown in Fig.3-5a.

In addition to this, from initial experiments, it was found that the backpressure is a key parameter in this AFSCE process to create an effective bonding. Backpressure is applied by a separate hydraulic system which consists of a hand pump, needle valve, release valve and a pressure gauge as shown in Fig 3-5c. Therefore it is possible to set the backpressure to certain value before experiment. In every experiment the backpressure is set before performing the extrusion. The carried out experiments and the outcomes are summarized in the Table 3-1

Table 3-1: Summary of the AFSCE experiments shows the outcome of the various experimental cases.

Experimental case number	Test conditions	Outcome
Experiment 1	• 300°C without backpressure • 10.5 mm Al core diameter	• At The free end, the copper and the aluminum were not aligned due to different flow velocity of core and sleeve • It was confirmed no bonding was occurred
Experiment 2	• 300°C With 200Mpa backpressure • 11 mm Al core diameter	• During the ejection process of sample, flush out was noticed which made difficult to remove tungsten punch from the container. • The extruded specimen was split into two pieces along the axis of extrusion and checked for bonding • It shows the evidence for bonding
Experiment 3	• 300°C With 200Mpa backpressure • 2 samples were used in this extrusion • Steel disk of 1mm were placed in between the samples and between sample and punches to prevent flash out. • 10.5 mm Al core diameter for the 1st sample • 11.0 mm Al core diameter for the 2st sample	• Flush out was minimized by using steel disk of 3mm on the top (3×1mm) • Maximum force for the extrusion was measured ~ 20 tons • Successful bonding was formed • It was prevented that the punch hitting the die during the extrusion by placing two samples.
Experiment 4	• Similar steps of the experiment 3 was followed • 10.0 mm Al core diameter for the 1st sample • 10.0 mm Al core diameter for the 2nd sample	• Flush out minimized by using placing steel disk of 4mm on the top (4×1mm) • Maximum force required for the extrusion was ~ 22 tons

			• Successful bonding was formed
Experiment 5	• Similar steps of the experiment 3 was followed • 10.0 mm Al core diameter for the 1st sample • Solid steel rod was placed as the second dummy sample		• Experiment was discontinued as the force reached 35 tons • It was due to the second solid steel sample stuck in-between the top two containers. • It could be due to misalignment or the die set was not tightened properly • Therefore it was decided to keep the second piece from a soft material, and the accuracy of assembly must be checked before the extrusion using a dial gauge
Experiment 6	• Similar steps of the experiment 3 was followed • 9.5 mm Al core diameter for the 1st sample • 9.0 mm Al core diameter for the 2nd sample		• Flush out minimized by using placing steel disk of 4mm on the top (4×1mm) • Maximum force required for the extrusion was ~ 22 tons • Successful bonding was formed • Results which is similar to experiment 4

After these initial experiments and successful bonding formation at 300˚C with 200 MPa back pressure conditions, the project was only considered to concentrate with 10.5mm inner diameter sample to perform further investigation. Therefore a number of samples were fabricated with 10.5mm aluminum core diameter with 13 mm outer copper diameter composite samples.

3.2.1.3 Material characterization using hot torsion tests

Two materials, pure copper C11000 (99.90% copper) and pure cast aluminum, were used in this experiment to make a composite sample. In order to obtain stress-strain behavior of the materials, hot torsion test was performed at 300°C and the torque-twist data were converted to the stress-strain curve using the technique presented elsewhere [120]. The characterization of the base metals carried out using a hot torsion test rig shown in Chapter 5. The AFSCE heating cycle was applied to the torsion test samples before running the torsion test. The torsion test sample is shown in Fig.6a. The flow curves were mathematically modeled using the following expression:

$$\text{Aluminum } \sigma = \frac{130.2\varepsilon - 0.3689}{\varepsilon^2 + 3.494\varepsilon + 0.1443} \quad (3)$$

$$\text{Cupper } \sigma = \frac{98.32\varepsilon^2 + 10.37\varepsilon + 0.3378}{\varepsilon^2 + 0.03161\varepsilon + 0.01549} \quad (4)$$

where σ (Mpa) and ε are effective stress and strains in a uniaxial loading mode.

The mathematical models and experimental constitutive data are shown in Fig.3-6b

(a)

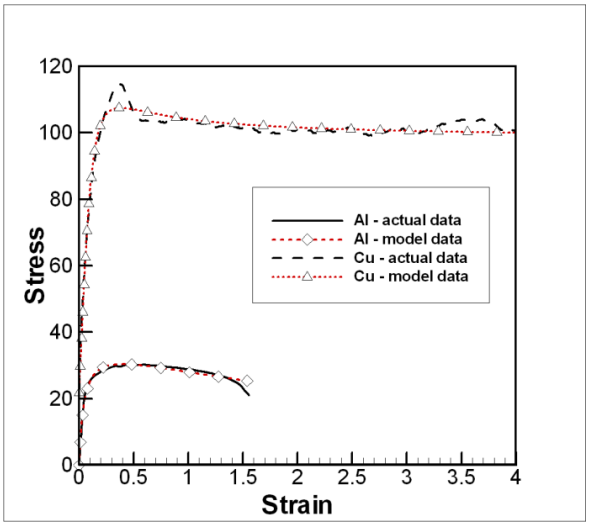

(b)

Fig. 3-6 (a) Example of aluminum torsion test sample inside the heating conduction material to characterize the material hot torsion test and (b) estimated and measured stress-strain of copper and aluminum of this study at 300°C

3.3 Macro scale investigations of the AFSCE processed samples

An extruded composite sample with core diameter of 10.5mm was investigated for strength measurements. Fig.3-7a shows the composite Cu/Al specimen after AFSCE with two distinct zones: zone 1 with grooves and a groove free zone 2 corresponding to the extruded and the non-extruded zones, respectively. A 1mm thick sample normal to the cross section of zone1 was sliced from the AFSCE specimen by the EDM wire cutting. Low voltage and low current were used during the wire cutting to avoid the heating of the sample. Wire cutting of the DBT slice prevents introduction of art effects and change in properties of the bonding layer which can occur by other slicing techniques. It can be seen from Fig.3-7b that copper thickness in the disc shape sample is uniform and the sample is axisymmetric.

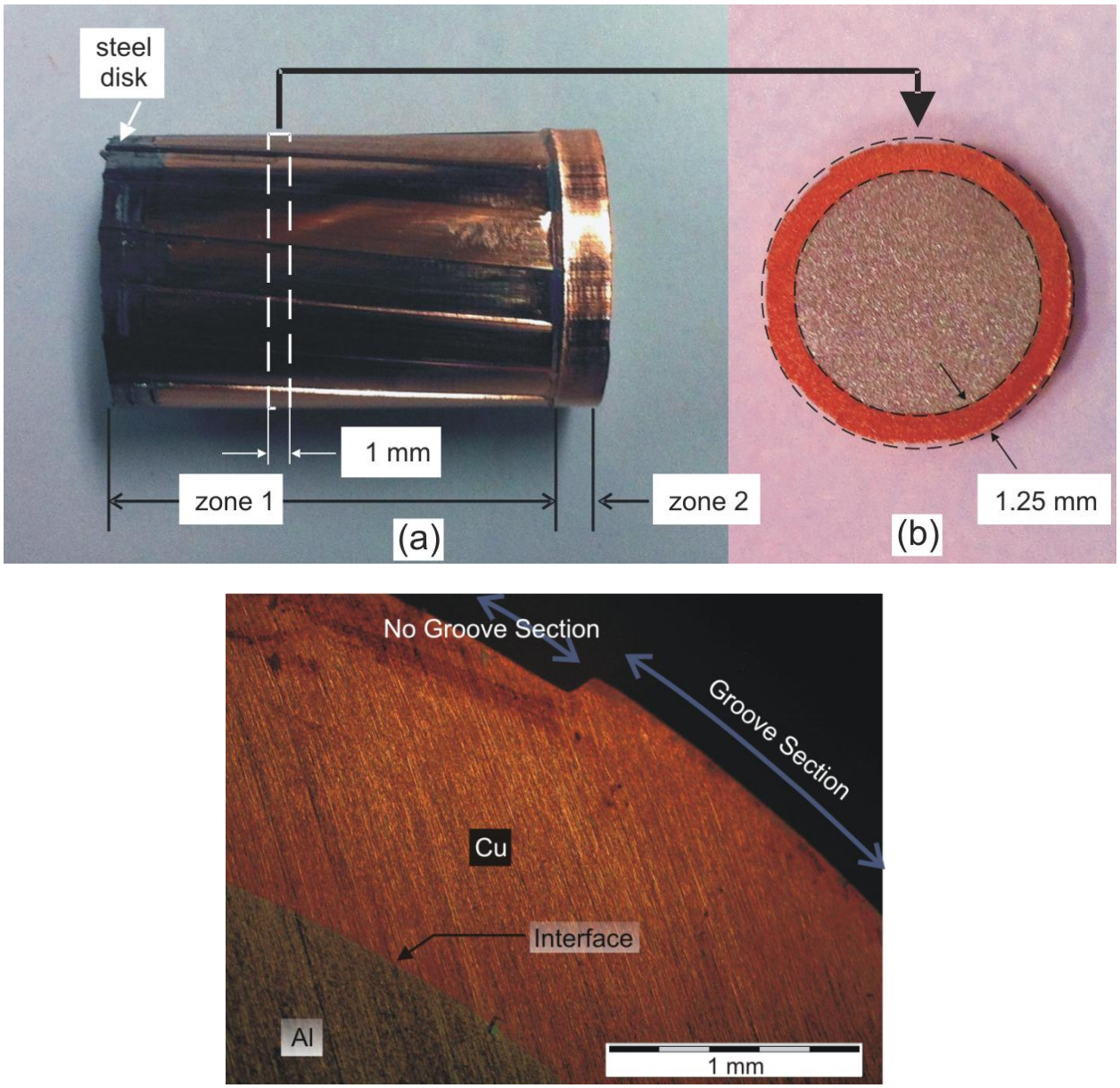

Fig. 3-7. (a) Longitudinal section view of the copper aluminum specimen, (b) cross section of the sliced DBT sample, (c) cross section of the AFSCE processed composite interface.

During the AFSCE, the cross section of the composite sample changes slightly due to the presence of the grooves. To ensure that the change of cross section and its subsequent fitting of the metals together are not interpreted as the bonding strength, two of the fabricated composite specimens were cut longitudinally along the axis of extrusion. The parts were not separated even after applying a 50 N shearing force tangent to their interfaces of the sample. In addition to this, it was confirmed by optical microscopy that the radial plastic flow of material during AFSCE was limited to the vicinity of the grooves

and did not distort the circular cross section at the interface. As shown in Fig. 4, an optical microscope image, there exist no radial cross sectional change along the interface. This indicates the radial plastic deformation mainly occurred in the copper region. It can be seen in Fig. 4 that the copper–aluminum interface remained fully circular after the AFSCE.

3.3.1 Bond Strength Investigation using a Dedicated Blanking Test (DBT)

Formation of a cylindrical bonding surface during the AFSCE prevents utilization of standard lap shear test to measure the bonding strength under pure shear conditions. Therefore, a modified axi-symmetric lap shear test was developed for this experiment which was similar to a normal blanking examination. The modified test allowed for application of shear along the bonding interface which was increased gradually until shear failure occurred along the bonding interface. In this work, we will refer to the test as “dedicated blanking test (DBT)”. The punch moved vertically to apply a shear blanking force along the interface, and its load displacement data were logged through the entire stroke of the punch. The extruded composite rods were sliced using a wire cutting method by electro discharge machining (EDM) before the DBT. The extruded composite specimen comprised of a 10.5 mm aluminum core with EDM slices of 1, 1.5 and 2 mm thicknesses were made for the subsequent DBTs.

A schematic diagram of the DBT is shown in Fig. 8 loaded with the DBT sliced sample shown in Fig. 7b before application of the load to measure bond strength. The detail discussion of the DBT design is discussed in Chapter 5 using numerical modelling technique.

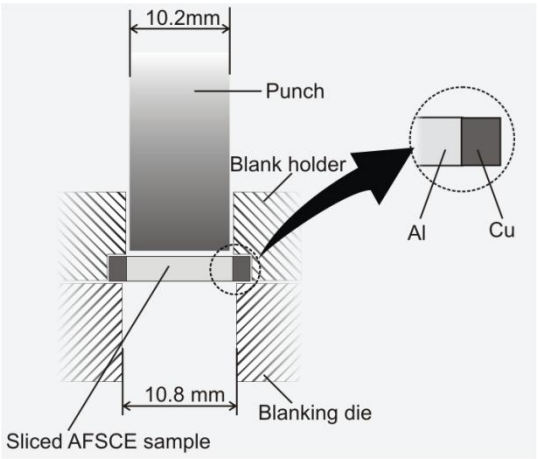

Fig. 3-8 The dedicated blanking test rig to measure bonding shear strength

To establish a reference stiffness curve, an aluminum disk sample of 1mm thickness was made out of an identically extruded section and was blanked using the DBT with the same 10.5mm DBT set. The solid 1mm aluminum sample required a DBT shearing force of $F_r = 1950N$ to fail with a typical elastic-plastic behavior as shown in Fig.3-9. Similar measurements for composite samples with various thicknesses revealed that the maximum blanking load increased with an increase in thickness of AFSCE specimens. It can be seen in Fig. 3-9 that the relationship between the thickness and the maximum DBT force is non-linear. This is due to the fact that for higher thicknesses the failure mode deviates from a simple shear failure which increases contribution of bending to failure for higher thicknesses.

Further to this, the composite sample with 1mm thickness required 1289N shearing load for bond failure at the interface which was below, F_r , value 1950N for pure aluminum. The lower than expected strength of the composite sample is most likely due to Al/Cu interface which could include formation of a thin composite like bond layer. This interface layer strength to some extent is expected to be lower than shearing strengths of both aluminum and copper due to presence of imperfections at the boundary. Also the sudden drop in the DBT results, Fig.3-9, indicates the brittle nature of this interface. Further study is required to verify the mechanism for bond formation at AFSCE interface which seems to have a brittle inter metallic nature. The lower than expected strength for the bond is discussed in Section 3.3.3.

Stress discontinuity and stress concentration at the interface due to sudden variation of the composite specimen properties at the boundary suggests a brittle failure from a continuum mechanics point of view. In order to further understand the bond failure, micro-structural investigations were performed on the AFSCE specimens interface and their corresponding fracture surfaces were analyzed.

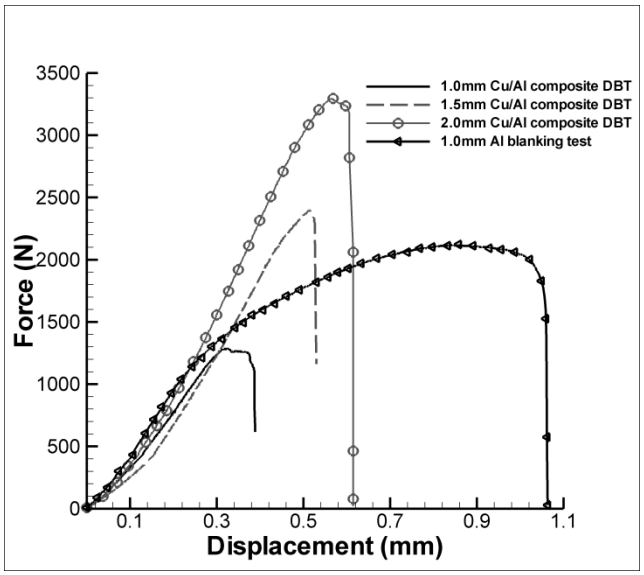

Fig. 3-9 Dedicated blanking test results plotted for shear force against the punch stroke

3.3.2 Characterization of Interface between copper and aluminum after the application of AFSCE process

Upon completion of the AFSCE, the bonding strength in shear along the interface was investigated. Optical and scanning electron microscopic techniques were also used to characterize the interfacial features of the hybrid bonding layer. The EDX (Energy-dispersive X-ray spectroscopy) analyses were performed at a number of points along the interface to investigate the nature of the interface layer formed after the bonding.

Fig3-10a shows an optical microscopy (OM) of the interface. It is almost a gap-free interface which shows details of the nearly perfect contact between the two metals. In Fig 3-10a, only a small part of the interface is visible due to the relatively large magnification. To show continuous generation of the layer through the entire joint, a low magnification SEM image of the interface is shown in Fig. 3-10b. The layer is a uniform dark band of about 0.5μm in thickness which has formed and distributed evenly at the Al-Cu interface.

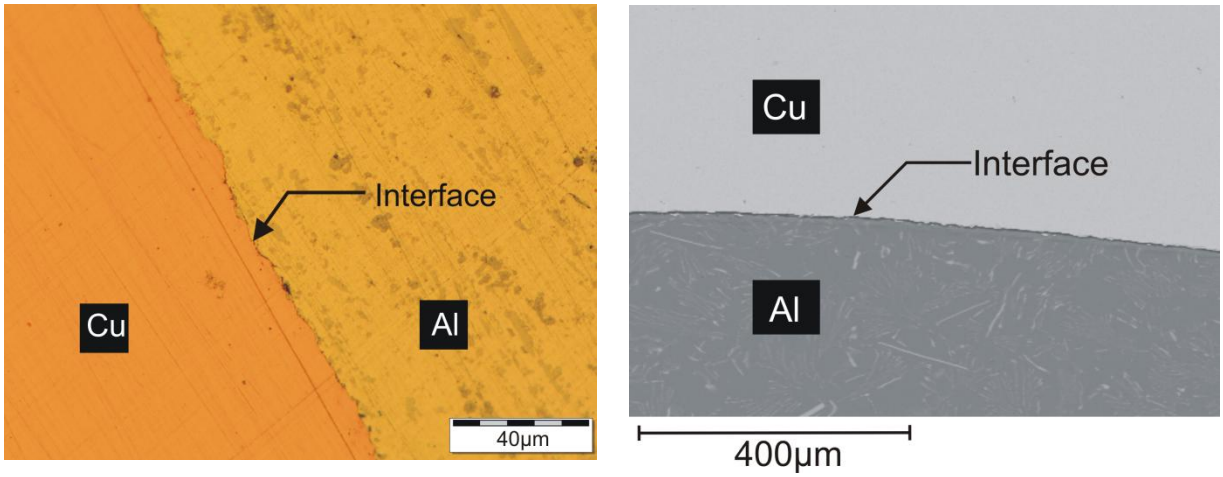

(a) (b)

Fig. 3-10. (a) Optical micrograph image of Cu/Al interface after extrusion (b) Back scatter electron (BSE) image of Cu/Al interface

In comparison, the optical microscopy image of the pre-extruded composite interface (from zone 2 of Fig.3-7a) shows a clear straight line as shown in Fig. 3-11.

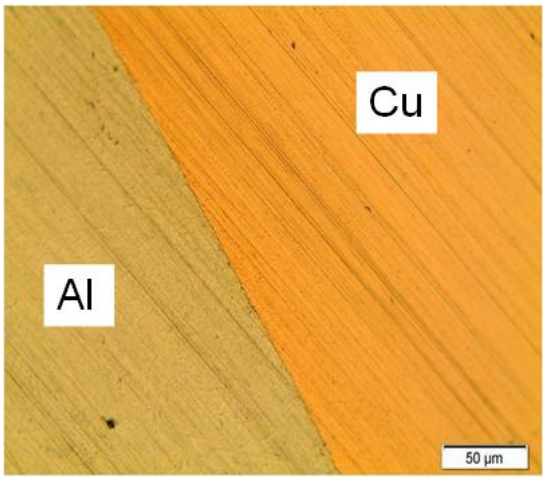

Fig. 3-11. Optical micrograph image of Cu/Al interface of the pre-extruded section from zone 2 of an AFSCE sample

Back Scatter Electron (BSE) image obtained by SEM (Fig. 3-12a) confirmed the presence of a nearly constant thin layer of approximately 0.5µm. this was visible between copper sleeve and the aluminum core. In order to confirm the occurrence of diffusion and the formation of a bonded layer, three points,

labeled as 1, 2 and 3 in Fig. 3-12a were examined using the Energy-dispersive X-ray spectroscopy (EDX) technique. The EDX spectra of three points are shown in Figs. 3-12b-d.

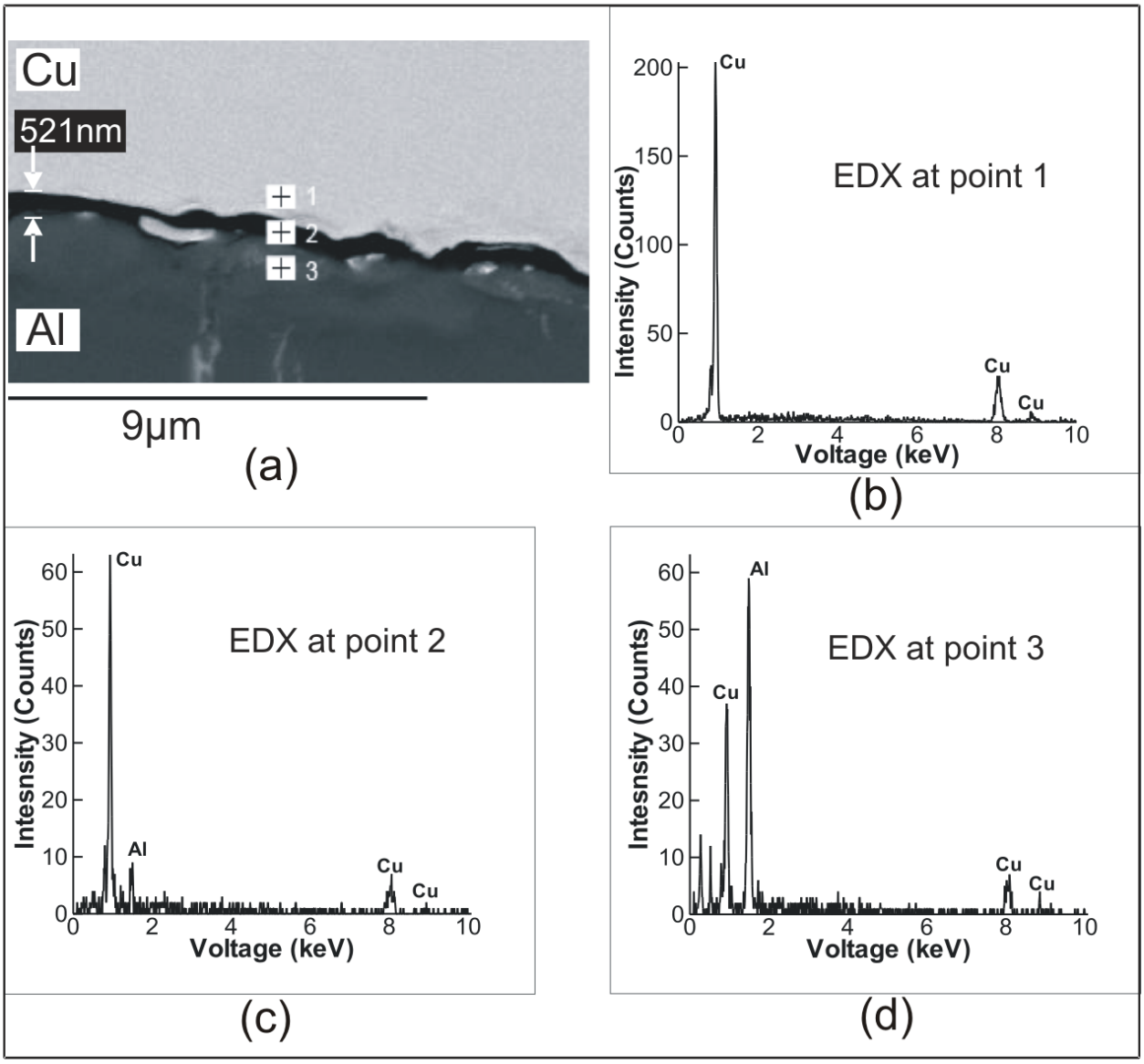

Fig 3-12. SEM image and EDX spectra from points 1, 2 and 3. (a) Back Scatter Electron (BSE) image of Al/Cu interface, (b) EDX at point 1, (c) EDX at point 2 and (d) EDX at point 3

According to the EDX analyses, point 1 (Fig. 3-12b) had mainly copper traces without any aluminum peak present. This is in contrast to EDX results at point 2 (Fig. 3-12c) which shows the amount of copper decreased from 200 counts to 65 counts with aluminum peak appearing with 10 counts. This suggests that sufficient drive for diffusion has been produced at the interface for conditions of this study. The

EDX results at point 3 (Fig. 3-12d) revealed further increase in aluminum peak with slight decline in copper counts compared with previous point. The higher counts for aluminum at point 3 compared to point 2 in the specimen was expected due to further increase in distance from interface towards aluminum core. These observations suggest that during the AFSCE process a favorable condition for diffusion of copper and aluminum has been created leading to formation of a thin interface layer. This is in agreement with the findings on other copper and aluminum bonding processes under high pressure such as cold spray [121].

The EDX results are typically estimated based on a measurement within a footprint volume and therefore are not point values. The EDX results are evaluated using an interaction volume technique, which can be modeled by using Monte Carlo Simulation. This provides a relatively low spatial resolution of measurement and therefore the results should be interpreted with caution.

SEM examinations of the fractured surfaces were performed to investigate the mechanism of the bonding layer failure. The fractography images of the shear failure at the interface are shown in Fig. 3-13. BSE images Fig. 3-13a and Secondary electron (SE) image Fig. 3-13b revealed the compositional contrast and the topography of the fracture surface, respectively. Presence of bright region which indicates copper and the dark region which indicates aluminum suggests that the bond layer did not fracture through a single material and the bonding residuals were not homogeneous.

More detailed analysis of the 1 mm thick composite material interface revealed a brittle fracture behavior which is in agreement with the load-displacement behavior shown in Fig.3-9. Brittle fractured surfaces of the composite structure after blanking tests are shown in Fig.3-13. The fractured pure aluminum surface is shown in Fig.3-14. The Fig 3-14 revealed a significantly higher number of dimples and grain boundary pull outs in aluminum sample. These pull outs and dimples were indicative of ductile fracture for aluminum specimen which were absent in fractography of the AFSCE processes composite material interface in Fig.3-13c. It is speculated that similar event as aluminum could occur in copper fracture.

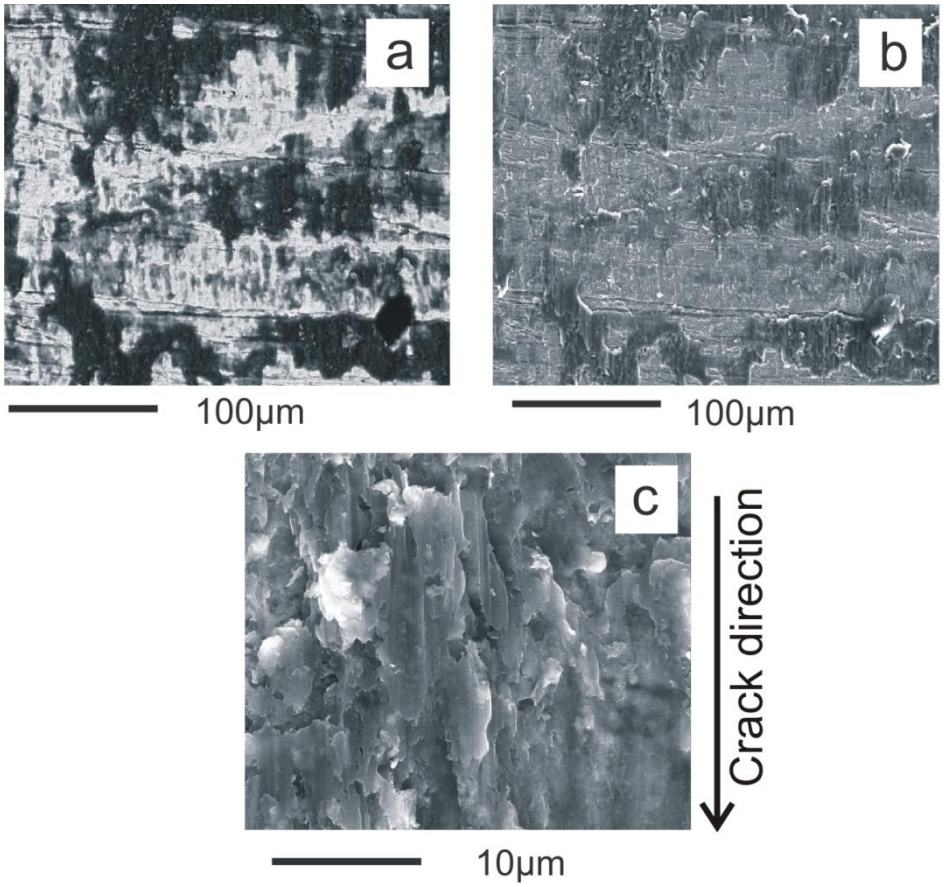

Fig. 3-13. (a) Back Scatter Electron (BSE) image of AFSCE sample after shear failure (b) Secondary Electron (SE) image of AFSCE after shear failure (c) SE image shows the aluminum on copper ring of the AFSCE sample.

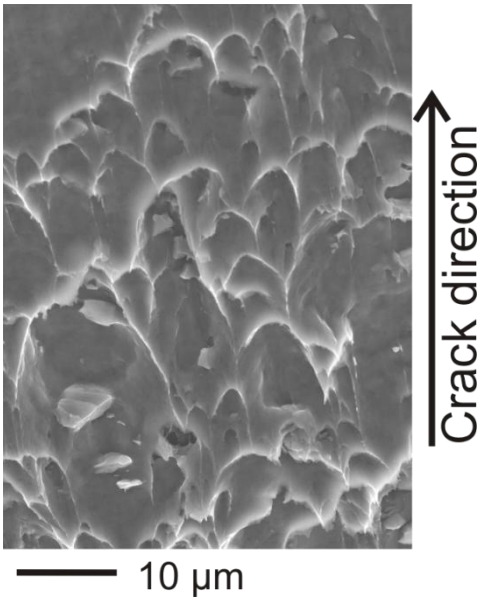

Fig. 3-14. SE image of aluminum fracture surface shows ductile failure

The introduced AFSCE process revealed an achievement of zero shape change effect in the composite extrusion for the applied process conditions. This was with respect to simultaneous bond formation at the manufactured Cu/Al hybrid rod interface. Further study is required to understand the nature of the interface and parameters that affect properties of the hybrid material produced through this method. Such process has the potential to be utilized as an advanced rapid manufacturing with cost effectiveness in energy and material consumption.

3.3.3 Evaluation of the bonding mechanism

The lower than expected strength of the joint is most likely due to the presence of a 'thin composite like bond layer' at the Al/Cu interface where a combination of metallurgical bonds and mechanical interlocking are present. In Fig.3-10a, the insufficient joints at the interface shown as dark spots and scars are negligible compared to the gap-free interface. As shown in the results in Fig. 3-9, the strength of the interface layer is lower than the shearing strengths of both aluminum and copper. This could be partially due to the presence of gaps and the contaminants (e.g. oxides) entrapped, shown as dark spots, at the interface. The sudden drop in the DBT results, Fig.3-9, indicates the brittle nature of the interface layer.

Three parameters relevant to the weak hybrid bonding are considered here, viz. a broken oxide layer, a formation of intermetallic layer at the interface and an insufficient diffusion. In a typical diffusion bonding process, it is possible to form broken oxide layers which are made up of the surface oxide of the parent materials [21, 22]. Also, formations of intermetallic compounds are well known for bimetal joining processes and diffusion welding (see for example Sasaki et al. [122], Manesh & Teheri (2003)[123], Kalpakjian[20] and Kazakov [21]). However, the EDX results shown here are inconclusive on the formation of an intermetallic layer. This is because the EDX results were estimated based on the interaction volume beneath the footprint which provides a poor resolution compared to the layer thickness of 0.5mm as shown in Fig. 3-12a. Further investigations are needed to confirm the formation of intermetallic layer at the Al-Cu joint. Finally, insufficient diffusion is mainly due to an inadequate holding time, temperature, pressure or a combination of all. By increasing back pressure in the assembly shown in Fig. 3-1b, the diffusion is expected to improve.

From a strength view point, the aforementioned parameters suggest two weakening mechanisms, stress concentration and discontinuity of flow stress in the radial direction at the interface. These are due to sudden property changes in an extremely narrow radial distance [124, 125]

3.4 conclusions

An axi-symmetric forward composite spiral extrusion (AFSCE) process is proposed to fabricate hybrid rods in a single step. An analytical frame work of the AFSCE process was developed based on quadratic velocity field with two extreme boundary conditions of fully sticking and fully sliding were considered. To demonstrate the AFSCE process, an experimental case study of a hybrid rod fabrication with heating and back pressure was performed for Al/Cu composite rods. A dedicated blanking test used in this investigation revealed successful bond formation during the AFSCE process which was below the strength of reference aluminum of this study. SEM-EDX technique and fractography analysis revealed an interface layer with a layer thickness of 0.5µm at the copper aluminum bond interface with sudden failure of the bonding. The differences between the reference pure aluminum failure and the composite sample failure were compared using the dedicated blanking tests (DBTs) and their facture studies. These early promising results show that the AFSCE process provides good dimensional control on both the core and clad layer. The introduced single step approach for AFSCE process and the established bonding at the interface are beneficial for industrial applications where manufacturing of hybrid rods with broad range of energy and material saving are considered. Further investigations of the fabricated AFSCE samples were carried out and discussed in the following chapter.

Chapter 4:
Characterizations of the AFSCE extruded Copper Clad Aluminum composite

Chapter 4: Characterizations of the AFSCE extruded Copper Clad Aluminum composite

4.1 Introduction

It has been suggested that the contact between copper and aluminum at elevated temperatures with a high pressure process conditions may produce a material bond by inter-diffusions at the interface by facilitating atomic movements across the boundary [20-22]. Formation of Intermetallic Compounds (IMCs) at the interface has been reported for copper clad aluminum bonding cases [21, 105, 108, 126, 127]. Such intermetallic layer increases the strength of the interface, but limits the ductility as suggested by Sasaki et al.[122] and because of its brittle nature [20, 122, 128] reduces the bond strength as suggested by Bae et al.[128]. Moreover, joining Cu–Al has been recently investigated by many researchers, for example using brazing processes with various filler materials such as Zn–Al–Ce in [129], Al–Zn in [130] and Zn–3Al in [131]. However the brazing process produces significant amount of IMCs and makes significant micro-structural changes in the parent materials at very high temperatures which are not preferable.

In the chapter 3, Al–Cu hybrid metal composite was successfully fabricated by AFSCE at 300 °C with a 200 MPa backpressure and a dedicated blanking test was performed to measure the bond strength of the fabricated composite samples. The process conditions with a high pressure and an elevated temperature could lead to the formation of both IMCs and ultra-fine grains at the interface. It is known that the concurrent shear deformation, high pressure and temperature create a bond at the interface during the AFSCE process but due to the inaccessibility of the interface, very limited direct observations can be made at the interface zone. The exact mechanism behind the creation of bonding is not clear. Therefore, in order to understand the bonding mechanism and the parameters that affect properties of the hybrid metal composite require further investigation.

In this chapter Scanning Electron Microscope/Focused Ion Beam (SEM/FIB), X-Ray Diffraction (XRD) and Electron Backscatter Diffraction (EBSD) techniques are used to investigate the nature of the interface. Moreover, the strength changes across the sample along the radial distance in the copper and aluminum

due to the AFSCE process are determined using micro-hardness tests and the copper region hardness changes are compared with the EBSD micro-structural results. It is found that the bonding is a near flawless mechanical interlocking at the interface which agrees well with bonding shear strength measurement. The bonding shear strength at the interface is higher than shear strength for the pure aluminum. The deformation mechanisms in various regions were also accommodated by a formation of ultra-fine grains (UFGs) and crystal orientation changes in various regions of copper sleeve, were confirmed by micro-hardness distribution across the copper region and the EBSD results from various sampling points.

4.2 Micro hardness measurements along the transverse section of the AFSCE samples

Micro hardness measurements on the transverse section were carried out to study mechanical property changes across the AFSCE composite sample in the radial direction particularly in the vicinity of the interface. Three samples were tested to investigate the hardness behavior along *x* and *y* directions and their average values were used to plot the hardness behavior as shown in Fig. 4-2. The Vickers micro-hardness was measured according to ASTM: E384 11e1 standard across the radial direction along the two perpendicular radii for aluminum and copper shown in Fig. 4-1b. Given the kinematics of Axi Symmetric Forward spiral extrusion (AFSE) / AFSCE, a finer spacing was chosen near periphery of the die. A Wolpert Group Micro-Vickers hardness tester with 100 gf (gram force) load was used. Measured hardness values of unprocessed materials were used to compare the hardness changes in the composite material. The average hardness values of unprocessed materials also included in the Plot Fig 4-2.

The transverse section is marked in the mid-section of the AFSCE processed sample in Fig 4-1a. Dotted lines are used in Fig. 4-1b to show the deviation of the sample transverse section, groove and valley, from a real axi-symmetric (circular) section.

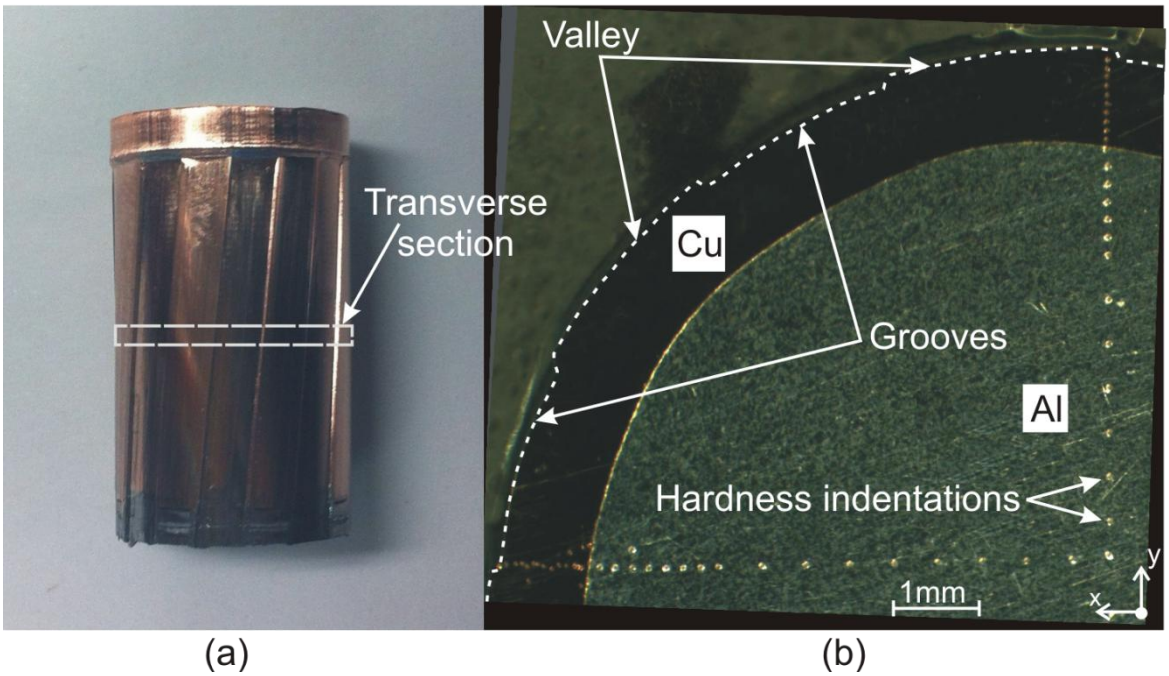

Fig. 4-1. (a) Processed Cu/Al AFSCE sample showing the transverse section of the testing sample (b) Micro hardness indentation pattern along the vertical and horizontal radii on the "transverse section" of the processed AFSCE sample

4.2.1 Micro hardness results along the cross section of the AFSCE sample and unprocessed parent materials

Vickers hardness tests were performed and the hardness measurements were plotted as a function of radial distance from the interface as shown in Fig. 4-2. A normalized distance has been used in Fig. 4-2 to show the position of hardness measurements in the radial direction; a zero distance (chosen at the interface) marks the origin of the radial coordinate system. The positive and negative sign conventions for the normalized distance are respectively used to distinguish the measurements relevant to Cu and Al zones. Two measurement paths were respectively chosen along Cu and Al base metals which are located at the left and right side of the origin. The first path, along the *x*-direction in Fig. 4-1b, has a normalized distance of $r = -5$ at the center and $r = 0$ at the interface. The second path, along *y*-direction in Fig. 4-1b, is overlaid with the first path data and shown in Fig. 4-2. The boundary conditions for the two paths are slightly different; given the fact that *x*-direction measurement was along the grooved zone of the die and the *y*-direction was along the valley zone (see Fig. 4-1b).

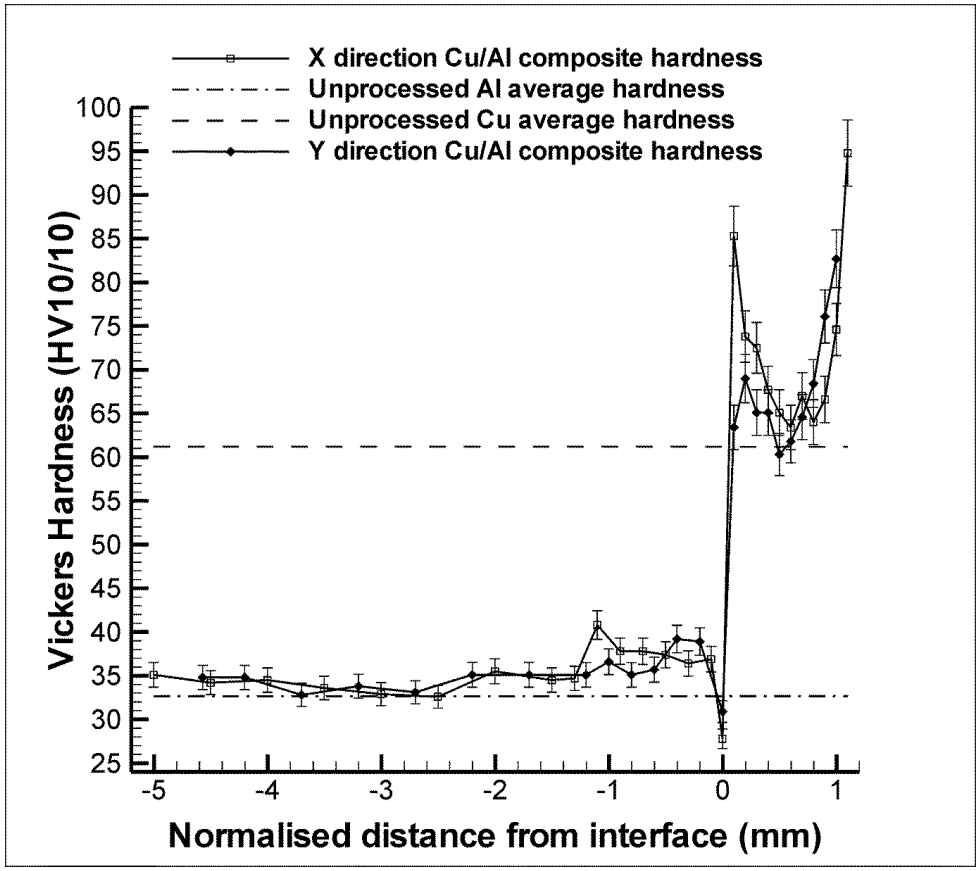

Fig. 4-2. Micro hardness measurements versus normalized distance for AFSCE Cu/Al composite specimen and average hardness of as received (un processed) copper and aluminum used in this fabrication process

Micro-hardness distribution in Fig. 4-2 shows a complex trend particularly in copper. Owing to the slightly different boundary conditions along the two paths, the measured hardness along x does not fully coincide with the measured values along y direction; localized deformations near the helix grooves, makes the process non axi-symmetric [132]. Farhoumand et al. demonstrated that the AFSE process creates a linear axi-symmetric result for the concentric core and non axi-symmetric shell region near the periphery of the sample because of the groove effect [132]. Therefore, strain accumulations along the two paths are slightly different.

Considering an initial hardness of 32.65 HV10/10 for aluminum as received, a slight increase in the aluminum hardness (37.8–38.9 HV10/10) was noted near the interface. Noting that the AFSCE process was conducted at 300 °C, which approximately is the annealing temperature of the aluminum which prevents significant work hardening and hardness changes in the aluminum. Near the interface and near the outer periphery of copper, two hardness maxima have developed with a minimum in the middle of

the two maxima. As shown in Fig 4-2, these two hardness maxima in copper are relatively higher than the average hardness of the unprocessed copper and the hardness minima of the copper is approximately equal to that of unprocessed copper which is 61 HV10/10. In addition to this, aluminum has lower "strain hardening exponent" compared to copper. This partly explains the large work hardening effect near the interface of the base metals. The significant strain hardening near the interface in the copper region did not create any micro-cracks. A similar hardness discontinuity at the interface of a copper clad aluminum was also reported [118] where the bimetal was produced by a forward extrusion process. In addition to this, care must be taken in measuring and interpreting hardness measurements very near to the interface or at the interface. This is because of material / property discontinuity at this zone. Therefore large indentations and false hardness measurements are very likely at the interface region. Such indentations lead to lower than expected hardness values at the interface (lower than both aluminum and copper).

Using Equal Chennel angular Pressing (ECAP) process, Llorca-Isern et al. [133] reported highly elongated copper grains near the Cu–Al interface and Cu outer periphery with less deformation at the centre of copper. Their findings comply with the experimental hardness measurements (Fig. 4-2) in the current study. Therefore variation in hardness during the AFSCE can be due to the microstructural changes within the composite structure that will be discussed in Section 4.5 and Section 4.6.

In the AFSCE process, boundary condition of the specimen at the exit (the backpressure) prevents longitudinal protrusion of aluminum. A large friction between copper and aluminum is expected to develop at the interface improving aluminum flow, induced by deformation of the copper. These complicated events could lead to slight tapered interface in the longitudinal direction as shown in Fig. 4-3. Consequently, both base metals deform tri-axially during the AFSCE which bring a complexity in the interpretation of the deformation based on the hardness distribution. In consideration of these follows, a simple explanation of deformation patterns during the AFSCE process and hardness changes in the materials are presented in Section 4.2.1.

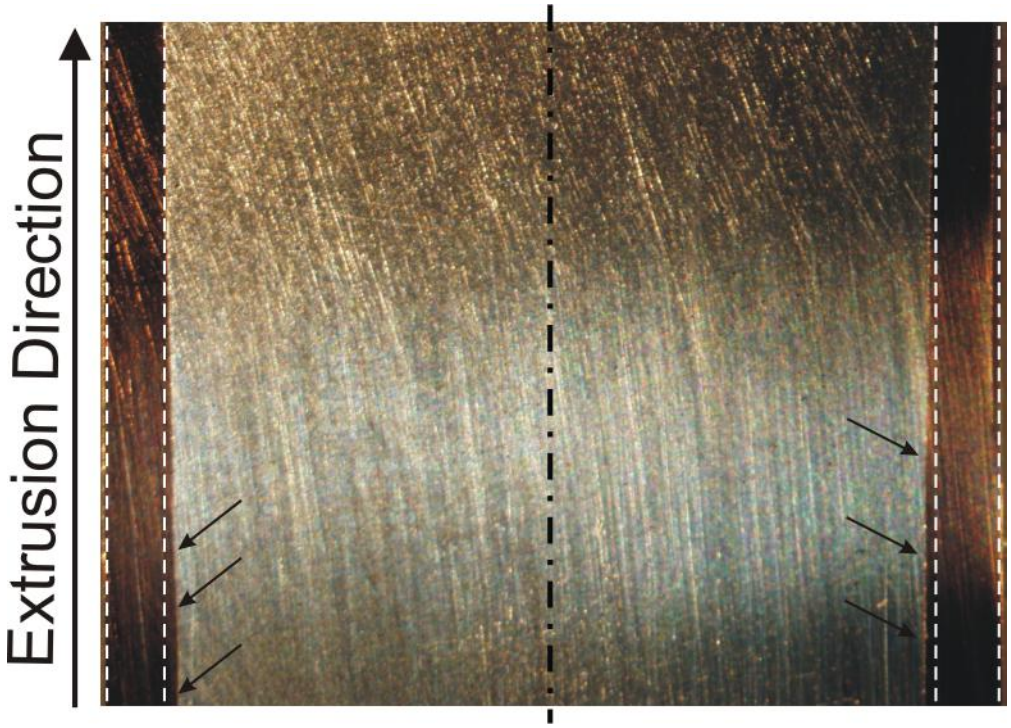

Fig. 4-3. Longitudinal section of the AFSCE sample, tapered interface due to radial deformation

4.2.2. Kinematic description of the AFSCE process and interpretation of hardness results

Let us consider the velocity vector at a typical point P, $\vec{V}_P$, in the metal composite sample (either in Al or Cu) described by its cylindrical coordinates r, z and θ in radial, axial and tangential directions respectively. The origin of the Coordinate system is at the centre of the die at its entry plane. The velocity could be resolved into radial, longitudinal and circumferential components using the unit vectors:

$$\vec{V_s} = \vec{V_r} + \vec{V_z} + \vec{V_\theta} = V_r\,\vec{e}_r + V_z\,\vec{e}_z + V_\theta\,\vec{e}_\theta \qquad \text{Eq. 4-1}$$

Given the bullet shape free surface of the AFSCE sample at the exit, reduction in the area of the copper annular in the axial direction shown in Fig. 4-3 and the kinematics of the AFSE [82], the following assumptions on the AFSCE's velocity filed are made:

$$V_r \propto r.z \qquad \text{Eq. 4-2}$$

$$V_\theta \propto r^2.z \qquad \text{Eq. 4-3}$$

$$V_z \propto \frac{z}{r^2} \qquad \text{Eq. 4-4}$$

The components of strain increment in the cylindrical coordinate system could be correlated to the velocity components (see [82] for details). The hardness distributions in Fig. 4-2 correspond to a "transverse section" with a fixed value of "z". Based on the proposed velocity components, for a given z, the trends for the "radius dependent" increments of strains (i.e. $d\varepsilon_{zz}$, $d\varepsilon_{rz}$, $d\varepsilon_{r\theta}$ and $d\varepsilon_{z\theta}$) could be described as:

$$d\varepsilon_{zz} \propto \frac{1}{r^2} \quad \text{Eq. 4-5}$$

$$d\varepsilon_{rz} \propto r + \frac{2}{r^3} \quad \text{Eq. 4-6}$$

$$d\varepsilon_{r\theta} \propto r \quad \text{Eq. 4-7}$$

$$d\varepsilon_{z\theta} \propto r^2 \quad \text{Eq. 4-8}$$

It can be shown that other "non- radius dependent" strain components (i.e. $d\varepsilon_{rr}$ and $d\varepsilon_{\theta\theta}$) are zero. Based on equations 5 to 8 and the von-Mises yield criteria, a general descriptive expression for the effective strain at the point P could be considered by decomposing the effective strain, $\bar{\varepsilon}$, into two functions:

$$\bar{\varepsilon} \cong f_d(r) + f_a(r) \quad \text{Eq. 4-9}$$

$f_d(r)$ and $f_a(r)$ are non-linear descending and ascending functions of r respectively which describe the radial work hardening behavior in Al and Cu. For each zone, there exists a critical radius before which the descending behavior and after which the ascending behavior is dominant.

Fig. 4-4a shows the trend for the aluminum zone; before a critical radius of $r = -2.6$, the hardness decreases with r (negative work hardening). After the critical radius, hardness increase with r is the dominant mode (positive work hardening). Fig. 4-4b shows a similar trend for the Cu zone; before a critical radius of $r = 0.68$, the hardness reduces with r but further increase in r increases the hardness. The small slopes of the curves in Fig. 4-4a could be due to small plastic deformation in the Al zone compared that in the Cu zone.

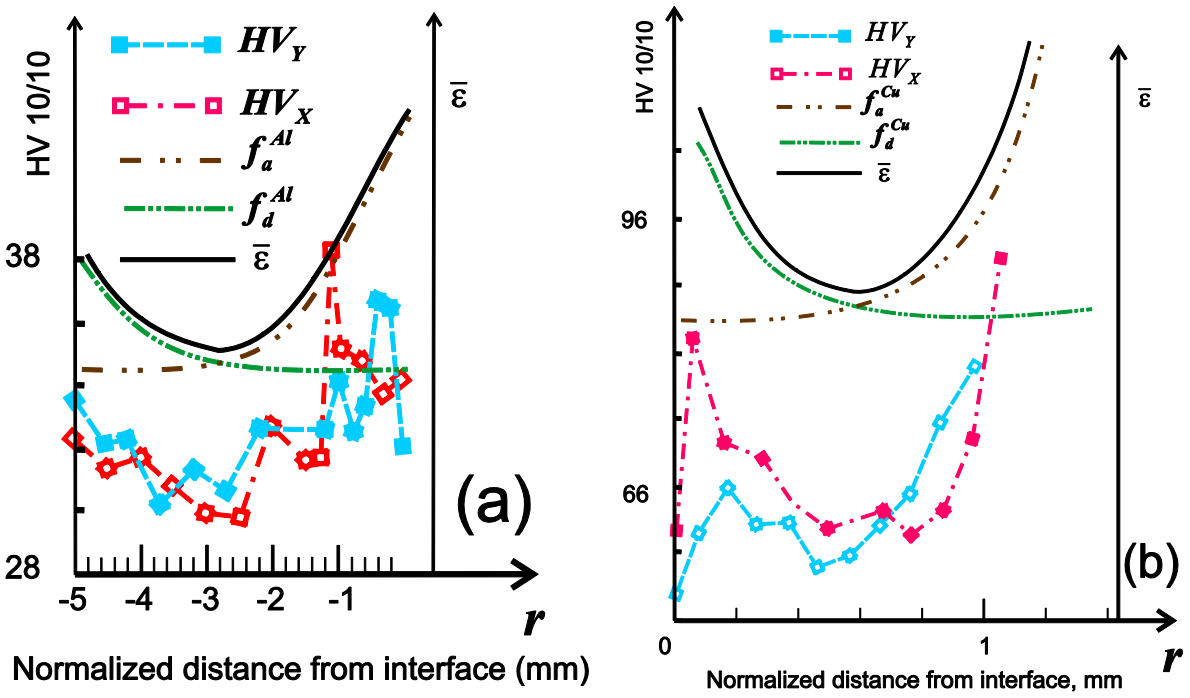

Fig. 4-4. Analytical results of AFSCE deformation using Eq. 9 and its comparison with the work hardening results (Fig.4-2), (a) for aluminum region (b) for copper region

Fig 4-4a and b are schematic illustrations of three dimensional nature of strain in the sample as indicated by expressions 2 to 8. The illustrations have been stretched in the radial direction to better demonstrate "cup shape" distribution implied by the expressions. . Based on the solution presented in [82], the effective strain at the interface ($\bar{\varepsilon}_a$ at $\mathrm{r} = \mathrm{r_a}$) can be estimated as follows:

$$\bar{\varepsilon}_a = \frac{r_a^2}{\sqrt{3} r_O^2} \tan\gamma \qquad (10)$$

where γ and r_O are the AFSCE's die helix angle and radius respectively. Predictions based on the work hardening model of Eq. 4-9 are overlaid with Fig. 4-2 and presented in Fig. 4-4a and b; these agree well with the experimental hardness distribution trends.

4.3 Focused iron beam dissection method to investigate the interfacial features

Two parent materials used in this experiment were a commercially-pure copper (Cu) annular and a commercially pure cast aluminum (Al) solid rod. Details of the process and constitutive behaviors of these materials can be found in chapter 3. To avoid dissection artifacts at the bonding interface, which could be introduced by standard mechanical grinding and polishing, a Focused Ion Beam (FIB) technique was utilized in this work to study interfacial features using an FEI Quanta 3D FEG FIB microscope. To minimize alteration of the interface and the formation of mechanical dislocations near the surface during the preparation, the FIB sample was cut from the middle section of the AFSCE extruded copper clad aluminum sample along the transverse section normal to the extrusion axis using a Buehler IsoMet low speed saw machine equipped with a diamond blade. The FIB milling location and the milled surface of the specimen are respectively shown in Fig. 4-5a and Fig. 4-5b.

Two approaches were chosen to reveal areas of interest. In the first approach, in order to prevent a collapse of the dissection, a thin layer of platinum was deposited across the dissection interface using FIB assisted chemical vapour deposition. The position of the dissection on the transverse section is shown in Fig. 4-5a and the platinum vapour deposition is shown in Fig. 4-5b. The second approach, without the platinum vapour deposition, was adopted to minimize the possible unwanted microstructural changes by the local heating to the sample. Initially a large beam current of 30 keV was used to quickly remove and mill the material across the interface. The high beam current milling produced a “curtaining effect” on the surface with debris in the milling area and uneven rate of milling in copper and aluminum regions (shown in Fig. 4-5b by arrow marks). To improve the surface finish of the FIB dissection, a subsequent fine layer was milled by 5keV low beam current sputtering using a slicing method. In order to identify the formation of inter metallic compounds (IMCs), oxide or carbide, Energy-dispersive X-ray spectroscopy (EDX) investigations along the interface were also carried out using 5keV exciting voltage at the FIB dissected region without Pt deposition.

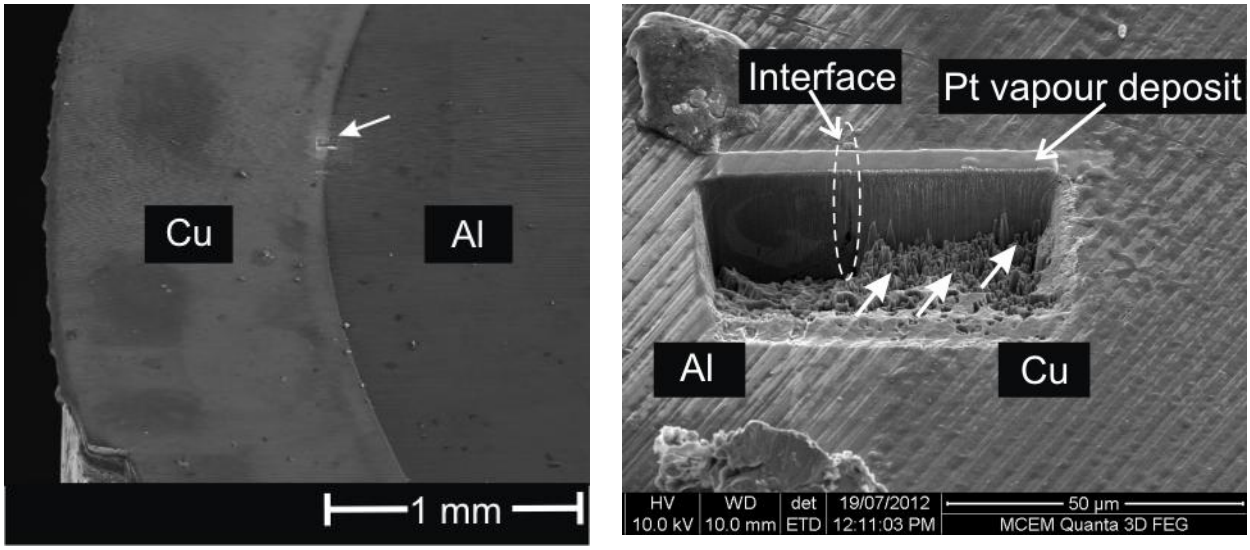

(a) **(b)**

Fig.4-5.(a) Focused ion beam dissection location at the interface (b) intermediate milling step prior to final surface finishing

FIB dissection with platinum vapour deposition and interface of base metals is shown in Fig. 4-6a. Fig. 4-6b and c show the FIB dissected surface of Fig. 4-6a with higher magnifications. Similarly, Fig. 4-6 d, e and f were produced for the interface of a FIB dissection without platinum (Pt) deposition. Relatively fine copper microstructural constituents (i.e. grains) are observed in the dotted boxed region in Fig. 4-6 a, b and c that are absent in Fig. 4-6 d, e and f. This is most likely due to rise in the local temperature during the Pt deposition. Platinum vapour deposit increases the local temperature that facilitates sub-substructure formation (localized annealing) near the surface when a small increase in temperature occurs.

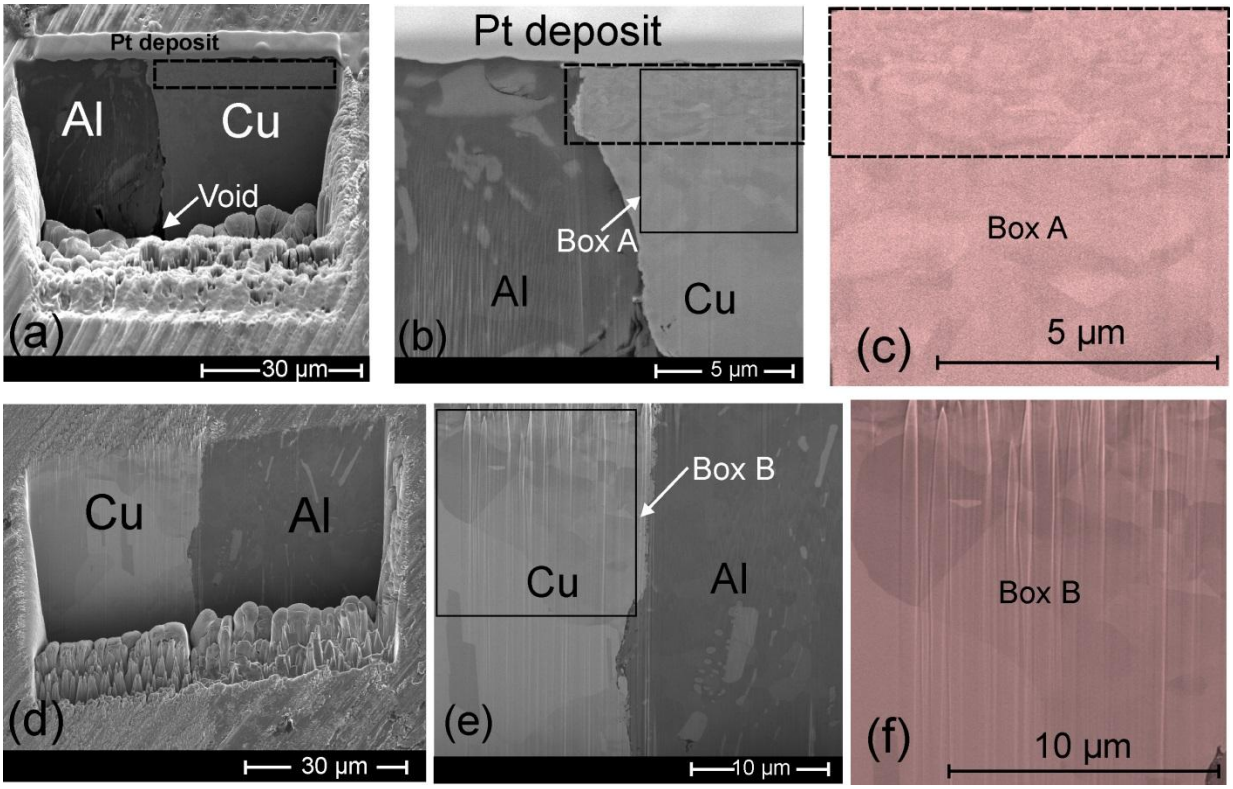

Fig. 4-6. (a) and (b) FIB dissection with Pt deposit, (c) higher magnification view of Box A (d) and (e) FIB dissection without Pt deposit (f) higher Magnification of Box B

4.3.1. Energy-dispersive X-ray spectroscopy (EDX) analysis to detect interfacial diffusion

Three EDX analyses were performed at points 1, 2 and 3 shown in Fig. 4-7 in the very close vicinity of the interface along FIB section shown in Fig. 4-6e. The EDX analyses were performed with 5keV exciting voltage to minimize the interaction volume of the EDX data. However the EDX results are not point values since they are typically estimated based on a measurement within a footprint volume. In addition to this, the standard EDX analysis has a minimum of 1% error because of non-flat topography of the sample, non-homogeneous distribution of elements and mathematical base database matching error. Three EDX results, corresponding to points 1 to 3, are respectively shown in Fig. 4-8a - c. Based on the EDX results, oxides or carbides at the interface between copper and aluminum are undetectable within the limits of EDX accuracy.

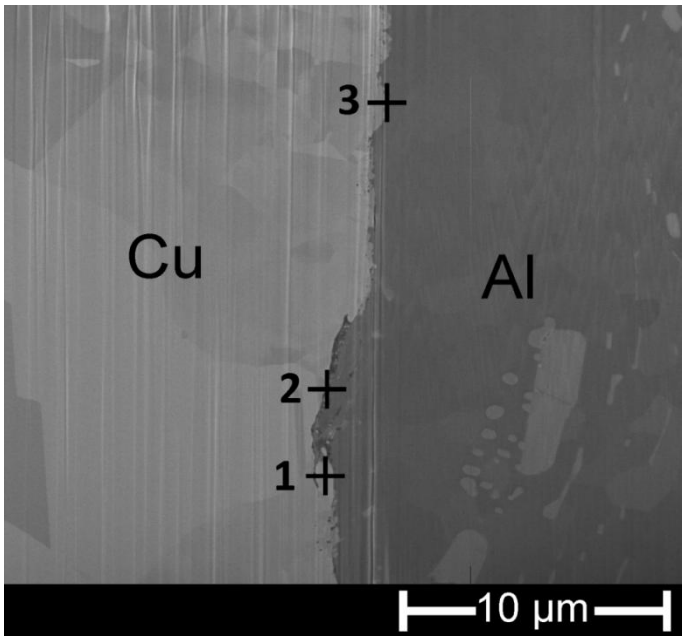

Fig. 4-7 SEM image with three EDX points shown in the FIB section without platinum deposition case

In the current literature, color contrast of the SEM image has been used to identify IMC layers [127, 128, 134]. But, the best achievable resolution of the FEI Quanta 3D FEG SEM is 7 µm with the standard installation and testing, in an ideal situation with a maximum resolution at 30kV condition. Therefore using the current SEM technique and the EDX analyses, intermetallic compounds were undetectable in the current work.

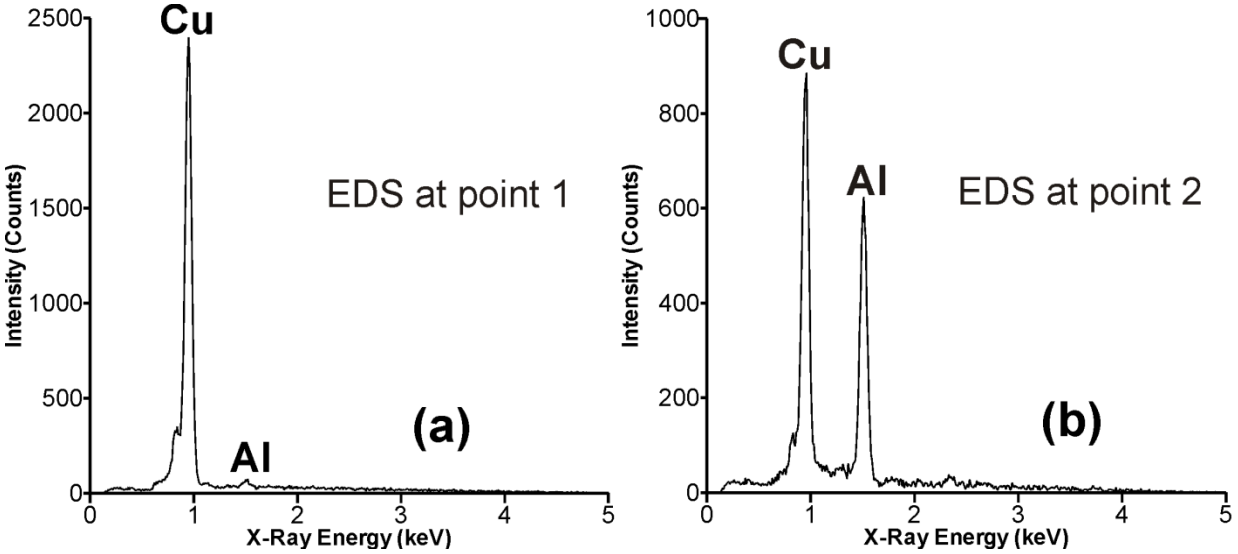

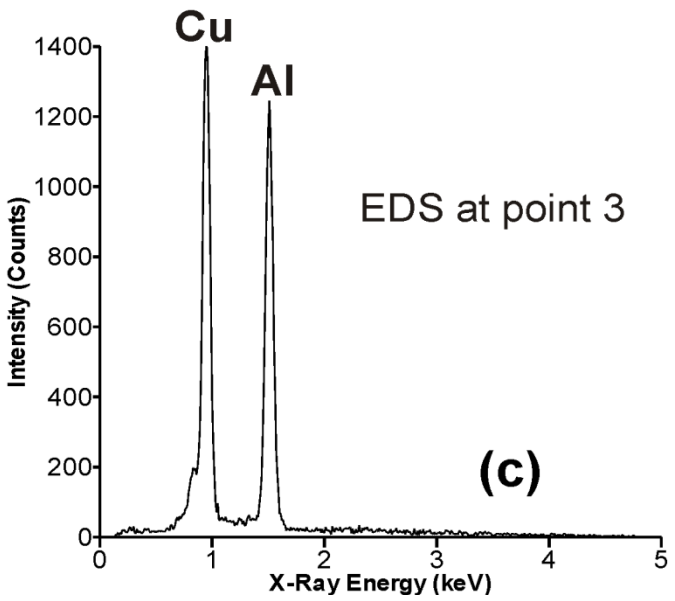

Fig 4-8 EDX analysis at the Cu/Al interface shown in Fig 4-7 (a) point 1 (b) point 2 (c) point 3

Both diffusion bonding and mechanical interlocking play important roles in a composite metal bond formation. Based on the SEM-EDX results shown in Fig. 4-6, 4-7 and 4-8, no detectable diffusion with the formation of intermetallic compounds were found at the interface. The FIB sections in Fig. 4-6b and 4-6e also show a near flawless and closely intact interface between copper and aluminum. Given the tubular and cylindrical geometry of the copper sleeve and aluminum core respectively, it is necessary to ensure that the change in cross section and its subsequent fitting of the components are not interpreted as a bond. This was confirmed by testing longitudinal cut sections of two fabricated composite specimens and the parts were not separated even after applying a 50 N shearing force tangent to their interfaces along the extrusion axis. In addition to this, observations at fractured interfaces confirmed traces of both metals in Fig.3-13. Therefore, it can be concluded that the bonding mechanism in this composite is most likely dominated by a mechanical interlocking. Based on this observation, the brittle fracture of the sample at the interface during the shear punch test will be discussed here.

4.3.2. Classification of the AFSCE composite based on bonding shear strength results and focused ion beam interfacial observations

For the mechanical interlocking shown in Fig. 4-6, bonding shear strength was calculated from “Dedicated Blanking Test” (DBT) results shown in Fig 3-9 and Fig 5-9. 3mm sample thickness results were avoided in this calculation because the results deviate from simple shear failure as discussed in Section 5.3.4. Based on the following equation 11, shear stress was calculated and shown in Table 4-1.

$$\tau = \frac{F}{\pi dt} \tag{11}$$

Table 4-1: Results of bonding shear strength of AFSCE samples and shear strength of pure Aluminum

Symbol in the equation	Variables	AFSCE sample	AFSCE sample	AFSCE sample	Pure Aluminum
t	Sample thickness (mm)	1	1.5	2	1
d	Failure punch diameter (mm)	10.2	10.2	10.2	10.2
F	Average force (N)	1300	2400	3300	1500
τ	Shear stress (MPa)	40.57	49.93	51.49	46

Based on the above calculation, the measured average shear stress of the AFSCE sample was ≈50.5 MPa. This measurement was slightly higher than the shear strength of the parent aluminum material (46 MPa). Assuming a 100% contact between the parent materials, the higher value suggests that the blanking (shearing) cracks produced by the DBT were distributed between Al and Cu with Al as the dominant crack arrester. Practically, in presence of the voids, as shown in Fig. 4-6a and 6b, the contact is not 100%. Therefore, the higher of that bonding strength value implies more significant role for Cu to arrest the blanking crack. Eliminating the voids can naturally improve the bonding strength. According to interlocking features shown in Fig. 4-6 and based on the classification presented in [6], the AFSCE product can be considered as a Mesocomposite metal.

4.4 X-Ray diffraction spectroscopy analysis to determine interfacial diffusion

A disk shape sample, similar to that prepared for the FIB investigation, was produced from the Al-Cu composite rod fabricated by the AFSCE. The sample was ground with 2500 grit emery paper before X-Ray diffraction (XRD) analyses. Polishing with diamond polish was avoided in the sample preparation as it may introduce carbon in the sample.

To verify formation of IMCs at the interface of the fabricated sample, XRD pattern was generated using Scientag Powder Diffractometer with a carbon monochromator. A Cu radiation with 1.54059 Å wavelength and a 1° divergence slit with a 2° receiving slit were used to obtain X-ray spectrums. Also, a scanning speed of 2°/ minute with a step size of 0.02° was chosen. The XRD results peaks were identified with X-ray spectrums database using Traces software platform.

One of the possible causes for the variation in hardness during the AFSCE process is micro- structural changes and IMCs formation at the interface. In addition to the EDX investigations, XRD analyses were also performed twice on the sample to check the formation of IMCs and the results are overlaid in Fig. 4-9.

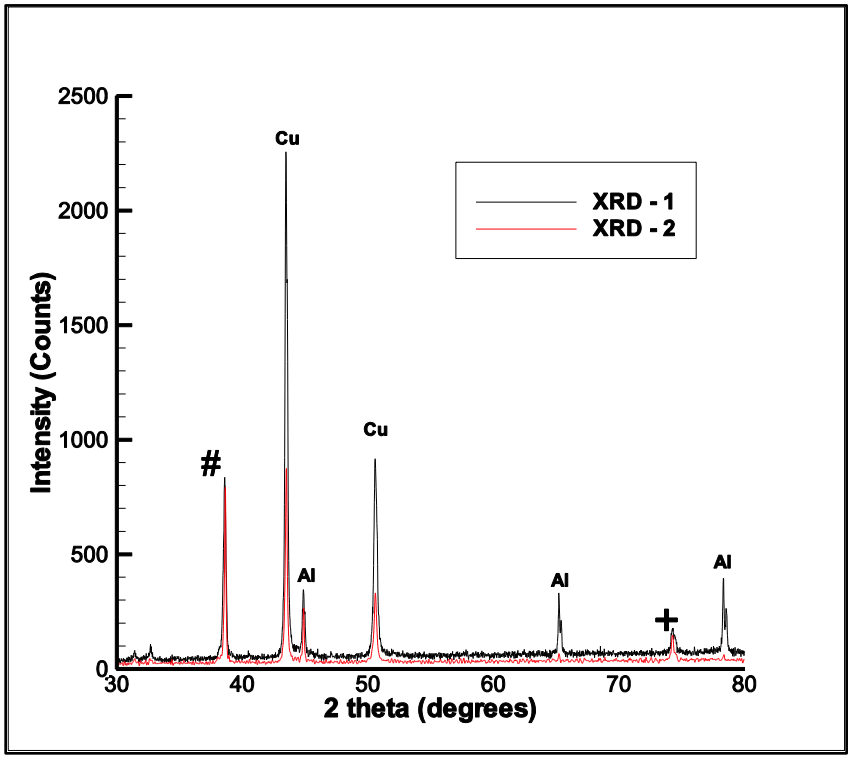

Fig. 4-9 X-Ray diffraction spectrum on composite sample (#: (74.28˚) - Al or / and Cu_9Al_4 or CuAl, +: (38.61˚) - Cu or / and Cu_9Al_4)

Kim et al. used a micro-XRD technique to investigate a copper wire bonding with aluminum pad [127]. In their study, they initially performed the XRD analysis on standard reference aluminum and copper, and eliminated those reference peaks from the final XRD results at the interface [127]. They found a number of peaks, including those corresponding to 2 theta (2θ) angles of 38.61˚ and 74.28˚ [127]. This study also contains two peaks similar to those reported by Kim et al. [127]; the two peaks in the Fig. 4-9 are

marked by # and + signs respectively. The first peak ('#') corresponds to 2θ angle of 38.61 ◦which may represent Al, or / and Cu_9Al_4 or CuAl. The second peak ('+') corresponds to 2θ angle of 74.28 ◦, may represent Cu or / and Cu_9Al_4. The peaks marked by # and + in the XRD spectrum in Fig. 4-9 are not conclusive peaks of Cu/Al IMCs. Also considering the very thin thickness of the interface between copper and aluminum with a layer thickness of ~0.5µm as shown in Fig 3-12a and poor resolution of the XRD for detecting IMCs, one cannot make conclusive remarks only based on the XRD results. These XRD examinations revealed two possibilities which were important to establish, intermetallic layer has not been formed during the process and the layer thickness was insufficient for detection by XRD.

4.5 Ultra-fine grain formation and investigation of crystal orientation changes using Electron Backscatter Diffraction (EBSD) analysis

Electron Backscatter Diffraction (EBSD) sample was produced from the AFSCE rod in a similar fashion with the FIB and XRD samples. The EBSD samples were carefully polished using 2500 grit emery paper followed by local electro polishing of a zone within the copper by masking the rest of the transverse section. The EBSD studies at three "sampling points" were conducted. The sampling points were chosen as point 1, 2 and 3 respectively located near Cu–Al interface, in the middle of the copper annular and near the Cu outer edge. The EBSD maps were obtained using the FEI Quanta 3D FEG SEM, and the data were analysed using TSL OIM Analysis software and compared with the reference EBSD spectrum of the copper as received. Crystal orientation maps and texture variations were investigated using the EBSD results. EBSD result of unprocessed copper as received was also obtained as a reference is shown in Fig. 4-10.

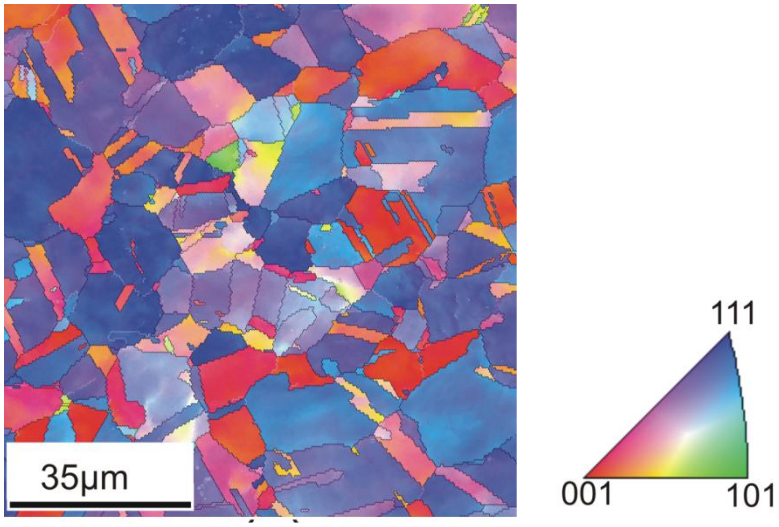

Fig. 4-10. EBSD crystal orientation map of as received copper before AFSCE process.

EBSD analyses were performed to investigate the micro-structural changes and the mechanism responsible for hardness distribution in Fig. 4-2 in the composite structure. Aluminum side EBSD work is not reported in this thesis as it was found that the pure cast aluminum material had large amount of indexing errors and poor pattern quality when trying to perform EBSD which makes the results of no practical importance and difficult to interpret. A ~5% difference in hardness measurement along *x* and *y* direction (shown in Fig. 4-2), suggests that the anisotropy due to the effect of valleys and grooves were insignificant and therefore EBSD work was only performed along one direction. Fig. 4-11a shows three "sampling points" at 1, 2 and 3 respectively correspond to near the interface, in the middle and near the outer edge of the copper.

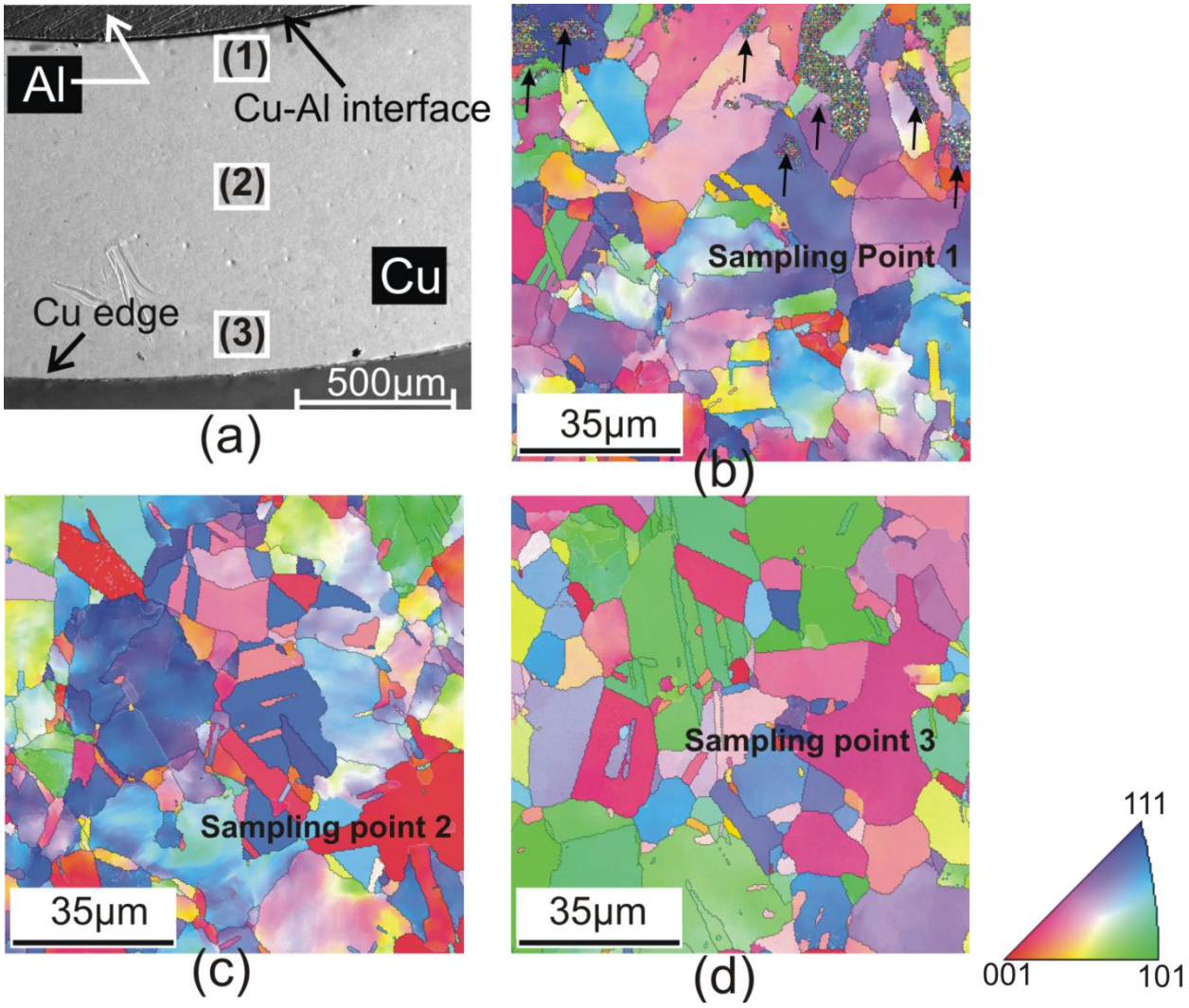

Fig. 4-11. Crystal orientation maps of copper deformed through AFSCE process (a) sampling points 1, 2 and 3 of the EBSD maps within the AFSCE specimen, (b) EBSD orientation map corresponding to point 1 near Cu–Al interface, (c) EBSD orientation map corresponding to point 2 in the middle of Cu region, (d) EBSD orientation map corresponding to point 3 close to the outer edge of the Cu

Crystal orientation maps of unprocessed copper and the copper regions in AFSCE composite sample and are respectively shown in Figs. 4-10 and Fig. 4-11. The crystal orientation at point 2 (Fig. 4-11c), shows similar distribution of as received copper crystal orientation (Fig. 4-10). Point 3 (Fig. 4-11 d), shows crystal closed pack direction <1 0 1> is dominant. Point 1 (Fig. 4-11b) shows similar crystal orientation distribution with a highly refined structure including UFG structure at locations close to the Cu–Al interface. The UFG formation at the interface is in good agreement with other studies of drawing process fabricated copper clad aluminum wires [122] and copper clad steel wires [135]. A formation of UFGs at the interface is mostly preferred than a formation of IMCs at the interface because of their brittle nature that could create a large stress concentration/stress discontinuity at the interface.

4.6 Micro hardness correlations with microstructural results and texture evolution of AFSCE sample

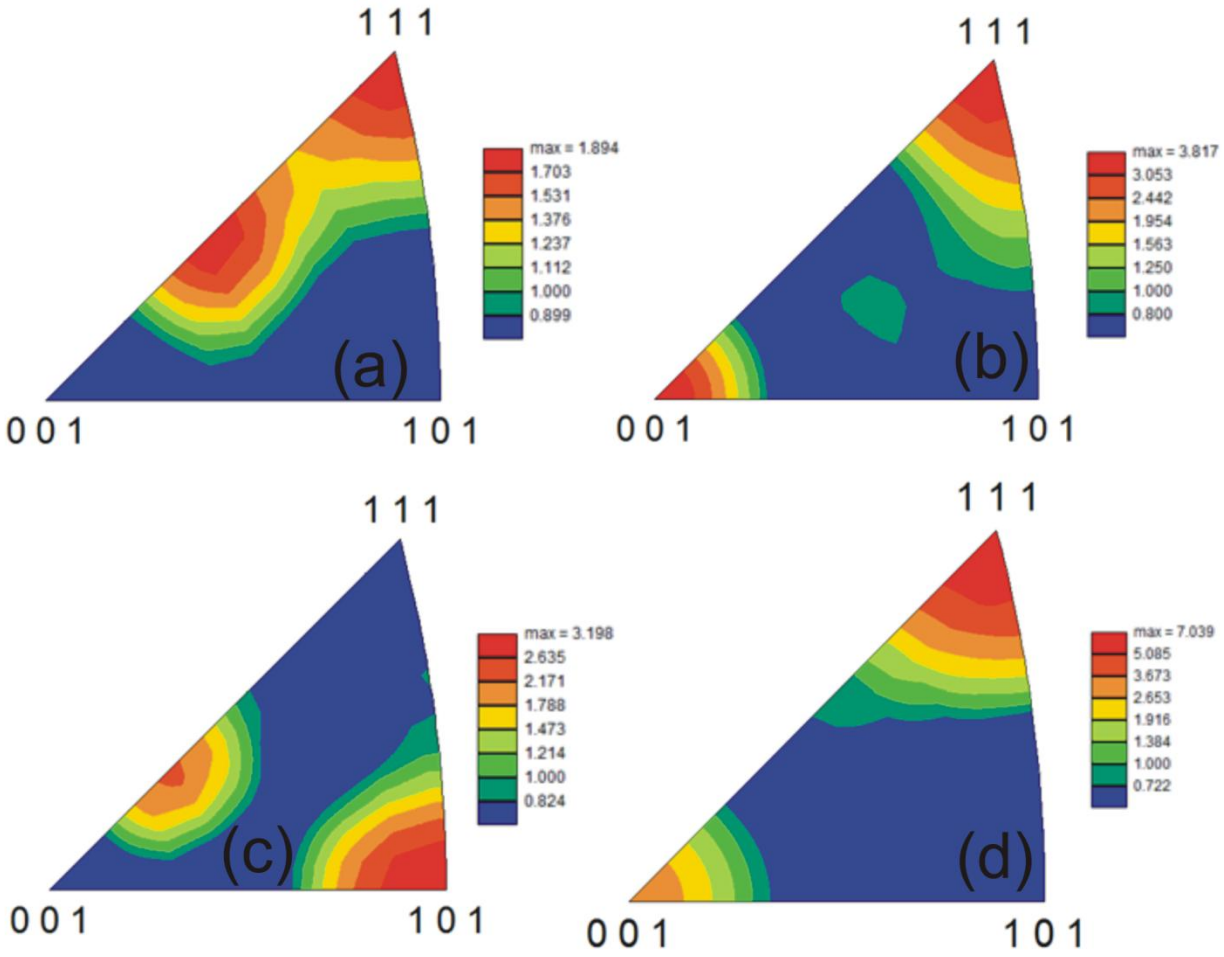

Fig. 4-12. Inverse pole figure (IPF) of copper deformed through AFSCE process (a) IPF corresponding to point 1 near Cu–Al interface, (b) IPF corresponding to point 2 in the middle of Cu region, (c) IPF corresponding to point 3 close to the outer edge of the Cu, and (d) IPF map of as received unprocessed copper.

Inverse pole figure (IPF) maps of as received copper and copper sampling points of AFSCE processed sample (Fig 4-11a) are obtained using TSL OIM Analysis software and shown in Fig 4-12. Texture at point 2 (Fig. 4-12b) is similar to the texture of the unprocessed copper, shown in Fig. 4-12d. This is an indication of less deformation in the middle region of the copper annular. In comparison with the unprocessed copper texture (Fig. 4-12d), the AFSCE processed composite textures were significantly changed particularly near the Cu–Al interface (Fig. 4-12a) and near the outer edge of the copper (Fig. 4-12c).

Crystal orientation map of point 1 (Fig. 4-11b) and texture at point 1 (Fig. 4-12a) show noticeable changes from results of as received copper. From these observations, it can be explained that the hardness change near the interface region occurred in the material by formation of UFGs and grain rotation. Formation of submicron grains and UFGs is a mechanism which, material accumulates the large strains. Grain rotation allows the material to accumulate the applied energy by aligning into preferred orientation and texture changes (texture related high energy planes). Comparison of misorientation angles with their number fraction is used here to further understand the deformation history at each sampling points.

The misorientation angles shown in Fig. 4-13 were plotted with normalized number fraction for comparison across the EBSD sampling points. Results in Fig. 4-13 shows that the microstructure in the Cu as received included some low angle grain boundaries, LAGBs; less than 15˚ in this study. The proportion of high angle grain boundaries, HAGBs, (> 15˚) was at its maximum at point 3 compared with other two sampling points. Considerable increase in HAGBs near point 3 is an indication of significant deformation where the [1 0 1] texture became dominant (Figs. 4-12c and Fig4-13). The minimum value for HAGBs corresponded to point 2 with slight decline in HAGBs compared with unprocessed copper. These are in agreement with the trend of hardness distribution shown in Fig. 4-2.

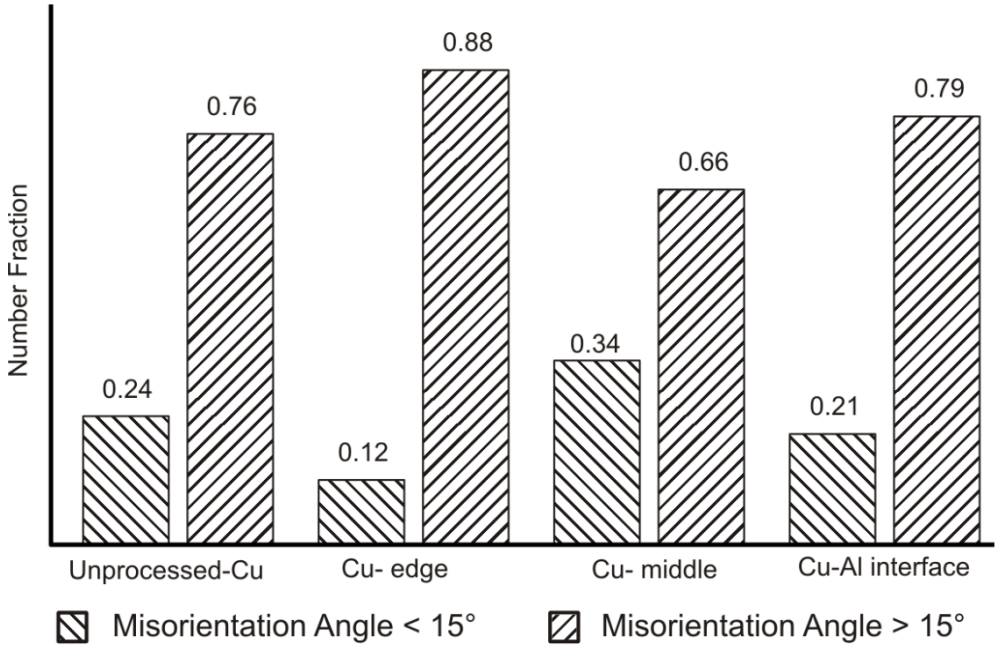

Fig. 4-13. Misorientation angles in number fraction for the unprocessed copper and three chosen locations in Fig. 4-11a, Cu-edge (sampling point 3), Cu-middle (sampling point 2) and near Cu–Al (sampling point 1).

The average grain size distribution is shown in Fig 4-14. Table 4-2 shows the number of grains in the distribution at those EBSD sampling points in Fig. 4-11a and in the unprocessed copper (Fig 4-10). In order to easily interpret the results, the cut off points for the grain size were chosen for grains below 1 µm (as submicron grains) and grain above 20 µm which are upper and lower limit grain sizes in the unprocessed copper. In comparison with the unprocessed copper, 17% submicron grains produced at the copper located close to the outer edge (point 3 in Fig. 4-11a) with a 2% of grains larger than 20 µm. A similar trend for grain size distribution is also observed for copper located in the middle (point 2 in Fig. 4-11a). However, at point 1 in Fig. 11 a, 61% of grains were in the submicron size range and 1% of the grains were larger than 20 µm.

Table 4-2: Number of grains used to calculate grain size distributions for the three sampling points in Fig. 4- 11a and copper as received

	Copper as received	**Point 3**	**Point 2**	**Point1**
Grain diameter < 1 µm	0	42	62	380
1 µm < Grain diameter < 20µm	342	205	226	244
Grain diameter > 20µm	0	6	7	4
Total Number of Grains	342	253	295	628

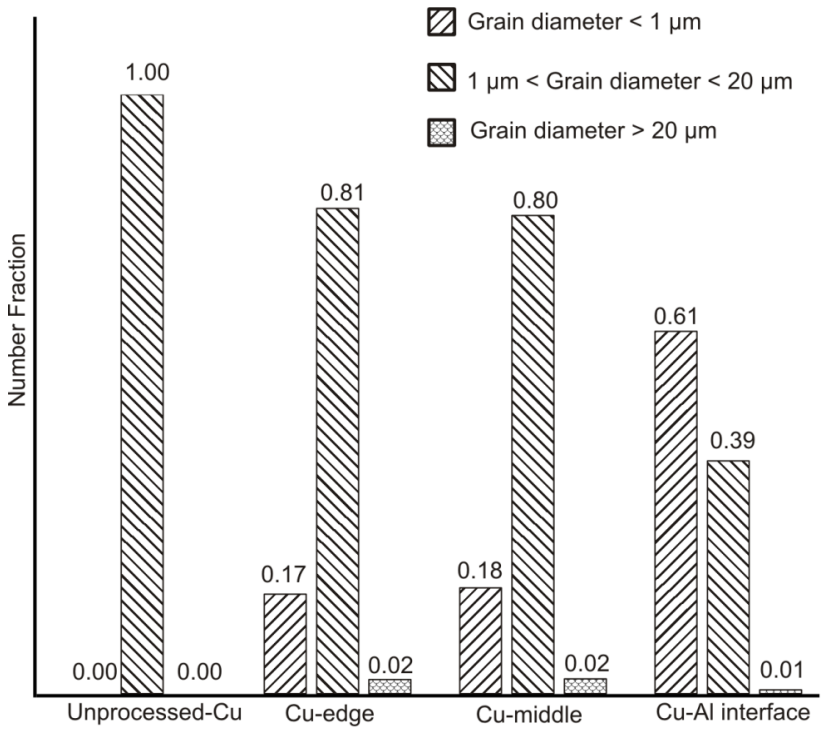

Fig. 4-14. Grain size distribution in number fraction for the unprocessed copper and three sampling points in Fig. 4-11a, Cu-edge (sampling point 3), Cu-middle (sampling point 2) and near Cu–Al (sampling point 1).

Presence of large grains with average grain size of greater than 20 μm after the AFSCE process could be interpreted as a grain growth due to an annealing effect. The applied heat using a heating jacket located around the die improved annealing at point 3 and point 2 compared with points 1. For the case of AFSCE, analytical estimation of strain cannot be used confidently because of simultaneous events of work hardening and annealing. However the distribution of the grain structure presented in this chapter is a solid evidence of grain refinement in the composite sample.

Concurrent annealing, grain refinement and work hardening in the material are governing the strain accumulation in the AFSCE processed composite material in this study. The presented results here are useful for further investigation and optimization of the AFSCE process to improve the bond leading to a stronger composite metal product. In terms of fundamental investigation, the mechanism responsible for grain refinement in the copper using the aluminum as a soft material provides opportunity for further investigation.

4.7 Conclusions

In this chapter, bonded interface features and strength changes of a copper clad aluminum rod fabricated by the AFSCE process has been investigated. The bond at the interface was found most likely created by a mechanical interlocking, using SEM / FIB, EDX and XRD investigations. The near flawless bond with bonding shear strength of approximately 50.5 MPa, demonstrated the potential of the process to fabricate copper clad aluminum composite rods with good bond strength. The complicated strain accumulation in composite samples was observed in hardness distribution which was explained using an analytical model. Hardness values at the interface and the outer periphery regions of the copper sleeve found to be significantly higher than those in its middle region. This minimum hardness value in the middle is approximately equal to that of unprocessed copper which is 61 HV10/10. A similar cup shape trend was also found in the extruded aluminum core. This cup shape behavior emphasizes a multidimensional deformation during the AFSCE process. A formation of ultra-fine grains (UFGs) in the copper sleeve near the interface with approximately 61% of the grains below 1 μm was also confirmed in this process using EBSD results. The grain refinement significantly contributes to the increase in copper hardness in the interface region. In contrast, deformation which led to the change in crystal orientation was the dominant mechanism for the hardness increase near the outer periphery of the composite structure. The EBSD analysis revealed that the AFSCE process has the potential to form UFGs as well as change crystal orientation in various locations of its sample. Therefore these investigations suggest that the AFSCE process can be used to produce architectural hybrid materials with specific localized property changes for modern engineering applications.

Chapter 5:
Validity requirements of a composite bond shear test using numerical and experimental analyses

Chapter 5: Validity requirements of a composite bond shear test using numerical and experimental analyses

5.1 Introduction

Hybrid materials have structural and multi-functional characteristics such as thermo, electrical, magnetic and optical properties. They can supply the growing material demand for many industrial applications which require a single material with a combination of multiple properties [1, 2]. Hybrid materials are especially attractive for special purpose applications because of their unique structural properties, when a combination of weight savings and high strength are required.

Structural properties of materials are key parameters for almost any engineering application. They are also important from a handling, machining, joining and fabricating point of view. Recently, architectured metal-based composites have been produced using different processing techniques (e.g. [4] and [105]). The structural performance of the composites depends on the mechanical properties of the base materials, the stress concentration at their interface and the bonding strength of the ingredients. Yet, measuring the interface bonding strength between the parent materials could be very complex. As a result, characterization of composites structural properties is more challenging than orthodox materials. For the case of metal-based composites with simple geometrical configuration, the interface bonding strength can be measured.

Blanking is a well known process used in sheet metal manufacturing to produce small samples through shear failure [12, 136, 137]. It has been utilized as a “small specimen test technique” [138] to determine the shear strength [139-141] and interfacial fracture toughness [142, 143] of materials when there is insufficient material for testing or material saving is considered. Assuming linear correlation between shear strength and tensile strength, many researchers used the test to interpret yield property of materials [139-141, 144-147]. The shear punch test has also been used to study the strength variations and strength gradient in Al/Ni – SiC composite samples [148], in plane stress local torsion samples [149], and in friction stir processed samples [150]. However, these simple blanking tests were performed with the assumption of either homogeneous material or homogeneous shear strain distribution in the failure

zone. Evaluation and interpretation of the shear strength at the interface of a composite material requires a more sophisticated approach due to the presence of two materials at the interface. Bonding strength of aluminum clad steel sheet fabricated by cold rolling and various subsequent heat treatment processes were evaluated using the Erichsen cupping test while it was used to assess the metal formability [123]. Bonding strength of bi-layered copper alloy and bi-layered aluminum alloy strips, fabricated using roll bonding, were tested using a peeling test according to ASTM: D903-93 [151, 152]. However, the aforementioned standard tests are not suitable for a solid rod fabricated in a core-clad fashion.

A shear strength test designed based on ASTM: F1044 was used to determine a bond shear strength of Hybrid Al/Cu clad rod fabricated using equal channel angular extrusion [109]. But, the standard is mainly applicable for a test between two flat surfaces when an adhesive or cohesive bond between two calcium phosphate coated plates or two metallic coated plates are involved [153]. The standard has also been extended for a bond created by any thermo mechanical joining process such as sintering or diffusion bonding [153]. However, the standard methods used in previous works cannot obtain a reliable measurement of the shear strength for the extruded composite Al/Cu clad rods because of their cylindrical geometry.

The interface bonding strength for a fabricated Al/Cu clad composite using axi symmetric forward spiral composite extrusion (AFSCE) has been investigated recently using a dedicated blanking test (DBT) IN chapter 3. Owing to the specific requirements of the “non-standard test”, the test parameters have to be carefully analyzed to ensure a reliable bonding strength measurement. The dimensions of the test rig, most notably its die clearance, are crucial in ensuring that the failure occurs at the bond interface between the two materials. Also, the effect of stress concentration and stress discontinuity at the interface because of the presence of two materials requires special care when interpreting the bonding strength; having two different materials near the interface and a sudden property change in the narrow interface region, and unavoidable stress discontinuity [124, 125] complicates the analysis. Therefore, in order to identify the required test conditions for an accurate bonding strength measurement, a finite element model of the test rig was developed, using Abaqus finite element analysis package, to assess the test and to investigate the test rig parameters. A new FE modelling was required because welding and joining simulation reviews over the past three decades do no not contain any FE study of bond shear failure of core clad composites [154-156]. The critical parameters in the numerical model were studied to develop a larger and more uniform plastic strain distribution at the interface and to minimize

stress concentration in other regions. The FE analysis findings gave the required parameters to ensure that the failure at the interface also includes a blank holder, which facilitates the sample positioning and prevents bending of the sample during the dedicated blanking experiments. Having the required rig built, it was utilized to measure the composite bonding strength for an AFSCE extruded Al/Cu clad composite sample.

5.2 Interfacial characteristics and the requirement for a numerical modelling

Fig.3-10a shows an optical microscopy of the interface of the AFSCE fabricated copper/aluminum composite sample. It is almost a gap-free interface which shows details of the nearly perfect contact between the two metals. Fig 3-10a shows only a small portion of the interface due to the relatively large magnification. Further investigation was carried out using Scanning Electron Microscope (SEM) technique, a uniform dark layer of approximately 1mm in thickness has been observed and distributed evenly at the Al-Cu interface as shown in Fig. 3-10b.

For further clarification of the interface layer and to avoid artifacts at the bonding interface, which could be introduced by standard mechanical grinding and polishing, a Focused Ion Beam (FIB) technique was utilized in this work to study interfacial features using an FEI Quanta 3D FEG FIB technique. Fig. 4-6d shows a FIB dissection of the interface and Fig. 4-6e shows SEM image of the FIB dissected interface at higher magnification show near flawless bond at the interface. Color contrast in SEM images has been used to identify IMC layers in the current literature [127, 128, 134]. But, the best achievable resolution of the FEI Quanta 3D FEG SEM is 7 μm with the standard installation and testing, in an ideal situation with a maximum resolution at 30kV condition. In addition to the FIB – SEM technique, X-Ray Diffraction and Energy Dispersive X-ray Spectroscopy were also used to investigate intermetallic compound at the interface. However using those aforementioned techniques there were no intermetallic compounds detected. Based on these observations it was concluded in chapter 4, that the bonding mechanism in this composite is most likely dominated by a mechanical interlocking.

Therefore it is important to investigate the strength of this composite joint to evaluate the material property. Therefore a dedicated blanking test was proposed to determine the shear strength at the interface of the composite structure. This test is designed to ensure the failure at the interface of the composite sample. To design this test and establish the critical test parameters such as sample thickness,

clearance and fillet radii, finite element modelling with hand in hand experimental investigations were performed as described below.

5.3 Methodology

5. 3.1 Blanking test to determine the shear strength at the interface of the core-clad composite structure

The dedicated blanking test is proposed to determine the bonding strength of the hybrid material and was conducted by using a specially designed rig to experimentally investigate the bonding strength between these two materials. A schematic of the DBT is shown in Fig. 5-1a. The longitudinal section view of an AFSCE sample is shown in Fig. 5-1b in which a DBT sample with a thickness "t" is also highlighted. A numerical design of the blanking rig will be explained in the following sections. The aim of the design is to cause the failure at the interface in an Al/Cu clad composite sample of thickness "t" with a uniform shear strain. A large clearance for example can develop multi axial stress components along the interface and consequently the measured blanking load deviates from the shear bonding strength at the interface.

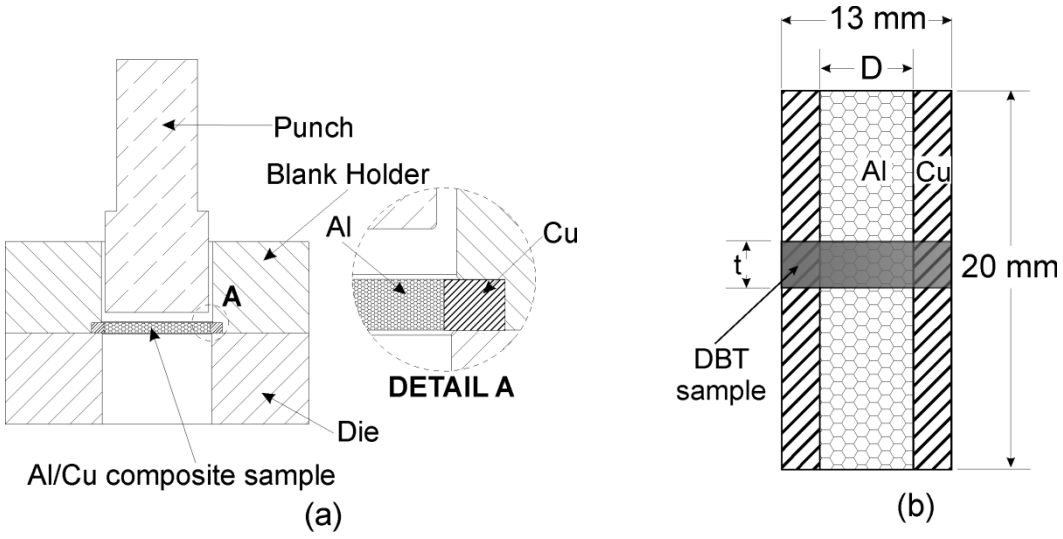

Fig. 5-1. (a) The dedicated blanking test rig to measure bond shear strength (b) AFSCE composite sample longitudinal section view with a highlighted DBT sample.

Optimizing the design parameters including clearance, sample thickness and tool fillet diameter is essential to ensure a development of pure and uniform shear at the bonding zone during the DBT. The optimum parameters were identified using finite element models of DBT. The model and its detailed results will be discussed in the following sections.

5.3.2 Stress strain behaviour of materials used in the numerical modelling obtained by using hot torsion test

AFSCE processing involves heating of the sample. The blanking test was performed on a sample at room temperature (20℃) for a hybrid material fabricated using the AFSCE process at 300°C. Therefore characterization of the base metals to be used in the numerical model was carried out using a hot torsion test rig shown in Fig. 5- 2a and Fig. 5- 2b. The AFSCE heating cycle was applied to the torsion test samples before running the torsion test. The heating cycle is shown in Fig. 5- 3a, where ε_F represents the fracture stain of a material at the end of the test. The testing sample was heated with a rate of 5˚C/min and cooled to room temperature at an average rate which was calculated and found to be 7˚C/min. A flow data obtained by the tension test cannot adequately represent the behavior of material subjected to the DBT as the latter involves large plastic strains with a shearing nature. However, the similarity of the deformation mechanisms in the hot torsion test and the DBT allowed the copper and aluminum stress strain behaviors to be derived from the torsion test and included in the DBT finite element model.

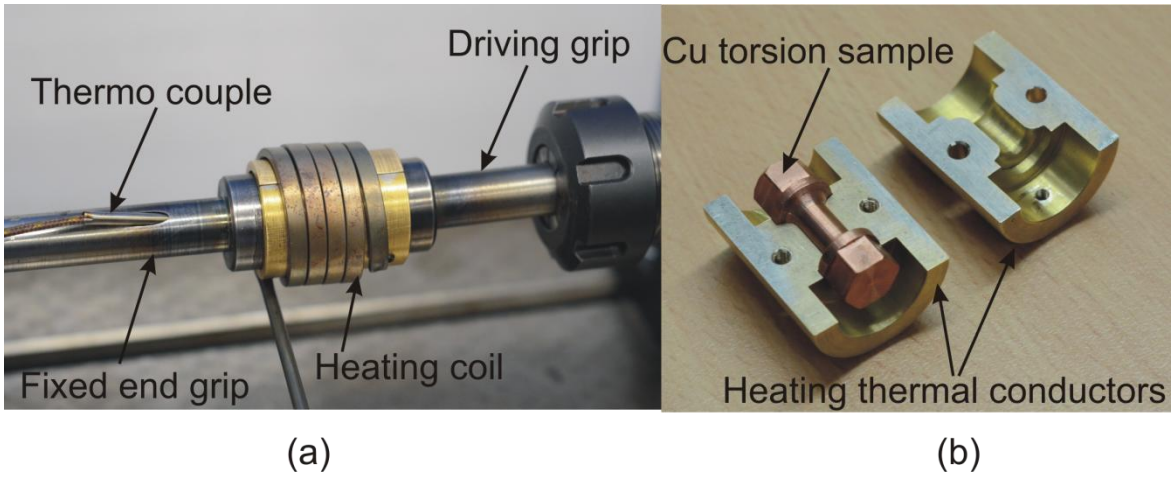

Fig. 5- 2. Hot torsion test setup used to characterize the flow behavior of the parent materials (a) hot torsion test assembly setup, and (b) heating casing setup of the cupper material shown here as an example.

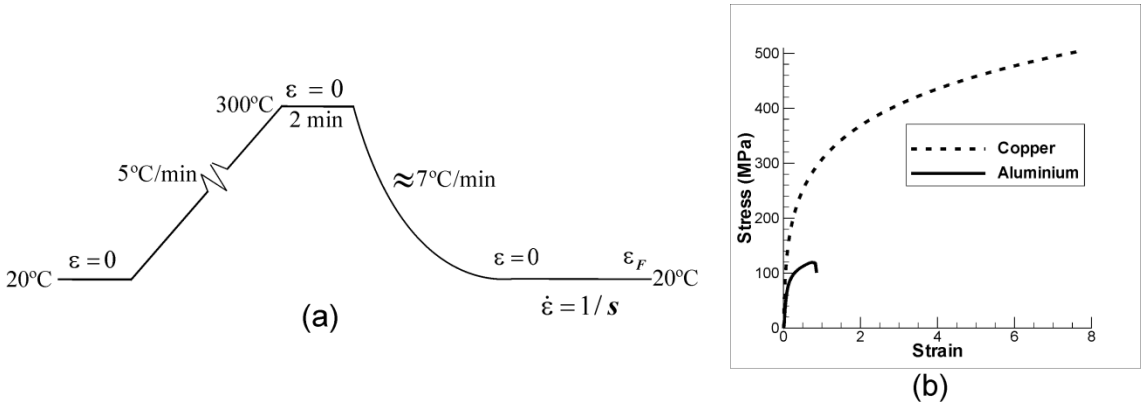

Fig. 5- 3.Hot torsion heating cycle and flow behavior (a) Heating cycle of torsion test similar to that of the AFSCE process, and (b) Flow behaviors of the materials at room temperature, initially were heat treated according to the heating cycle.

The finite element models used in this work are based on J2 plasticity formulation. The material model used in this study was established using a data modelling approach [157, 158]. Also due to the monotonic nature of the loading, a simple isotropic hardening behavior was considered in the simulations. The materials model was specified using stress against plastic strain in Abaqus explicit; this data was obtained using a hot torsion test rig. A technique presented in [157, 158] was used to convert the measured data to the flow stress data. The flow curves representing these flow behaviors were also modelled with the following analytical solutions for aluminum and copper respectively:

Aluminum $\sigma = 100.5e^{0.2097\epsilon} - 107.1e^{(-10.96\varepsilon)}$ (Eq. 5-1)

Copper $\sigma = 359.1e^{0.0463\epsilon} - 250e^{(-1.316\varepsilon)}$ (Eq. 5-2)

Where σ and ε are stress and strain of the materials.

5.3.3 The finite element modelling

An assembly of the DBT test rig, including the composite sample, was modelled using finite element as shown in Fig. 5- 4a including three major components; the punch, die and blank holder. An axi-symmetric model was considered to perform the numerical modelling using Abaqus/explicit algorithm. Fig. 5- 4b shows a longitudinally sliced composite metal sample at the onset of blanking. The numerical model simulates the blanking process to investigate the parameters such as sample thickness, clearance between punch and die and fillet diameter of the tools.

The material flow behaviours of the copper and aluminum presented in Fig. 5- 3b were utilised in the simulations. Two dimensional, axi-symmetric, bi-linear solid elements (CAX4R) with 4 nodes, reduced

integration and hourglass control were used to model the bimetallic material. The CAX4R elements have 2 degree of freedom per node. Punch, die and holder were meshed with rigid elements. A sufficiently fine mesh was chosen at the interface zone to capture the high gradient of the stress between the two materials.

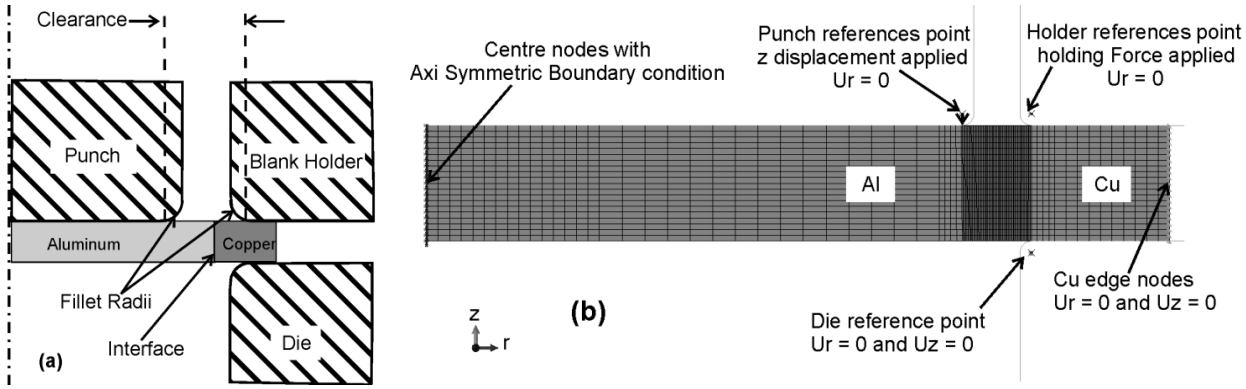

Fig. 5-4 Numerical model used to study the DBT design (a) Schematic diagram of blanking numerical model (b) meshed numerical model with boundary condition

The nature of blanking for a composite sample has to be clearly understood before the DBT raw data can be interpreted meaningfully. Given a correct design of rig, the measured shearing strength can be interpreted as the shearing strength of the bonding interface. The purpose of DBT is to break the bonded sample along its interface to evaluate the bonding strength via a pure shear action. Experimental works were carried out using the rig configuration parameters which ensured failure at the interface. These results were used to validate the finite element model.

Without using the required rig configuration, the small thickness of the bonding zone makes it challenging to achieve repeatable failure at the interface and to measure mechanical properties of the interface layer, which are directly related to the bonding strength of the composite. Therefore an Abaqus Finite Element (FE) model with macro features was utilized to design the DBT and to identify a suitable sample thickness, punch fillet diameter and the die clearance for successful failure of the specimen through shear stress at the interface.

5.4. Sensitivity analysis of the design parameters of the dedicated blanking test using finite element analysis.

5.4.1 Effect of the clearance between the punch and die on the equivalent plastic strain

Initially, a finite element model with large clearance between a 2 mm punch diameter and the die revealed a bending effect in the aluminum. This bending is not desired in a shear blanking test. In order to avoid the stress concentration of composite material and visualize the pure bending effect, the equivalent plastic strain (PEEQ) result for the aluminum is shown in Fig. 5-5. The simulation for the punch stroke of 0.5mm step confirmed bending near the punch region when the clearance between punch and the die was large.

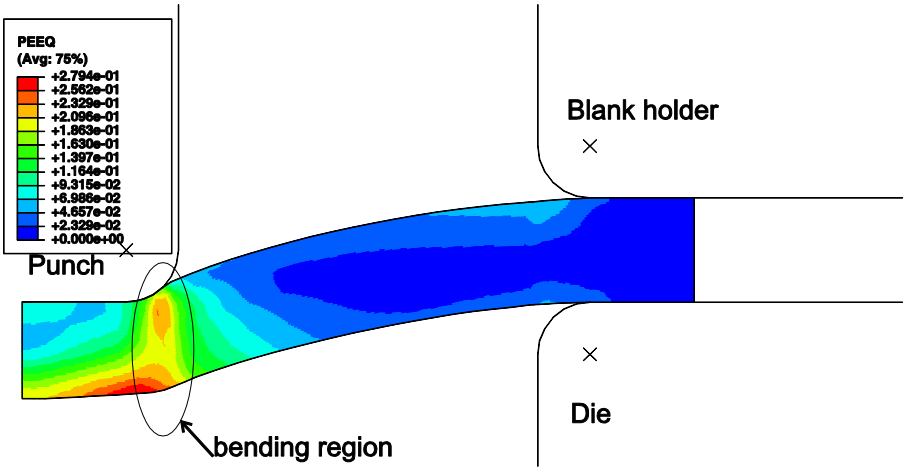

Fig. 5-5. Blanking model with 2mm punch diameter for a single material with large clearance shows bending of the tested material

Therefore the main aim of the clearance study was to determine the appropriate clearance which can be used to avoid the bending effect and create large stress at the interface, which can cause the interfacial shear failure to determine the bonding strength. In order to identify the appropriate clearance between the punch and die, various clearances between 0.2mm - 1mm were studied for a 1mm thickness sample with tools fillet diameter of 0.1mm. Equivalent plastic strain distribution results for three models with various clearances of 0.4mm, 0.6mm and 0.8mm are respectively shown in Fig 6a, 6b and 6c.

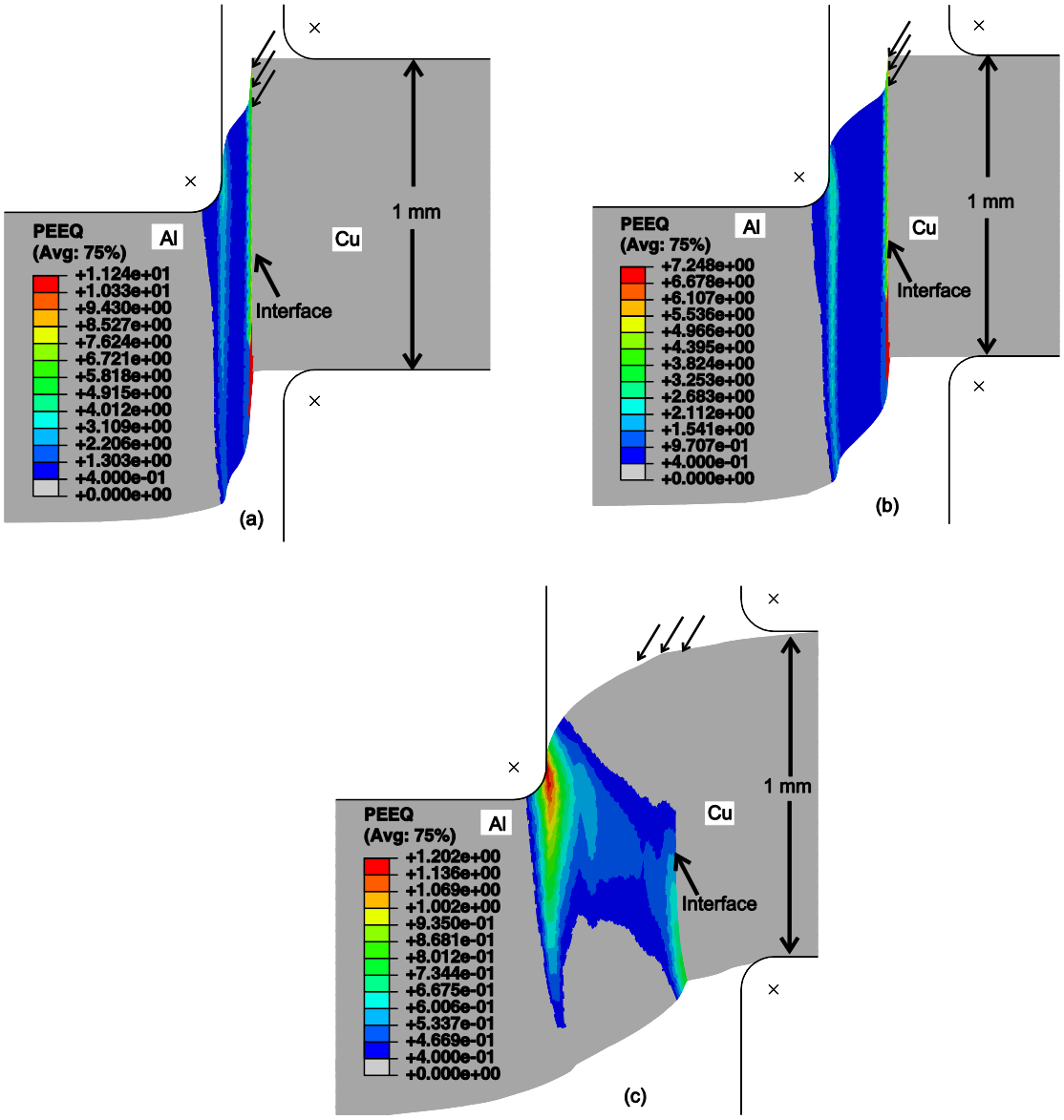

Fig. 5-6. Simulation results for Al/Cu composite sample clearance (a) 0.4 mm (b) 0.6 mm (c) 0.8 mm

Numerical models for a clearance equal to and larger than 0.8mm developed a large localised stress concentration near the punch region which deviated far from the interface region as shown in Fig. 5-6c. Numerical models with clearance of 0.6mm and 0.4 mm have developed significant plastic strain at the interface region ((Fig. 5-6a and Fig. 5-6b). Also, the clearance of 0.4mm and 0.6mm (Fig. 5-6a and Fig. 5-6b) did not show any significant variation in the strain distribution at the interface. In a comparison of both models (Fig. 5-6a and Fig. 5-6b) for punch movement of 0.5mm, the low clearance (0.4 mm) model developed a higher shear strain at the interface. However, the 0.4mm clearance model (Fig. 5-6a) also developed relatively higher strain near the punch region compared to that of the 0.6 mm clearance

model (Fig. 5-6b).In addition to this 0.4mm clearance model (Fig. 5-6a) developed the strain with large variation at the interface while 0.6mm clearance model (Fig. 5-6b) develops small variation of strain at the interface. Therefore, the 0.6mm clearance was the required configuration to predict the shear failure at the interface, which creates large stress at the interface with small stress in the other regions.

5.4.2 Effect of the composite sample thickness on the equivalent plastic strain

The numerical model as shown in Fig. 5-4b is used to find the suitable thickness of the composite sample for the DBT. In order to identify the appropriate sample thickness 3mm, 2mm and 1mm samples were considered for numerical modelling. These three models were studied with the same clearance of 0.6mm and with punch and die fillet radii of 0.1mm.

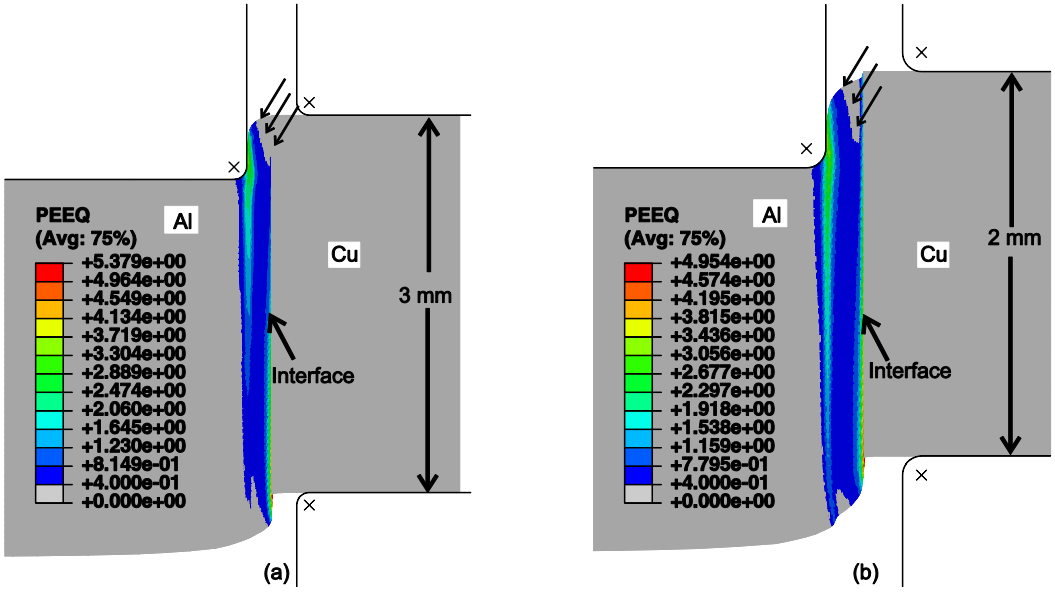

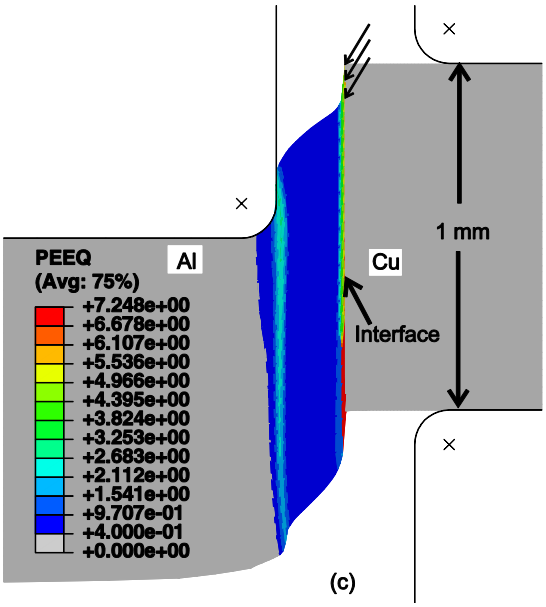

Fig. 5- 7. Numerical model simulations for the effect of Al/Cu composite sample thickness (a) 3mm (b) 2mm (c) 1mm

Equivalent plastic strain distribution of 3mm, 2mm and 1mm thick samples were respectively shown in Fig. 5- 7a, 5-7b and 5-7c. FE results revealed that shear strain developed at the interface of the 1mm thickness composite sample was more uniform (Fig. 5-7c) compared with other samples (Fig. 5-7a and Fig. 5-7b). FE results also showed a stress concentration at the interface similar to the theory of layered composite sample [124]. Moreover, no significant deformation was noticed in the Cu sleeve, which acts like a rigid member due to its significantly higher yield strength compared with Al substrate. In the top region, indicated by the arrows in Fig. 5-7a, 5-7b and 5-7c, the 1mm sample has higher plastic strain along the line of fracture than the thicker samples.

5.4.3 Effect of the punch and die fillet radii on the equivalent plastic strain

The numerical study was also performed to investigate the importance of the punch and die fillet radii on the DBT. Two cases of composite sample model with different fillet radii were studied using 1mm thickness sample and 0.6mm clearance model for 0.1mm and zero mm fillet radius as shown in Fig. 5-8a and Fig.5-8b respectively. The zero radii edges create significant stress concentration on the composite sample (Fig. 5-8b) at the punch point of contact, which is not desired for a DBT. In order to develop the fracture at the interface, the stress concentration must be avoided outside the interface region. In order to avoid the flow localization outside the target zone (the interface between copper and aluminum) and stress concentration at the contact points, 0.1mm punch and die edge radius were used The 0.1mm

punch and die fillet radius for the condition in Fig. 5-8a showed the largest stress in the sample to be at the interface region, which is required to ensure a pure and uniform shear at the bonding zone during the DBT.

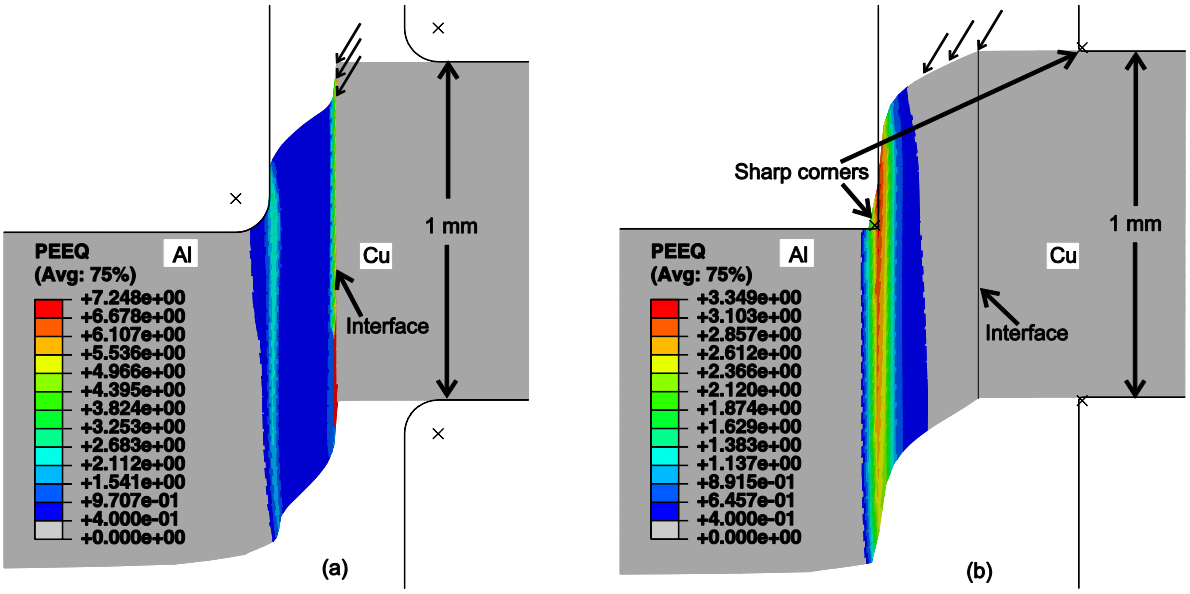

Fig. 5- 8. Simulation results for fillet radii effect on composite samples (a) 1mm thickness with 0.1mm punch and die fillet radii (b) 1mm thickness without punch and die fillet radii

The composite DBT rig design was finalized based on the numerical studies of the above three critical parameters: clearance, sample thickness and punch fillet diameter. According to the numerical studies the suitable thickness for sample was found to be 1mm. Moreover, the overall clearance of 0.6mm with 0.1mm punch and fillet diameter were identified to develop approximately uniform strain distribution at the interface region.

Therefore, it can be summarized based on the FE analysis findings, that for a given aluminum core diameter “D” (Fig. 5-1b), a punch diameter equal to (D-0.2mm) and a die diameter equal to (D+0.2mm) with the fillet radius of 0.1mm for punch and die and the holder maintaining a 0.6mm clearance between the punch and the die are required to ensure the failure at the interface region. Also, a blank holder with the same die diameter as shown in Fig. 5-1a is required to facilitate sample positioning and prevent bending of the sample during the test.

5. 4.4 Experimental work and results of dedicated blanking tests

In order to verify the bonding strength using the DBT test, specimens with 1mm, 1.5mm and 2mm were machined from10.5mm diameter Al core extruded composite samples. The slices were produced using an Electrical Discharging Machining (EDM) wire cutter to avoid unwanted stresses on specimens.

An Al disk sample of 13mm diameter with 1mm thickness was also cut from an identically extruded section to obtain a reference stiffness curve. The Al sample was blanked using the similar 10.5mm DBT set used for blanking composite material. The DBT load-displacement measurements of the sliced 1mm composite sample and the reference aluminum sample were compared with the predicted results of the FE model.

Contrary to the FE and the reference aluminum sample response, the measured composite DBT load-displacement response was almost linear in behaviour and all tested composite samples had a brittle fracture characterized by a sudden drop of the load at the fracture point. From the numerical model, it was clear that the thick samples cannot develop uniform shear strain distribution along the interface. In order to verify the behaviour, a number of sliced samples with 1-3 mm thicknesses were produced and tested by using the DBT. The maximum shear force needed at failure against the thickness of the sample is shown in Fig. 5-9.

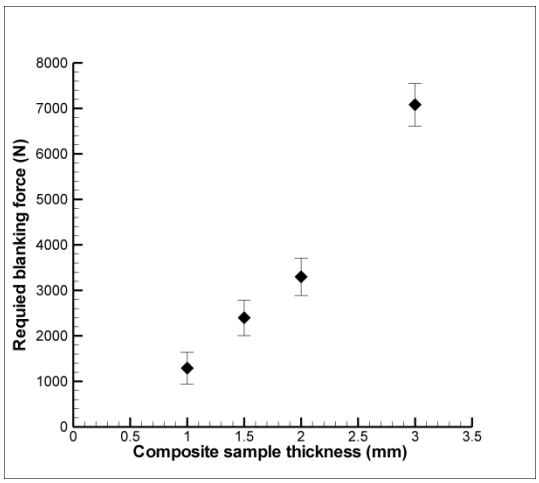

Fig. 5-9. Maximum blanking load (N) for 1-3 mm thick AFSCE extruded composite samples with a core Al diameter of 10.5 mm

As shown in Fig. 5-9, the maximum blanking load increased as the thickness of the sample increased. Results revealed that a simple linear co-relation between the thickness and the required force in the DBTs does not exist. Composite material behaviour deviates from a simple shear failure at higher

thicknesses. Furthermore, Fig. 5-9 shows that 3 mm blank required almost 6 times of the force required to blank the 1mm sample. Similarly, 1.5 mm thickness sample also required more than 1.5 times the blank force necessary for the 1mm sample. This was well agreed with the numerical model simulations which revealed a large uniform plastic strain at the interface does not develop for large thicknesses specimens (Fig. 5-7).

5.4.5 Comparison of finite element and experimental results

A load-displacement diagram for a 1 mm composite sample with 0.6 mm clearance and a 0.1mm punch die radii was obtained using the numerical model for a punch stroke of 0.5mm and shown in Fig. 5-10. Experimental load-displacement results for extruded pure aluminum and composite sample with 1mm thickness were obtained from experimental DBTs also shown in Fig. 5-10.

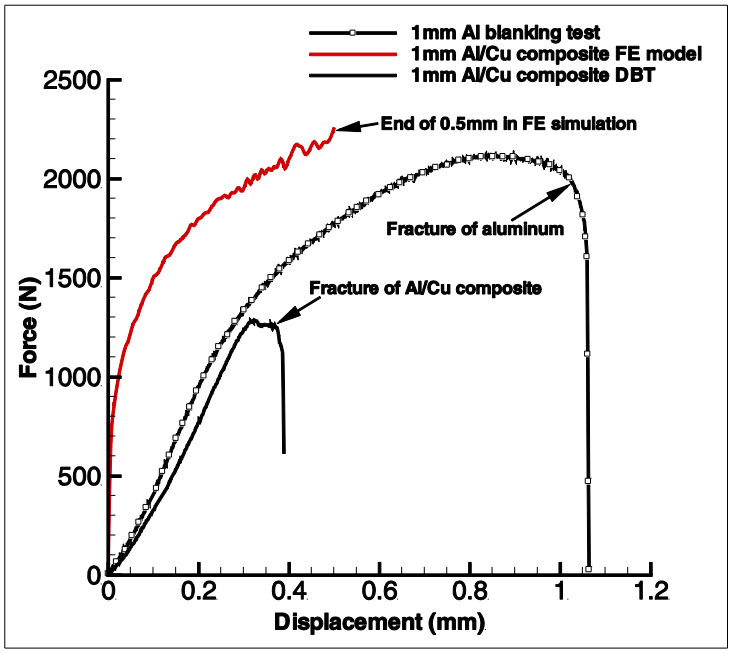

Fig. 5-10. Experimental and numerical load - displacement behaviors during shear blanking tests

The numerical model was solved as a non-linear and transient problem which is highly iterative in nature. This has led to small fluctuations in the predicted load-displacement shown in Fig. 5-10 which are mainly due to steps and sub steps of the simulation iterations. The variations of the slopes for both numerical and experimental results are due to the differences in punch movement used to simulate the numerical

solution and the punch velocity used in the experiment. In the numerical model the punch displacement boundary condition was specified but the punch stroke during the experiment was controlled by the motor head speed.

As shown in Fig. 5-10, the maximum load required to shear the Al disk sample ($\approx$1950 N) is approximately equal to the predicted maximum load obtained from the FE model. The measured strength of bonding is almost half of that obtained using the FE model. The discrepancy between the FE and the composite DBT results indicates that a full bonding, which has been assumed at the interface of the FE model, does not accurately represent the real situation and this has been confirmed using the bond fracture failure image shown in Fig. 5-11. A better understanding of the interface is required to lead to the development of improved predictive models for bonding. The DBT results for composite sample in Fig. 5-10 indicate that the shear failure is sudden, which resembles brittle failure while the pure aluminum clearly shows a ductile failure. This is in agreement with Fig. 5-11 where composite fracture surface and the aluminum fracture surface are shown.

Interfacial observations using Scanning Electron Microscope / Focused Ion Beam (SEM / FIB), Energy-dispersive X-ray spectroscopy (EDX) and X-Ray Diffraction (XRD) techniques confirmed that a near flawless bonding was created at the interface most likely through mechanical interlocking in AFSCE samples. The composite fracture micrograph also shows presence of aluminum residues on copper (Fig. 5-11a).This implies that aluminum as a softer material could be acting predominantly as crack arrester when failure occurred at the interface region. The sudden failure without full yielding of the composite material could be due to the limited ductility and high hardness near the interface resulting from work hardening and grain refinement as found in previous strength investigations. In contrast, fracture surface of pure aluminum shows ductile failure features such as a significant number of dimples which is in good agreement with the yield failure of the material.

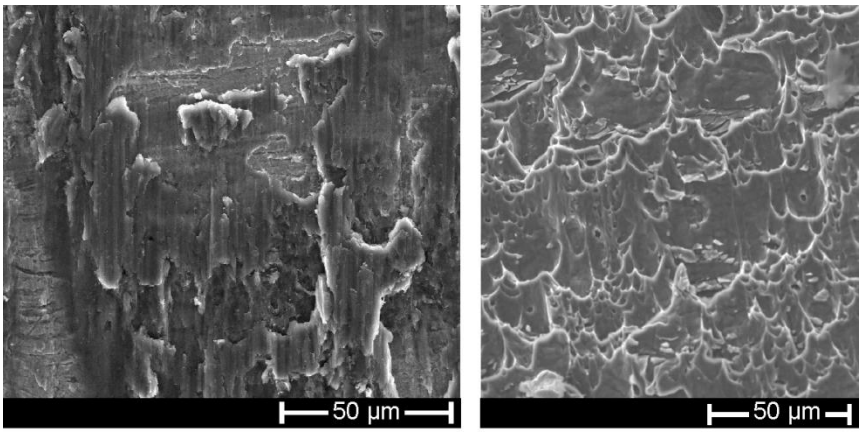

Fig.5-11. SEM images of DBT fracture surface (a) composite interface (b) pure aluminum specimen.

The weakening mechanism and the low shear strength of the bonding could also be due to a formation of diffusion bonding and intermetallic formation at the interface. In general diffusion bonding (DFB) can occur at the interface when the temperature is between 0.5Tm to 0.8Tm to promote the diffusion across the interface[22]. Diffusion bonding occurs by the phenomenon of atomic diffusion at elevated temperatures and a high contact pressure to be applied for an adequate contact/holding time[13]. Firstly, mass transport takes place in a DFB process by breaking the oxide layers on the contact surfaces, which facilitate the contact between the adjacent layers of different materials. This atomic diffusion creates a new metallic compound called intermetallic compound (IMC). Bonding dissimilar metals at room temperature may form mutually soluble or brittle IMCs which create a weak joint[20]. Typically, an Aluminum-Copper diffusion bonding forms various brittle IMCs such as Al2Cu, AlCu and Al4Cu9 at different temperatures[21]. Diffusion bonding of Al/Cu clad composite which was fabricated using ECAE process with varying temperatures from 100°C to 225°C varying by 25°C with various holding times of 20, 40, 60, 80 and 100 minutes at each of the temperatures were investigated for their shear strength of the bonding[108]. It was found that good bonding occurred at 200°C with a holding time of 60 to 80 minutes[108]. It was also noticed that increasing the temperature above 120°C adversely affected the bonding strength due to a formation and a growth of IMCs and oxide layers at the interface[108]. Therefore, it is also possible to have IMCs and oxides at the interface which could weaken the Al/Cu bonding. Earlier observations of the AFSCE samples also indicated that an approximately 1µm thickness of 'a thin composite like bond layer' develops at the Al/Cu interface which might be of intermetallic nature with the presence of oxides. However, intermetallic compounds or oxides were not detected in detailed examinations of AFSCE samples using FIB, SEM - EDX and XRD techniques.

But there were significant work hardening patterns observed in both aluminum and copper regions of AFSCE samples. The process conditions of 300˚C and back pressure of 200MPa with severe deformation led to micro structural changes including formation of ultrafine grains (grains size of less than 1μm) near the interface region of the copper substrate in the AFSCE extruded samples (Fig 4-11b). However, the numerical models were studied with homogeneous material flow behaviours with perfect bonding condition. This could result in over estimation of shear force required for failure that was confirmed in the numerical model simulations compared with the experimental results for failure. However, the composite bond with average bonding shear strength of approximately 50.5 MPa, which is higher than the shear yield of the aluminum (46 MPa) is promising for potential applications of these copper clad aluminum composite rods.

5.5. Conclusions

In this chapter, the shearing load needed to blank the Al disk out of a Cu ring in an AFSCE composite sample was measured and compared with the numerical results obtained using a developed FE model. The FE model was conducted for the composite sample to study the effect of sample thickness, clearance and fillet radius of the blanking tools on the strain distribution. Based on the carried out numerical studies, 1mm sample thickness was identified as the most appropriate sample thickness for the dedicated composite blanking test. Model estimations revealed a 0.6 mm clearance between the punch and die develops a large effective strain at the interface sufficient for failure to occur. The blanking tools fillet radius study showed that the blended edges with 0.1mm radii tools develop shear failure at the interface unlike the sharp cornered tool that caused failures at different places. Based on the numerical studies parameters of 1mm thick sample with the clearance of 0.6mm and fillet radii of 0.1mm was found to be a required configuration to determine the shear strength of a composite bonding. In addition to this, the FE model enhanced the understanding of composite blanking failure with the stress concentration scenarios which are different from a single material shear failure. The experimental results concurred with the numerical studies and provided consistent results when the parameters identified by the numerical model were used. Finally, the proposed design delivers a proper method that could be utilized to examine the bond shear strength of composite structures that includes interfacial failure.

Chapter 6:
Hybrid metal fabrication using Confined High Pressure Torsion (CHPT) process

Chapter 6: Hybrid metal fabrication using Confined High Pressure Torsion (CHPT) process

6.1 Introduction

Hybrid materials are attractive alternatives in modern engineering applications, which are designed based on their classifications on the choice of components, shape and length scale [1, 2]. In addition to the general classifications of hybrid materials, in recent years a special classification was considered as "architectured materials" which consist of a length scale defined by their inner architecture [4-6]. These materials are not only viewed for their architectural features, they also have multifunctional and structural properties to serve the increasing demand of the competitive material application. Especially new engineered materials provide various functional properties such as thermal insulation, magnetic properties, acoustic damping or energy absorption with enhanced additional structural properties such as weight reduction and high strength [5]. In this way, in order to cater the growing demand of these novel engineered materials, over the past decade severe plastic deformation (SPD) processes facilitate the manufacturing process to fabricate such materials with enhanced superior properties and provide room to produce new architectured materials [4].

Since Nilsson introduced a technique to manufacture Al/Cu clad composite rods, which can be considered as architechural hybrid material, using hydrostatic extrusion in 1973 [100], recently many researchers studied various techniques to fabricate the copper clad aluminum composite using different techniques. In this way, severe plastic deformation (SPD) processes have also been considered to fabricate hybrid materials as they reduce the required bonding temperature by leveraging the synergy due to high pressure and shear. Equal channel angular extrusion (ECAE) [51] and High Pressure Torsion (HPT) [73] are most well-known SPD processes. Recent years, the following SPD processes also considered to fabricate aluminum/copper hybrid metals by using ECAE [107, 108] and Cu / Al tube by High Pressure Tube Twisting(HPTT) [159].

In addition to this, AFSCE process also considered in this project to fabricate axi-symentric hybrid material. However, small disk shape composite specimen fabrication with near net shape, cannot be achieved using these processes. In addition to this, long piece of material required a very high pressure which reduces the life of press tools and die components. In addition to this, some elevated temperature process or additional heat treatment which increases the energy requirement to fabricate the final composite metal [107]. In order to fabricate a wide, thin, disk shape composite, a confined HPT process was proposed. This process can also compared to an additive manufacturing process because the final processed material does not required a lot of machining. As an example case study of a copper clad aluminum disk at room temperature was proposed to fabricate using a ring shape copper with a filler of aluminum powder in the confined HPT process.

The confined High Pressure Torsion (CHPT) process is presented in this chapter, which required less machining to obtain the final product because of no flash out of materials in this process. This confined HPT process having the advantages of increased pressure in the process material and reduce the material waste. In addition to this, this process introduces heterogeneity and higher localized deformation in the outer area of the material, which increases the life span of the final product. This process is also not required high pressure and elevated temperature which makes the process more attractive, as it can make significant improvement in the material property due to work hardening and grain refinement. The low pressure process condition also have an additional advantage on the lifespan of working tools and dies which is also beneficial in terms of operation.

In general HPT processes performed with large number of revolutions and high pressure (average of 15-60Rev with 2.5 to 15GPa) to achieve significant grain refinement in bulk material, and powdered materials [87, 90, 92]. However, this CHPT process allowed low pressure and only a few of revolution (up to 2 Revolutions with 1 to 1.5GPa) to investigate the effect of CHPT in the material property changes.

The CHPT process is initially studied for aluminum powder samples which aim to achieve grain refinement at room temperature. The process has its own controls on the number of revolutions, pressure and rotation speed of the process. The bottom punch rotates while the material is under the applied pressure, which develops a combination of a compressive and shear forces in the material. The confined nature of the process allows a “near zero external radial change” in the final product.

Firstly, initial experimental studies of the CHPT process using the aluminum powder material and post processing sample characterization are presented. After that, the hydrostatic pressure effect on the

composite samples which facilitate a multi-dimensional compression in the Al/Cu clad composite materials discussed in this chapter. Finally the experimental case studies of the fabrication of hybrid Al/Cu samples using the CHPT process are presented. Here the micro shear punch test, hardness tests and micro structural observations are used to characterize the process requirements and the successful copper clad aluminum composite fabrication.

6.1.1 Key features and implementation of the Confined High Pressure Torsion (CHPT) process

Initial experiments were performed using 16 mm nominal size punches and dies to process the material. The test rig assembly press is shown in Fig 6-1 a-c. The schematic illustration of the longitudinal section of the CHPT process assembly configuration is shown in Fig. 6-1b. The bottom punch facilitates the material to rotate about the vertical axis. In order to avoid un-wanted flash out of materials through the clearances (upper punch - die clearance and lower punch - die clearance), and trap the loose powder in place, small aluminum disks were placed on the top and bottom of each sample.

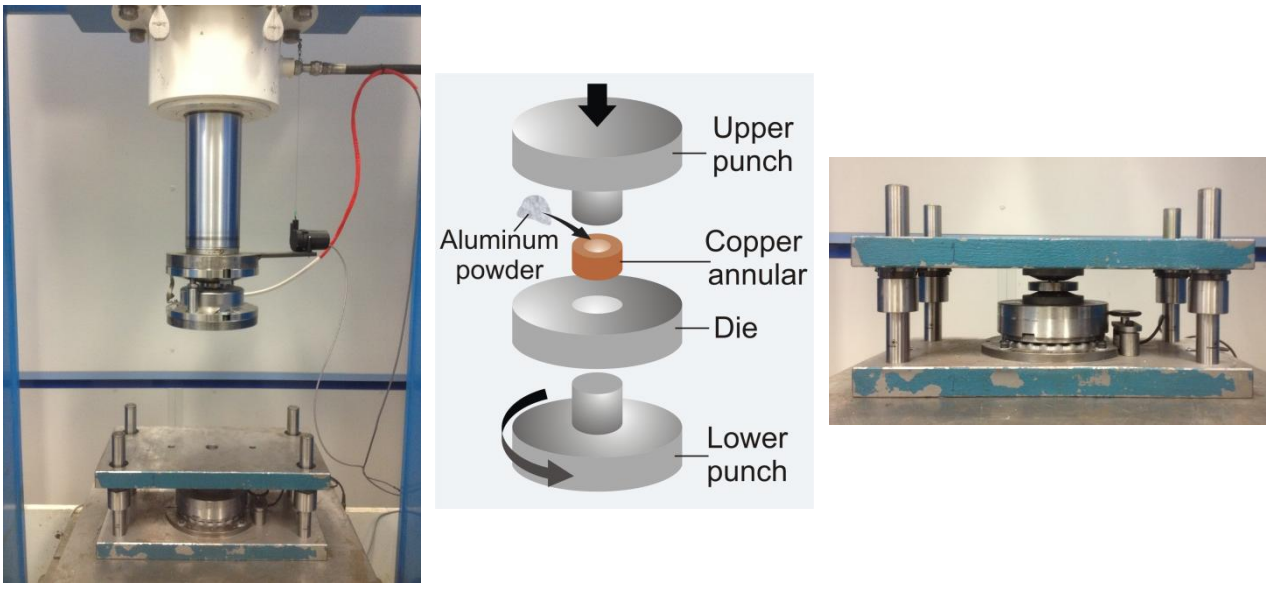

(a) (b) (c)

Fig.6 - 1. The CHPT test rig (a) The process on the hydraulic press (b) Schematic presentation of the CHPT process with copper annular and aluminum powder materials (c) CHPT process assembly prior to the processing

Main aim of this chapter is to investigate the basics of the CHPT process and axi-symmetric hybrid material fabrication using the process. Therefore the detail of the process is introduced in this section with stress development study, which brings the overview and nature of the process and suggests the

possibility of processing a successful fabrication of axi-symmetric hybrid material using this CHPT process.

6.1.2 Stress development in the sample during the CHPT Process

The mechanism for matching of the flow stresses at the core-clad interface is a key to understanding the powder-solid hybrid metal fabrication using CHPT. Estimating the flow stresses within the composite sample is an extremely difficult task due to the presence of two materials during the hybrid metal fabrication process. The powder with solid hybrid material fabrication makes the process very complex to understand. In order to understand the hybrid metal fabrication, it is required to fully understand the process effect on powder materials and bulk materials. Limited experimental observations at the interface can be performed to understand the deformation/stress distributions at the interface. Examples of potential observations include radial hardness distribution, grain size changes and texture distribution.

The multi-dimensional stress development in the CHPT process in a composite material has been noticed after a careful investigation of the longitudinal cut section of the composite Al/Cu sample was undertaken. Therefore, the multi-dimensional compression effect on the composite sample is also investigated to understand the stress development in the CHPT process for composite material. Furthermore, initial studies were also carried out on aluminum powder sample to understand the stress development on CHPT process prior to the Al/Cu clad composite material fabrication.

The CHPT process is more sophisticated to produce compacted greens than traditional powder processing methods, and achieved samples with higher density, which also eliminates the need for additional sintering step to obtain a processed material with enhanced material properties. The synergy effect of high pressure and shear deformation in this HPT process is an advantage to produce solid material in a single step process. In this chapter, a clear description of the process of producing green compacts by using the CHPT in room temperature is presented. This is then followed by the presentation of results and discussion on post processed material characterization of both aluminum powdered samples and copper/ aluminum hybrid samples.

6.1.3 Comparison of traditional powder compaction process and CHPT process

In the current research, an investigation of a new fabrication method of aluminum powder by CHPT is initiated. 99.70% pure aluminum powder, Al eckagranules® 75s is chosen to be the raw material to be

consolidated in the current project. This is due to its high malleability and ductility, soft, light weight and very compressible compared to other metals such as copper and iron. The mechanical property, where it is highly malleable is especially important in this study, as it provides an indication that it is highly formable and can be easily deformed plastically by compression without the occurrence of cracking or rupturing. On top of that, its light weight property also of interest in this study, as it would be advantageous to produce a light weight material with superior mechanical properties.

During the process, high purity aluminum powder, Al eckagranules® 75s is compacted into the disk shape using the CHPT process. The material was preferred to be performed at room temperature to avoid contamination and oxidation of aluminum powder and to achieve effective fabrication at low temperature. By implementing CHPT in powder consolidating process, the compacted sample formed is expected to have better mechanical properties, such as higher density or lower porosity, and smaller grain size than green compact formed by traditional compaction process. These properties would then give rise to the strength of processed material. This is certainly due to the rearrangement of powder particles during the process, where powder particles move primarily in two dimensions due to the concurrent torsional straining in HPT. In comparison with Hot Isostatic Pressing (HIP) process, the powder particles primarily move in the direction of the applied pressure in this process. Moreover, the amount of applied pressure has an effect on the density of the green compact formed. Typically, as the applied pressure increases, the porosity in the green compact would decrease, causing the average density of green compact to increase. Besides that, the size and size distribution of the pores are also functions of applied pressure. The relative shrinkage of I-pores, which is the internal pores within particle, and V-pores, which is the void between particles, increases with increasing amount of applied pressure [13]. However, average density of green compact can only be increased to a limit, where further increasing applied pressure will not cause any change in average density. This occurs when the porosity in green compact is fully eliminated [13].

The CHPT (HPT) process can also be used for powder consolidation as it satisfies the process requirements in a traditional powder processing technique. The CHPT process could also eliminate the step of additional sintering, to obtain a high strength material.

6.2 Experimental work of aluminum powder samples

The aim of the work is to study the CHPT process to fabricate powdered aluminum samples at room temperature. The microstructure and mechanical properties of the fabricated samples were investigated after the CHPT process with varying pressure and number of rotations of the sample.

6.2.1 Application of CHPT experiments to aluminum powder samples

Aluminum powder with 99.7% purity, Al eckagranules® 75s was used as the raw material to perform performing Confined High Pressure Torsion (CHPT) experiments. The SEM image of the powder particles is shown in Fig 6-2. Al eckagranules® 75s has spherical particle shape, bulk density of 1250 kgm^{-3} and average particle diameter of 28.0 µm based on the information provided by the supplier, SCM Metal Products.

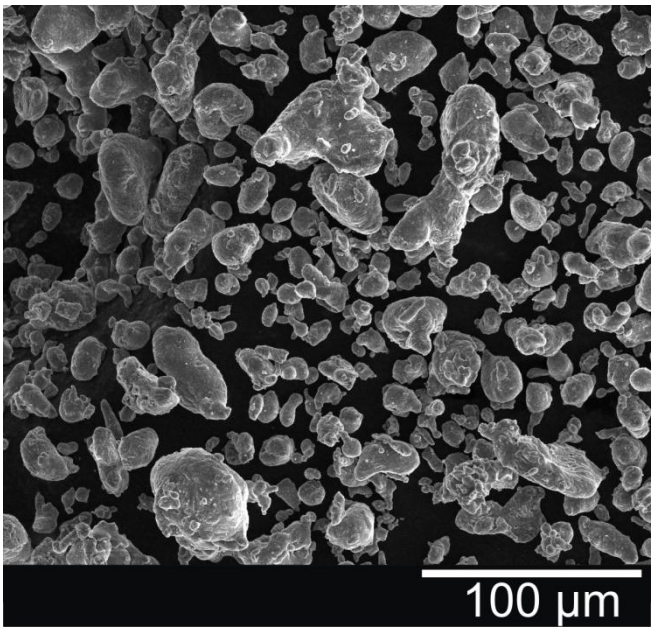

Fig.6 - 2 SEM image of the aluminum powder samples

The required mass of aluminum has been calculated prior to the experiment using mass density correlation in order to produce a sample of required heights. Density equation was used for calculation of mass of aluminum powder required. In the current study, samples with two different heights were produced, where it requires initial sample thickness of approximately 4mm and 6 mm including the

aluminum caps. It was found that the required mass for the initial sample thickness of 4mm and 6mm were approximately 1g and 1.5g respectively.

After that, the procedure of the experiment was started by cleaning the dies and punch. Sodium hydroxide (NaOH) solution was applied on the surfaces of the die cavity and punch to easily remove the residues of aluminum from previous experiments. The calculated amount of powder was securely placed within the die cavity by using two dome-shaped aluminum caps, each with 1 mm thickness and 16 mm diameter as shown in Fig 6-3a. The first dome-shaped cap was initially placed in the die and flattened using a hand press. This step eliminates the clearance between the cap and die would then be perfectly sealed after flattening the dome-shaped cap, hence preventing leakage of powder. The diameter of aluminum cap was made to be 16 mm so that it fits perfectly in the nominal size of the die. It is extremely important to prevent any occurrence of leakage of the aluminum powder as it may cause flash out of material during the processing. The calculated amount of aluminum powder was then poured into the die, and the second dome-shaped cap is placed on top and flattened to seal the aluminum powder within the die cavity as shown in Fig 6-3b.

(a) (b)

Fig 6-3 (a) The dome-shaped cap used in the CHPT process (b) Picture of actual die with powder contained between two flattened dome-shaped caps

Then, the die was placed in the Servo-Hydraulic FIHPST rig as shown in Fig 6-4. The whole test rig was tested for its concentricity and alignment during the installation stage, the punch was guided using four pillars during the test to avoid misalignments.

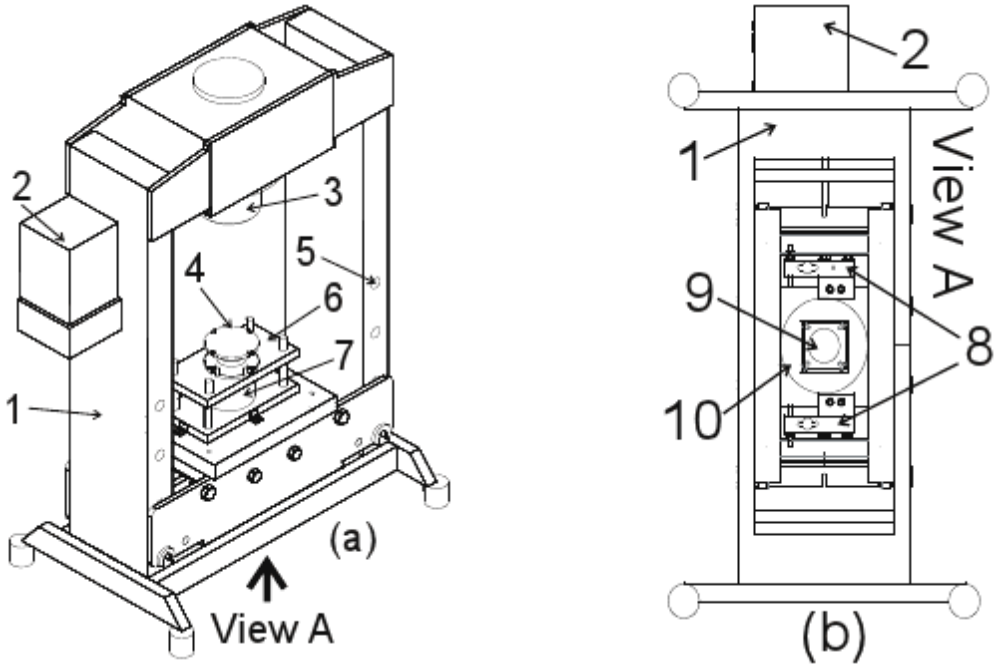

Fig 6-4 Serve-Hydraulic FIHPST Rig. (1) Frame (2) Hydraulic control power supply unit (3) Compression ram (4) Compression load cell (5) Height adjustment holes (6) Vertical guide pillars (7) Friction induced high pressure shear die (8) Torque load cell (9) Hydraulic motor (10) Torque cell reaction plate

In order to start the test rig, firstly process pressure (1 GPa or 1.5 GPa) was applied. After that the clockwise torsion was applied using the toque motor to apply concurrent torsional straining under the high pressure condition. The pressure was applied by the hydraulic press using the compression ram and the torsional straining was applied from lower part of the test rig. The test parameters for a particular test, pressure and number of revolution were controlled by using DAQFactory software interface. The DAQFactory software platform also provides a graphical user interface for the automation of Servo-Hydraulic FIHPST rig and which helps to monitor ram displacement, rotation angle and pressure force.

After the required number of revolution, the punch was lifted up and a processed sample was successfully removed from the test rig with the aid of a hydraulic jack. The process was repeated for 5 different combinations of pressure and number of applied revolutions. The specifications of parameters for each samples produced are summarized in Table 1.

Table 6-1: Specifications of parameters for various cases of samples produced by the CHPT process in room temperature

Case	Al powder weight (g)	Applied pressure (GPa)	Number of revolution (1 rev=360 degree)	Average total sample height after the process with caps (mm)
1	1.0	1.5	1	3.863
2	1.0	0.5	1	4.160
3	1.0	1.5	2	3.832
4	1.5	1.5	2	4.843
5	1.5	1.5	-	4.803

The experiments of "case 5" were conducted without applying torsional straining to study the consequence of torsional straining on the samples produced. In the current research, cases 1 and 2, where only 1 revolutions of concurrent torsional straining, were compared to investigate the effect of increasing pressure on the microstructure of samples produced. The samples with cases 4 and 5, which were produced with 1.5 GPa applied pressure, were compared to study the effect of number of revolutions of concurrent torsional straining on the mechanical properties of samples produced. The results of all the samples were also compared to the microstructure and mechanical properties of 99.999% pure bulk aluminum samples and aluminum alloy AA5005 – H34 to study the effectiveness of the CHPT process.

6.2.2 Post processing characterization using micro hardness test and micro shear punch test

6.2.2.1 Micro shear punch test to evaluate the shear strength of the processed samples

In order to investigate the mechanical properties of the produced samples, micro shear punch test was used as an appropriate technique to identify the local variations in the shear strength of materials. The micro shear punch test was performed using the test rig shown in Fig 6-6a. Miniaturizing sample test technique is well suited and experimentally feasible to identify the local strength variations in the processed sample. This test is similar to a small punch test which was originally developed for assessing the ductile–brittle transition temperatures (DBTTs) [160] shear strength [139-141] and interfacial fracture toughness [142, 143] with limited amount of materials. Micro shear punch test

(MSPT) is similar to the dedicated banking test described in chapter 5, based on a blanking operation to evaluate shear strength of a material. The micro shear punch test samples were secured between a stripper and a matrix, shown in Fig 6-6b, to minimize the effect of bending during the test. The shear punch was guided using a punch guide with a built in linear bearing.

The shear strength of a material can be calculated using the MSPT results and material shear strength equation Eq.6-1.

$$\tau = \frac{F}{\pi d t} \qquad \text{Eq.6-1}$$

Using this eq. 6-1, shear stress τ can be estimated by dividing the shear force F by the shearing area. Here d and t are respectively corresponding to the punch diameter and sample thickness.

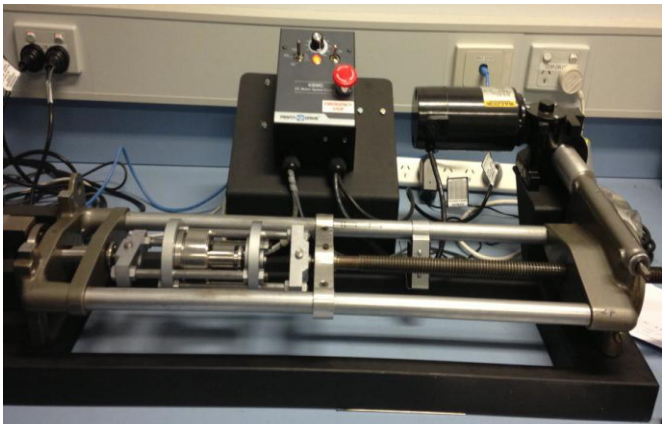

Fig 6-5 Micro shear punch test rig

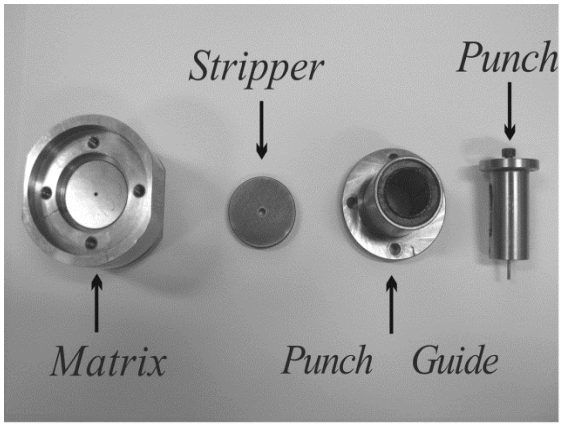

Fig. 6-6 Internal parts of the MSPT assembly

In order to study the distribution of strength and density of the samples produced by CHPT, samples were manually ground to a 2mm thickness. The grinding step removes the top and bottom caps of the samples. This step also help to achieve the exact sample thickness with both (top and bottom) parallel surfaces. The manual grinding process also prevents the sample from any damage during the preparation stage as this eliminates the requirement for climbing the samples on a wise or collet. The manual grinding of the samples also removes small amount of material at a time. The CHPT sample from "case 4" was tested using micro-shear punch tests (MSPTs), at various radial distances.

After the MSPTs, the sample from case 4 is shown in Fig 6-7a. For each test (S1-S5), shearing load versus displacement was obtained and plotted as shown in Fig 6-7b. For comparisons pure bulk aluminum sample with 2mm thickness was also tested using the same MSPT rig. MSPT results of the pure bulk aluminum sample are also overlaid in Fig 6-7b. From the graphs, yield strength and ultimate shear strength were determined. The weight for each blanks produced in each test were also carefully measured on a scale with six decimal precision. Given the volume of each blanks, the density of each blanks produced along the respective radial distances of the sample can be obtained. Furthermore, the average density of the produced blanks also gives an indication of the amount of porosity in the sample, where higher average density indicates a low porosity in the sample.

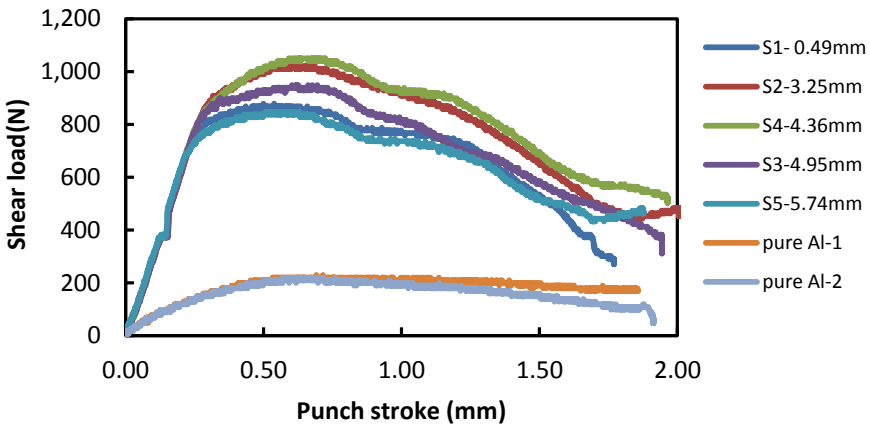

(a) (b)

Fig 6-7 (a) Sample case 4 (1.5 GPa with 2 revolution process condition sample) after micro shear punch test and (b) Shear stress versus normalized displacement for sample case 4 obtained using micro shear punch test with MSPT results of pure bulk aluminum samples

The shear yield strength along the radial distance of sample case 4 (1.5 GPa, 2 revolution) does not have significant variation. The shear yield strength varies between 59.07 MPa to 72.33 MPa. The 72.33MPa shear strength was obtained at the radial position of 4.3551 mm from the center. On the other hand, shear yield strength of pure bulk aluminum sample was found to be 14.335 MPa. This is significantly lower than the shear yield strength of a sample from “case 4”. This was further investigated in Section 6.2.3 using grain size measurements of both processed samples and the pure bulk aluminum sample.

For a material with smaller grain size, there is a greater ratio of surface area to volume, which also indicates that there is a greater ratio of grain boundary to dislocation. Grain boundaries play an important role in hindering the dislocations from movement, hence resulting in higher shear yield strength. Therefore, it shows that concurrent torsional straining has a significant effect on the strength of the sample produced, considering that both samples were consolidated with the same amount of applied pressure. The results showed good agreement to the average grain size presented in the section, where the bulk aluminum sample has a relatively large average grain size of 223 μm and sample case 4, which has an average grain size of 10.512 μm. The average grain size of the processed aluminum powder sample in case 4 is significantly smaller than the average particle diameter of 28.0 μm in eckagranules® granules 75s aluminum powder.

The ultimate shear strength of the samples was also determined. It is defined as the strength of a material against structural failure at which material fails in shear, and this point can be determined from the highest load point of curve. Ultimate shear strength varies from 83.23 MPa to 102.6 MPa in the CHPT processed sample. An overall increasing trend in ultimate shear strength along the radial distance is also observed, which is analogous to the trend of shear yield strength obtained using the MSPTs. The sample from “case 4” also have significantly higher ultimate shear strength than that of bulk aluminum sample which can be explained due to the larger average grain size of the bulk aluminum sample.

The density variation in the high pressure torsion samples were investigated using the blanks produced from micro shear punch test. In order to determine the density, masses of each blank were firstly measured by using a high precision measuring scale. Based on the thickness and diameter of little blank, 2 mm and 1.5 mm respectively, volume was calculated to determine the density of each blank. Density of the blanks varies between $2.63 gcm^{-3}$ to $2.41 gcm^{-3}$. This density variation can be negligible, and may be due to several influential factors, such as error tolerance of sample thickness and final shape of the very small blanks. Therefore, from these results, the average density of the sample was calculated as $2.54 gcm^{-3}$, which is higher than that of pure bulk aluminum, $2.17 gcm^{-3}$. Therefore, it may be concluded that the CHPT process has significantly increased the density of the powder material by more than factor of two from row powder material density of $1.25 gcm^{-3}$.

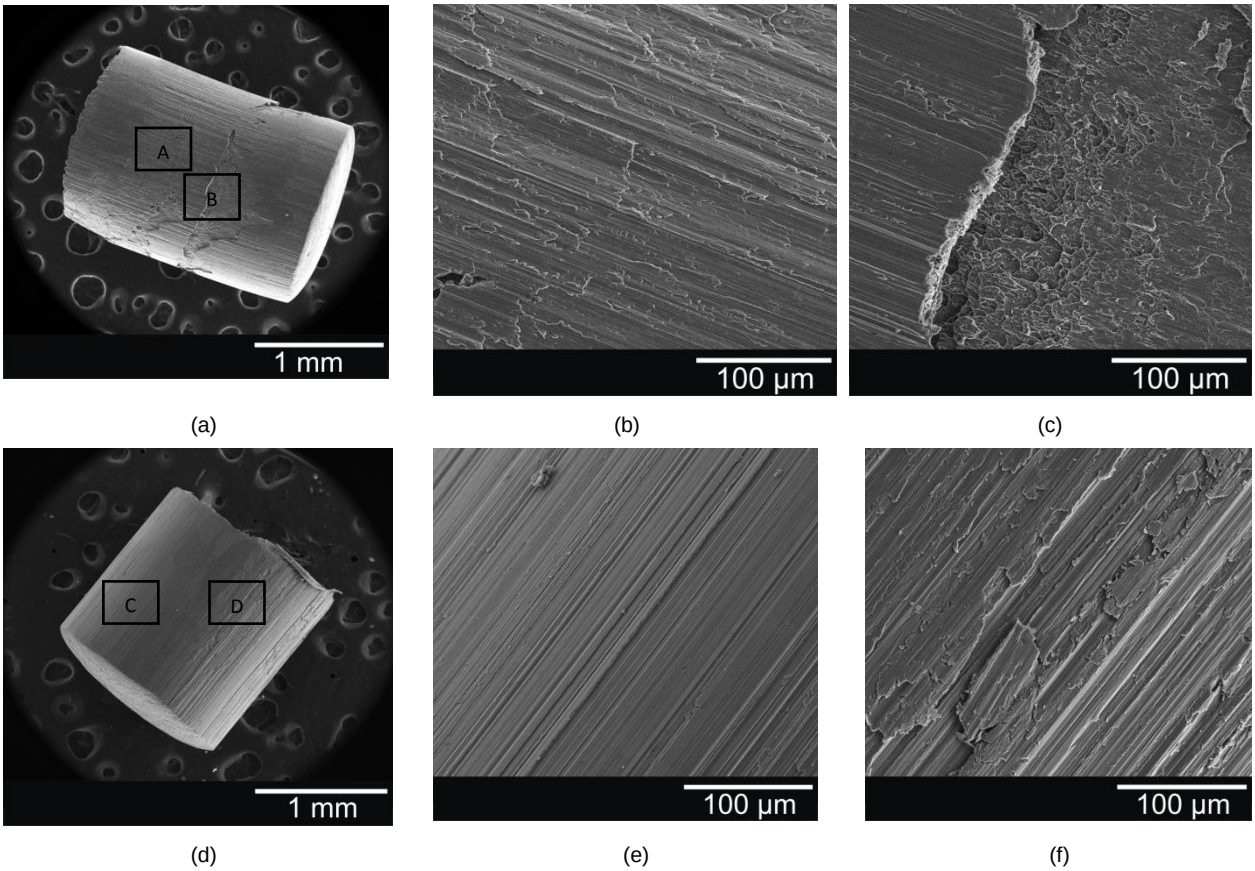

Fig 6-8 (a) Secondary Electron (SE) image of the cylinder blank from micro shear punch test of the CHPT processed sample with 1.5GPa and 2 revolutions after shear failure, (b and c) SE image shows the shear failure surface of the CHPT processed sample with 1.5GPa and 2 revolutions from box A and B respectively (d) SE image of the cylinder blank from micro shear punch test of the pure bulk aluminum sample after shear failure and (e and f) SE image shows the shear failure surface of the pure bulk aluminum sample view of Box C and D.

The cylindrical surfaces of the CHPT processed aluminum sample from "case 4" after MSPTs are shown in Fig.6-8a-c. The surfaces of the bulk pure aluminum after shear failure are shown in Fig.3-8d-e. shear failed surfaced of the CHPT processed sample (Fig 6-8a-c) revealed a significantly higher number of boundary pull outs compare to the pure bulk aluminum sample in Fig 6-8d-f. All the images in Fig 6-8 show ductile shear failure for CHPT processed sample and pure aluminum sample after MSPTs.

Samples from "case 5" (processed with 1.5 GPa pressure without torsion) were also tested using MSPT. However, any reliable data was not obtained from the MPST of those samples as they failed in an overloading low ductile fashion across the sample as shown in Fig 6-9a. A fractured sample and fractographic image of the sample are respectively shown in Fig 6-9a and in Fig 6-9b, obtained using OLYMPUS SZX16 optical microscope and Joel 7001F scanning electron microscope.

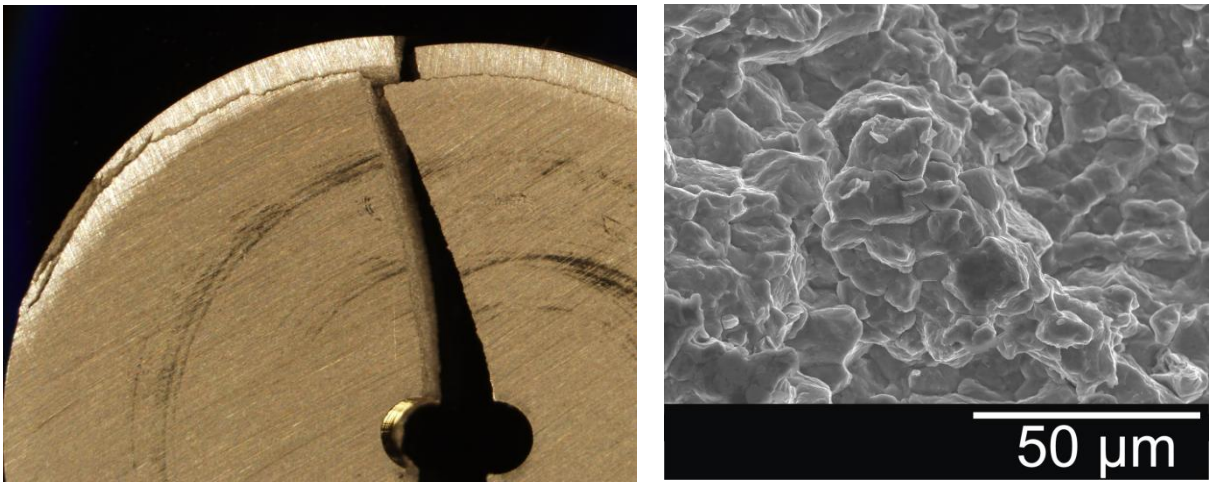

(a) (b)

Fig 6-9 (a) Fractured sample case 5 (1.5 GPa with 0 revolution process condition sample) after micro shear punch test and (b) Fractography image of the case 5 sample (1.5 GPa with 0 revolution process condition sample) after overloading low ductile fracture.

This is a clear indication, that the samples from “case 5” (1.5GPa, no revolution) failed under overloading fracture during MSPTs, showed that these sample have low ductility. The fracture surface also shows low ductile facture behavior of the sample. The concurrent torsional straining introduced, extensive plastic deformation which enhances the material property of the CHPT processed aluminum powder samples from “case 4”. This showed good correlation with a previous study, where the strength level of Fe alloy with 10 wt% aluminum sample consolidated with one revolution of concurrent straining is slightly higher than that of a sample consolidated without any torsional straining [77].

In order to justify the enhanced property of this CHPT processed aluminum samples, properties of an aluminum alloy of AA5005-H34 were also used to compare with the CHPT processed sample properties. Ground 2mm MSPT samples from perpendicular section of rolled aluminum alloy AA5005-H35 were prepared and tested using MSPTs. The overlaid results with the MSPTs results of samples from case 4 are shown in Fig 6-9. Although, the aluminum alloy AA5005-H35 has a slightly higher percentage of elongation at the failure point than that of the CHPT processed sample, the CHPT processed powdered samples has higher yield strength, higher ultimate shear strength than the alloy.

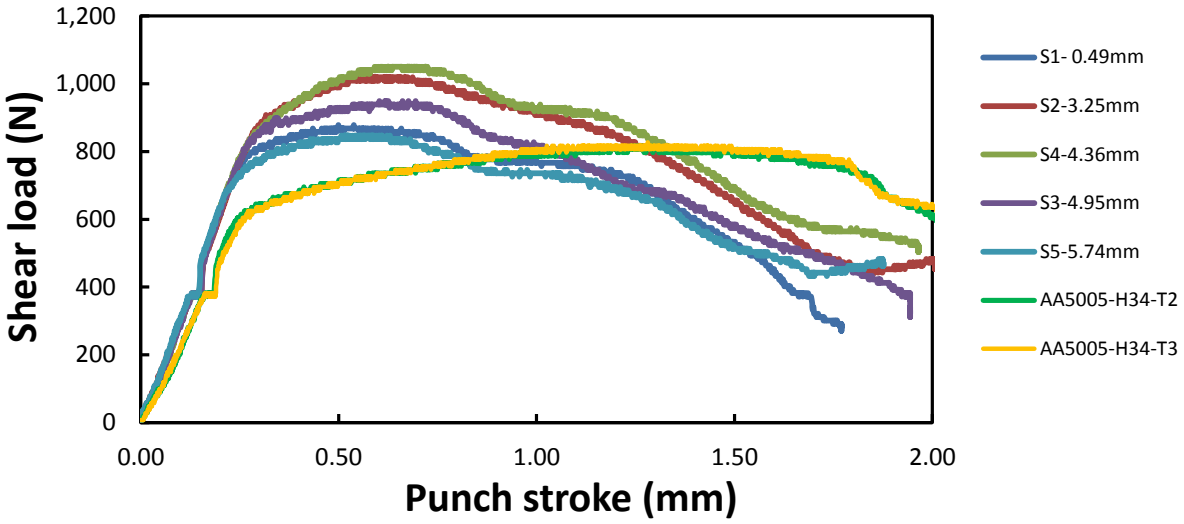

Fig 6-10 Shear stress versus normalized displacement for sample case 4 (1.5GPa with 2 revolution process condition) obtained using micro shear punch test with MSPT results of aluminum alloy AA5005 – H34

These preliminary results showed that the CHPT process is an enhance mechanism to produce high strength samples with high density compaction of powder under the hydrostatic pressure and torsional shearing. This process introduces a single step approach for powder processing which eliminates the need for sintering to achieve high density compacts.

6.2.2.2 Micro hardness test to investigate the hardness changes in the processed material and bulk aluminum sample

In order to verify the micro shear punch test results and investigate the localized strength changes in the processed material, micro hardness measurements were performed for a processed aluminum sample from “case 3”. The micro hardness tests were performed using 10g load with 15 sec dwelling time. These measurements were taken using a Matsuzawa micro hardness tester MHT-1 according to ASTM: E384 11e1. The obtained micro hardness results for the sample from “case 3”, is shown in Fig 6-11.

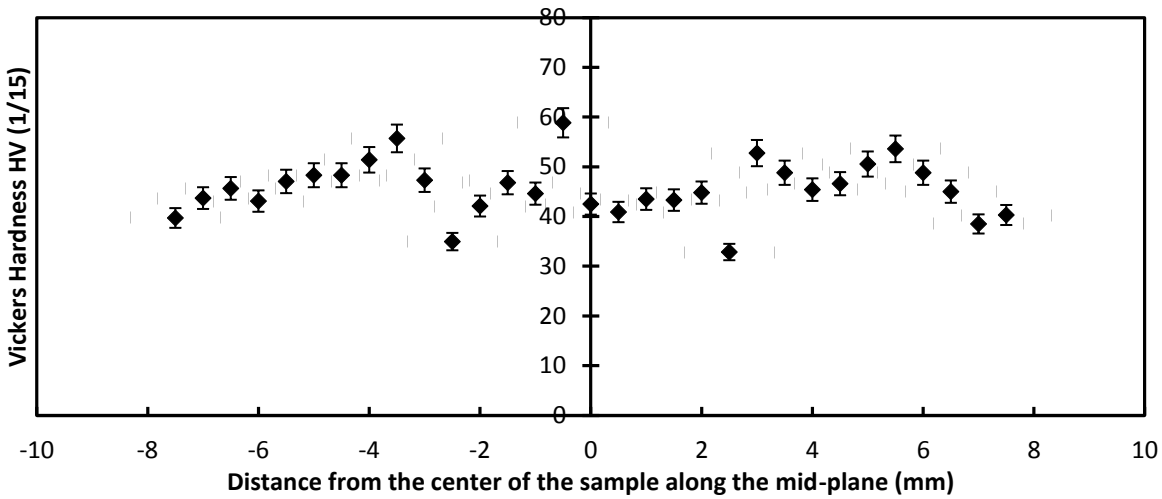

Fig 6-11 Hardness variations in the CHPT processed aluminum powder material against the distance from the center of the sample along the mid-plane in the cross section of the sample from case 3.

In order to avoid the variation in hardness distribution in top and bottom surfaces as described in an HPT process [77], the hardness measurements were taken along mid-plane of the cross section of the processed sample. The hardness result has an average of 45.67 HV 1/15 for the CHPT processed sample with the processing condition of 1.5GPa with 2 rotation sample from "case 3". The average hardness of pure bulk aluminum and aluminum alloy were also measured to compare with the CHPT processed sample. The pure bulk aluminum sample has average hardness of 17.7 HV 1/15 which is significantly lower than that of the CHPT processed sample. In addition to this, the aluminum alloy AA5005-H35 has an average hardness value of 53.2 HV 1/15 which lies between the lowest and the highest limits of the processed material's hardness value.

Although the micro hardness measurements showed a good agreement with the micro shear punch test results of the sample, the micro-hardness testing cannot deliver an accurate measurement with small load as they only measures the surface strength instead of the cross sectional thickness area of the specimen. Therefore, micro-shear punch test is more suitable for strength measurement of the specimens. In addition to this, micro shear results of partially compacted specimens give meaningless results as the indenter could be inside a pore or in a fully compacted area. However, the hardness results shown in Fig 6-11 confirm that the sample does not have a vulnerable area with significantly lower hardness.

6.2.3 Micro-structural evolution of CHPT processed powder samples

In the current research, mechanical properties of sample cases 4 and 5 were investigated to study the effect of the number of revolutions of concurrent torsional straining on the mechanical properties of the samples. These results were then compared to the mechanical properties of 99.999% pure bulk aluminum sample and aluminum alloy AA5005-H35. The investigations of mechanical properties of samples were performed using micro-shear punch test and micro hardness test techniques. Although the MSPTs give good estimation for the CHPT processed sample, the overloading fracture of the sample from "case 5" brings the need for further investigation to understand the role of torsional straining in the CHPT samples. Therefore, optical microscopic investigations were performed on the circular cross section and longitudinal cross section of the samples from case 4 and 5. The sample cross section convention is shown in the Fig 6-12. In addition to this, the pure bulk aluminum micro structure was also investigated to verify the grain size of the material.

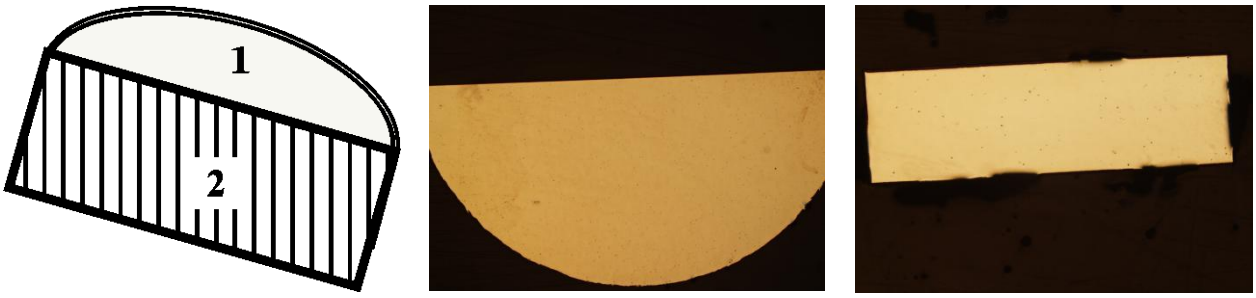

(a) (b) (c)

Fig 6-12 (a) Polished section view used here for convention (b) The circular cross section of the sample after final polishing corresponding to the surface 1 (c) The longitudinal cross section of the sample after final polishing corresponding to the surface 2

The samples were cold mounted and prepared using grinding and polishing. The samples were ground using emery paper of 180, 500, 800, 1250, 2500 grades, then diamond polished using 1µm diamond colloidal suspension, followed by oxide polishing of the samples were performed. After that the samples were etched using 1% hydrofluoric acid (HF) solution. The microstructure images from the cylindrical surface of the sample from "case 4" are shown in Fig 6-13.

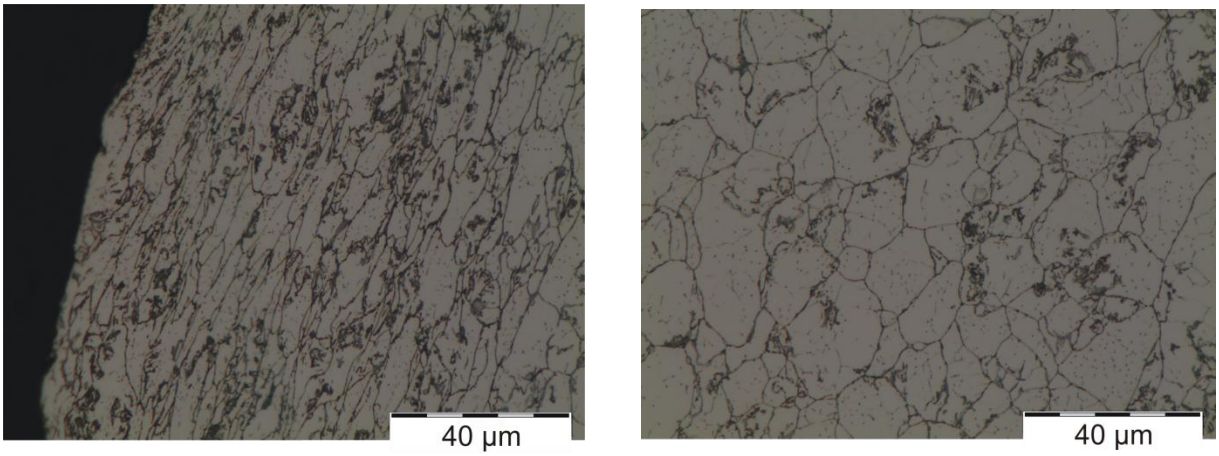

(a) (b)

Fig 6-13 (a) Microstructure of sample from case 4 at the surface 1 near the periphery of the sample (b) Microstructure near the center of the same sample from surface 1 (circular cross section)

In these images elongated grains were observed close to the periphery of the surface 1 while regular shape grains were observed inside the surface 1 of the sample from “case 4”. The microstructure images of the surface 2 of the sample from “case 4” are also shown in Fig 6-14. Although the micro-structure of the surface 2 has the similar pattern to the surface 1 in the sample from “case 4”, significantly higher number of particles is elongated in the surface 2. The overall elongated grain structure in the longitudinal section (surface 2) with low magnification is shown in Fig 6-14a. The evolution of the grain structure from region close to the periphery to inner regions of the surface 2 are shown in Fig 6-14 b – d. Fig 6-14b shows highly elongated grains close to the vicinity of the periphery region of the sample from “case 4”. In contrast, the grains become less elongated inside regions of the sample from case 4. This can be due to the effect of torsional straining that was large at the edge of the sample, which caused the edge of the samples to experience the highest strain. Theoretically, a finer grain size would lead to a higher strength in material. This non-uniformity of micro-structure in a single sample introduces varying yield strength properties in a single material. These materials can be used in application where a local region of a material requires high strength compare to other regions of the material [149, 161, 162]. In addition to this, the non homogenies nature of the grain can be resolved by introducing more revolutions of concurrent torsional straining to the sample to obtain homogeneous material property throughout the processed sample.

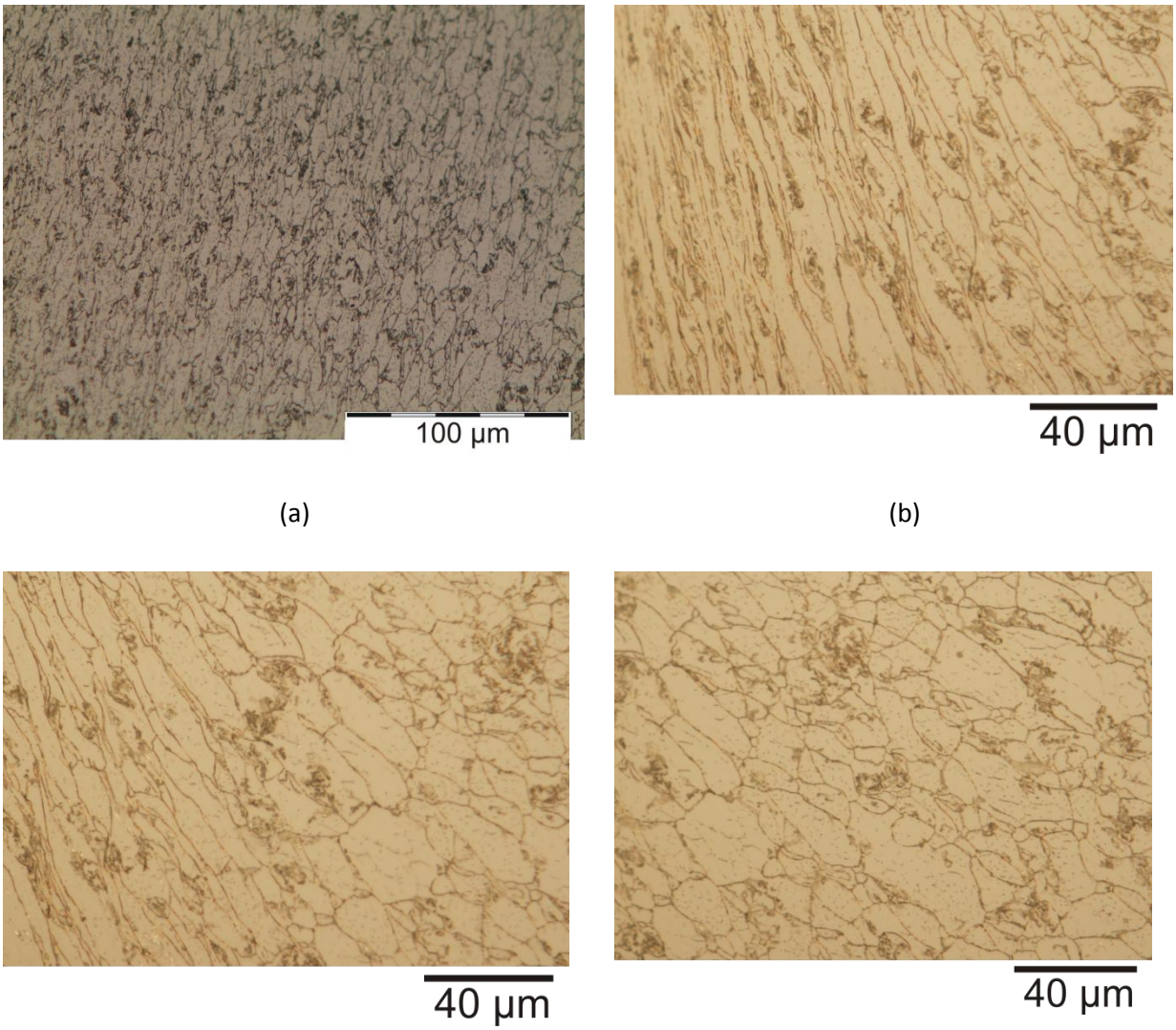

Fig 6-14 Microstructure of sample from case 4 at the surface 2 (longitudinal cross section) (a) overall micro structure with low magnification (b)near the periphery of the sample (c) between periphery and the center of the sample (d) region far from the periphery of the sample

The microstructure images of the surface 1 and 2 of the sample from “case 5” are respectively shown in Fig 6-15a and b. The elongated grain feature is absent in both circular and longitudinal cross sections (surface 1 and 2) of the sample from “case 5”. This has a good agreement with the predictions that the torsional straining change the grain structure into more elongated shapes in the CHPT samples.

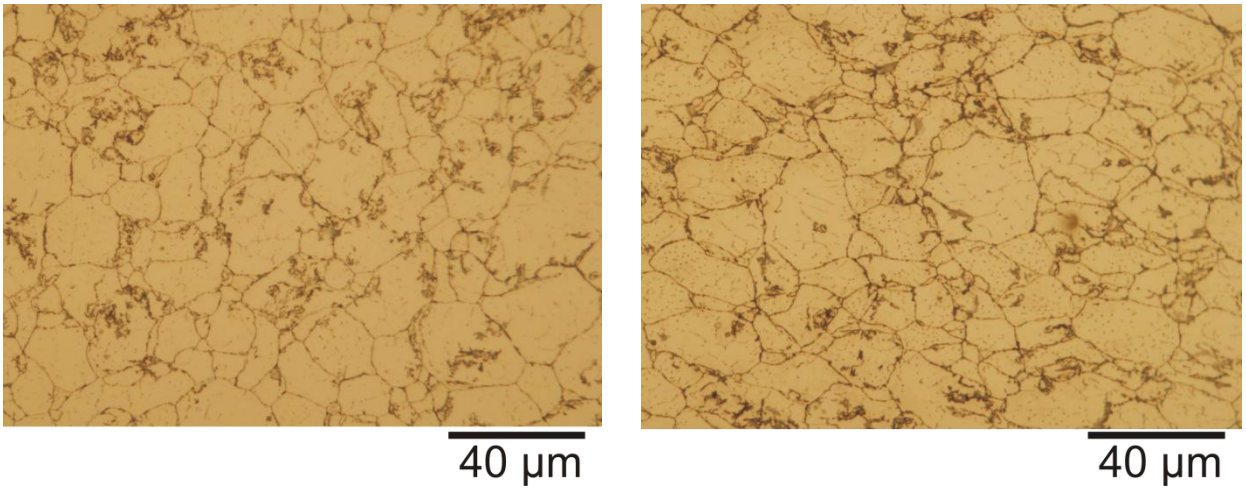

(a) (b)

Fig 6-15 Microstructure of sample from case 5 produced with 1.5GPa pressure without rotation (a) from the surface 1 (circular cross section) and (b) from the surface 2 (longitudinal cross section)

These results were compared with the grain structure of the pure bulk aluminum and the aluminum alloy AA5005-H35. The micro structure of the 99.999% pure bulk aluminum and the aluminum alloy AA5005-H34 are respectively shown in Fig 6-16a and b. it can be clearly noticed that the pure aluminum sample and aluminum alloy have relatively large average grain size of 223 µm and 192 µm respectively, which is significantly larger than average grain size of the CHPT processed aluminum powder samples, which can contribute to higher strength of the CHPT processed material.

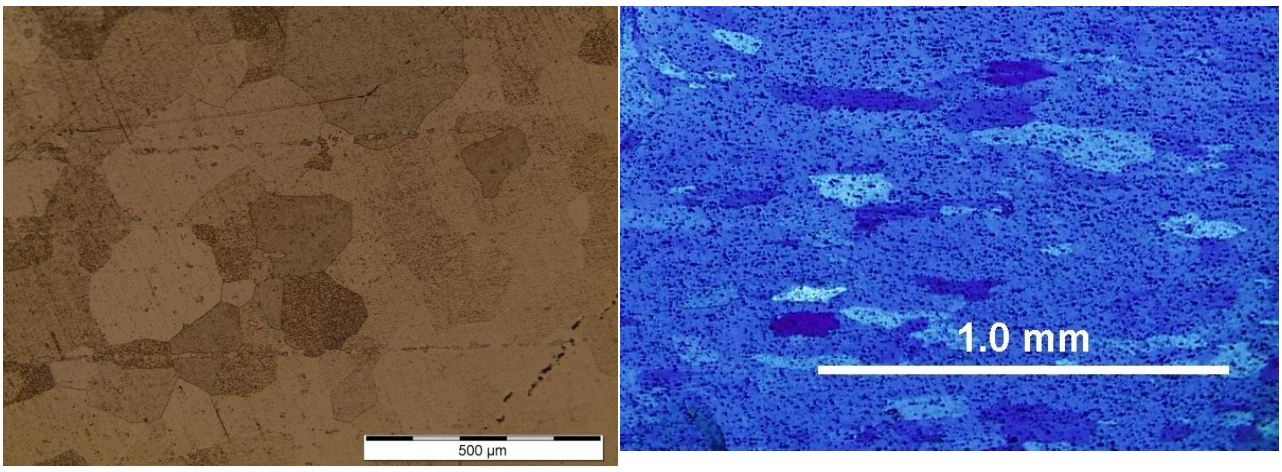

(a) (b)

Fig 6-16 (a) Microstructure of the pure bulk aluminum sample (b) Microstructure of the aluminum alloy AA5005 – H35

6.3 Experimental work of the Aluminum/Copper clad composite sample

The aim of the work is to study the CHPT process to fabricate Aluminum/Copper clad composite samples at room temperature. The microstructure and mechanical properties of the fabricated samples were investigated after the CHPT process with varying process parameters

6.3.1 Application of CHPT experiments to fabricate copper clad aluminum samples

6.3.1.1 Copper clad aluminum samples fabrication using CHPT

Before conducting the experiment, the die and punches were prepared by following the same procedure in Section 6.2.1. Then, a domed-shaped aluminum cap (Fig 6-3a) was placed into the die and using a hand press, flattens to seal the gap as shown in Fig 6-3b. A 4 mm height copper ring is placed on top of the flatten aluminum cap. Immediately before placing the copper ring into the die, it was mechanically cleaned using a 2500 grade emery paper to remove the oxide layer and washed with deionized water. Copper rings with 16mm outer diameter and 2mm thickness were used in these experiments. After that, aluminum powder was slowly poured inside the copper ring. The weight of the aluminum powder was measured using weight measurement scale. The cavity was filled with approximately 0.54g of aluminum powder every time. Another domed shaped cap was placed on top of the copper and powder surface inside the die, and flattened using the hand press. The initial arrangement of the CHPT test rig without die and sample is shown in Fig 6-17a. After that, the prepared sample with the die was placed on top of the lower punch, shown in Fig 6-17b. A hydraulic lift was used to slowly bring the top punch in the guided pillars until it sits on top of the sample shown in Fig 6-17c.

(a) (b) (c)

Fig.6 -17 The CHPT test rig (a) before placing the sample and die on the test rig which shows the top and bottom punches (b) after the sample and die were placed on top of the lower punch and (c) after bringing the top punch in contact with the processing sample

Then, the servo-Hydraulic FIHPST rig (Fig 6-4) was operated using computer controlled DAQ factory software. The Al/Cu clad composite was processed with 1.5GPa hydrostatic pressure with 2 revolutions of applied torsion. After processing the samples, macroscopic features of the processed samples were investigated. The images of the processed composite sample and the top aluminum cap are respectively shown in Fig 6-18a and 6-18b. These macroscopic images show the torsional deformation lines in both composite aluminum/copper sample and the aluminum cap.

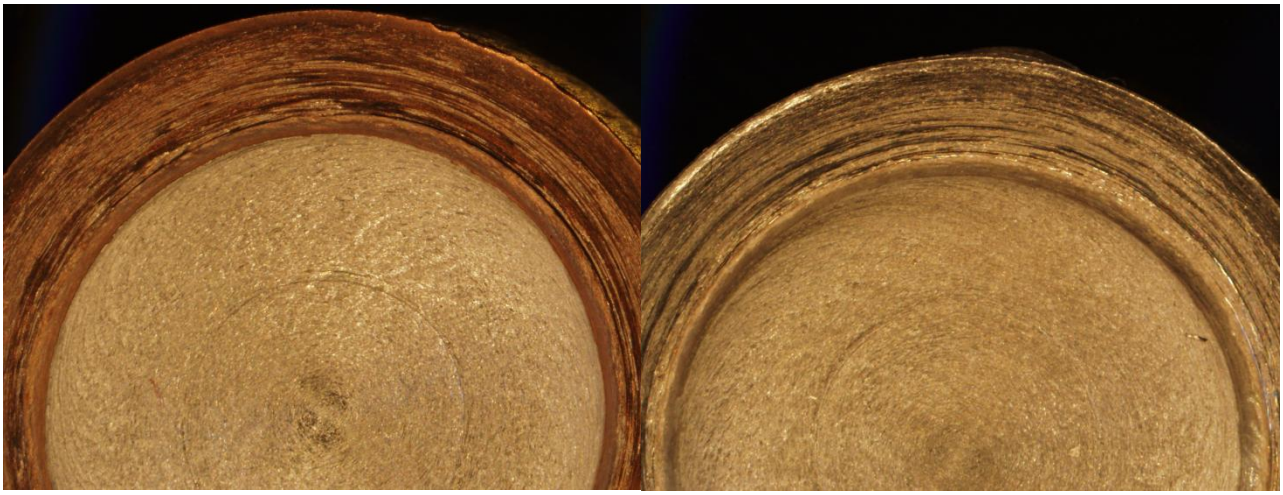

(a) (b)

Fig.6 -18 macroscopic features of the CHPT processed aluminum/copper composite sample (a) the cylindrical cross section view of the Al/Cu composite sample after removing the top cap and (b) the cylindrical surface of the top cap after CHPT process.

The sample cross sections and processed parent materials were investigated using Quanta 3D FEG scanning electron microscopy shown in Fig 6-19 a-d. The longitudinal section of the aluminum/copper composite fabricated using CHPT process is shown in Fig 6-19a. The interface image (Fig 6-19a) clearly indicates a 3D flow of materials during the process where the inner wall of copper was deformed at the interface during the process.

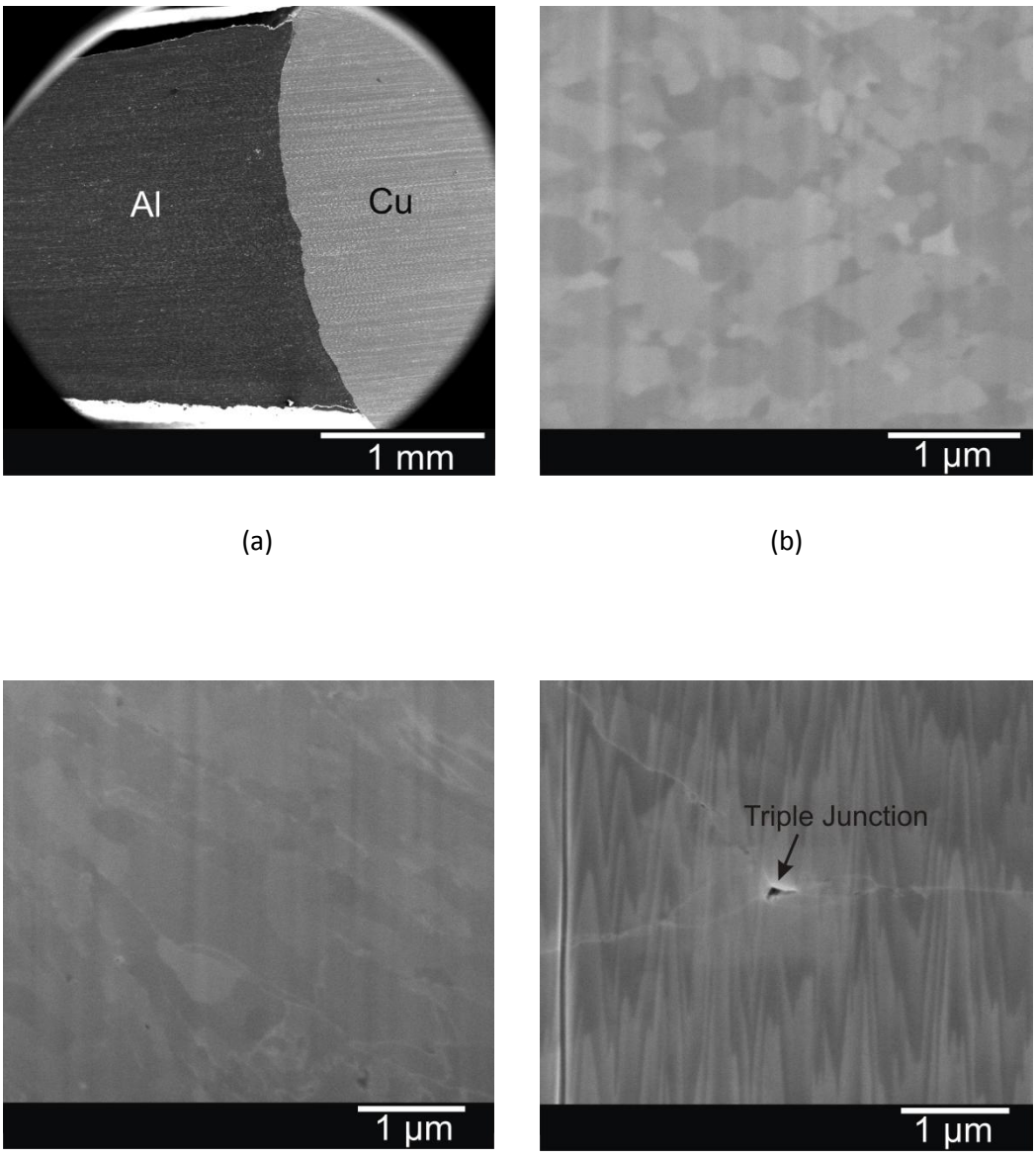

Fig 6-19 (a) longitudinal cross section of the Al/Cu composite after CHPT process (b) sub-micro structure of the copper region (c) sub-micro structure of the aluminum region (d) aluminum region shows a triple junction formed by 3 grains

The parent materials have a higher possibility to form fine microstructural constituents (i.e. grains) during the CHPT process. The formation of sub-structure in the copper region and the aluminum region are shown in Fig 6-19 b and c respectively. Fig 6-19d shows a triple point inside the aluminum region of the CHPT processed composite sample. However, the difficulty to the sample and presence of

multiple components (copper, aluminum powder and aluminum caps) while they are under processing made it was difficult to determine the deformation and stress development during the composite Al/Cu composite fabrication. In order to further understand the required process parameters and the role of torsional straining a multi-dimensional compaction was studied for the Al/Cu composite samples

6.3.1.2 Investigation of multi Multi-dimensional compaction using compression only copper clad aluminum sample.

In order to obtain a better understanding of the hybrid metal fabrication using the CHP process, an intermediate step of a multi-dimensional compaction of the raw aluminum powder inside a copper cavity was studied. A dome shaped aluminum cap placed to seal the gap between the dies. After that, the preparation steps in Section 6.3.1.1 were followed until the upper punch was placed on top of the sample. Then different pressure was applied to the sample and the sample was hold for 5 minutes after the desired pressure was reached. After 5 minutes, the power was turned off and the pressure was dropped itself to zero value. Then, the ram was moved away from the process rig. The experiment was repeated by varying the applied pressure. The parameters of the experiment are shown in Table 2.

Table 6-2: experimental parameters used in multi-dimensional compaction

Test No.	Sample diameter (mm)	Applied load (kN)	Pressure (GPa)	Weight of the Al powder (g)	Holding time (s)
1	**16**	**300**	**1.5**	**0.54**	**300**
2	**16**	**200**	**1.0**	**0.53**	**300**
3	**16**	**300**	**1.5**	**0.53**	**300**
4	**16**	**200**	**1.0**	**0.53**	**300**
5	**16**	**100**	**0.5**	**0.54**	**300**

After successful fabrication of the Al/Cu clad composite sample using multi-dimensional compaction, detailed investigation of the microstructural and mechanical properties of the greens product were performed. The micro-structural porosity investigation and mechanical testing of the composite Al/Cu samples are presented in the following sections.

6.3.1.3 Porosity investigation in Al/Cu composite sample fabricated using multi-dimensional compaction

The ground fabricated sample from multi-dimensional compaction is shown in Fig 6-20a. The micro-structures of the samples fabricated with various pressures are obtained to measure the average

particle size after the multi-dimensional compaction. The samples were ground to their mid-plane to observe the multi-dimensional compaction effect and to avoid discrepancies along the longitudinal axis of the sample. Micro structure from the samples fabricated using 1.5GPa, 1GPa and 0.5Gpa are respectively shown in Fig 6-20b-d.

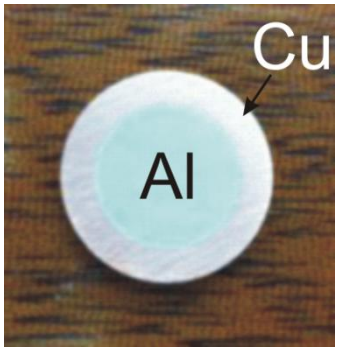

(a)

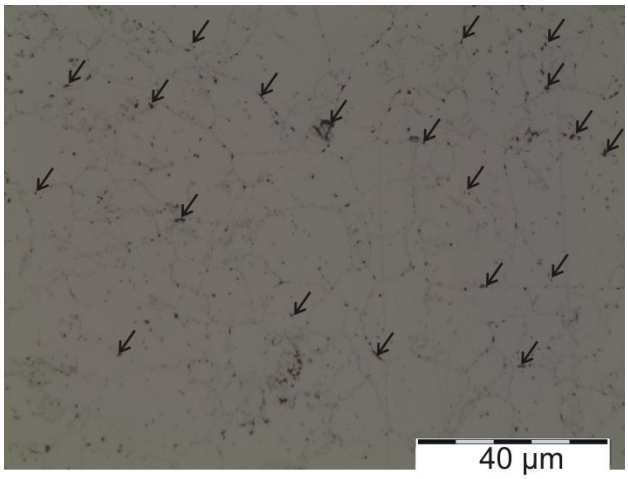

(b)

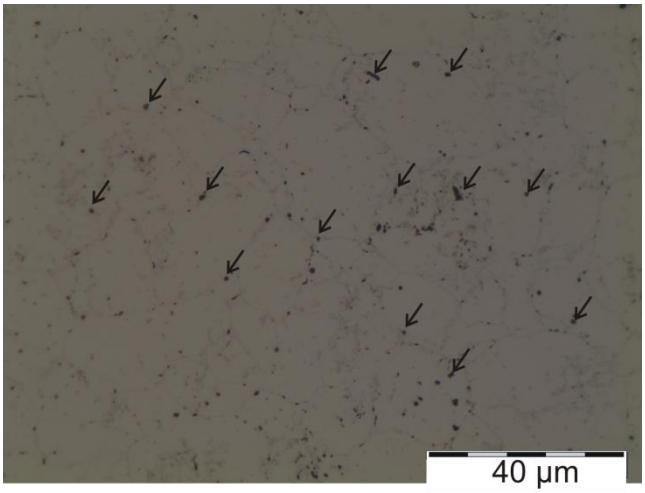

(c)

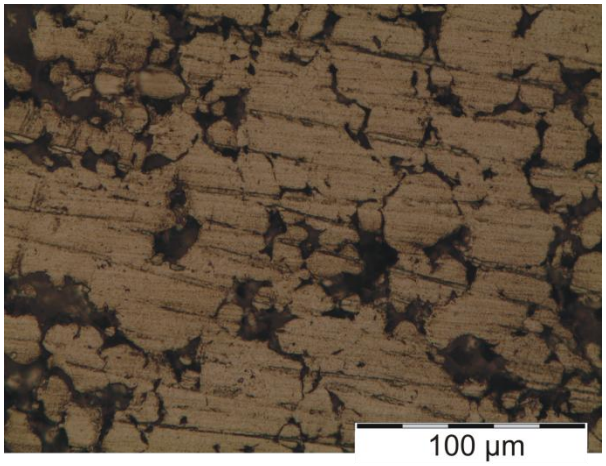

(d)

Fig 6-20 (a) Fabricated Al/Cu composite sample after grinding to 2mm (b) Aluminum region of the sample experience 1.5 GPa pressure (c) Aluminum region of the sample experience 1.0 GPa (d) Aluminum region of the sample experience 0.5 GPa

The pore size decreased by increasing the applied pressure at the same time particle density increased in the aluminum region of the fabricated Al/Cu composite sample. In addition to this, average particle size for the 1.5GPa, 1GPa and 0.5Gpa were found to be 16.24µm, 17.71µm and 26.52µm respectively. The aluminum powder used in these experiments has an average particle size of 28µm, which is slightly higher than the sample fabricated with 0.5GPa pressure. The 1.5GPa applied pressure in the multi-dimensional compaction caused 42% reduction in average aluminum particle size.

6.3.2 Post processing characterization using hardness test and micro shear punch test

The micro shear punch test (MSPT) was used to study the strength of Al/Cu composite fabricated using CHPT process and multi-dimensional compaction. MSPT results of Al/Cu composite sample processed in CHPT using 1.5GPa pressure with 2 revolution of torsional straining was compared with multi-dimensional compaction sample fabricated with 1.5GPa applied pressure. The micro shear punch tested sample and the MSPT results of the CHPT processed sample are shown in Fig 6-21a and Fig 6-21b respectively.

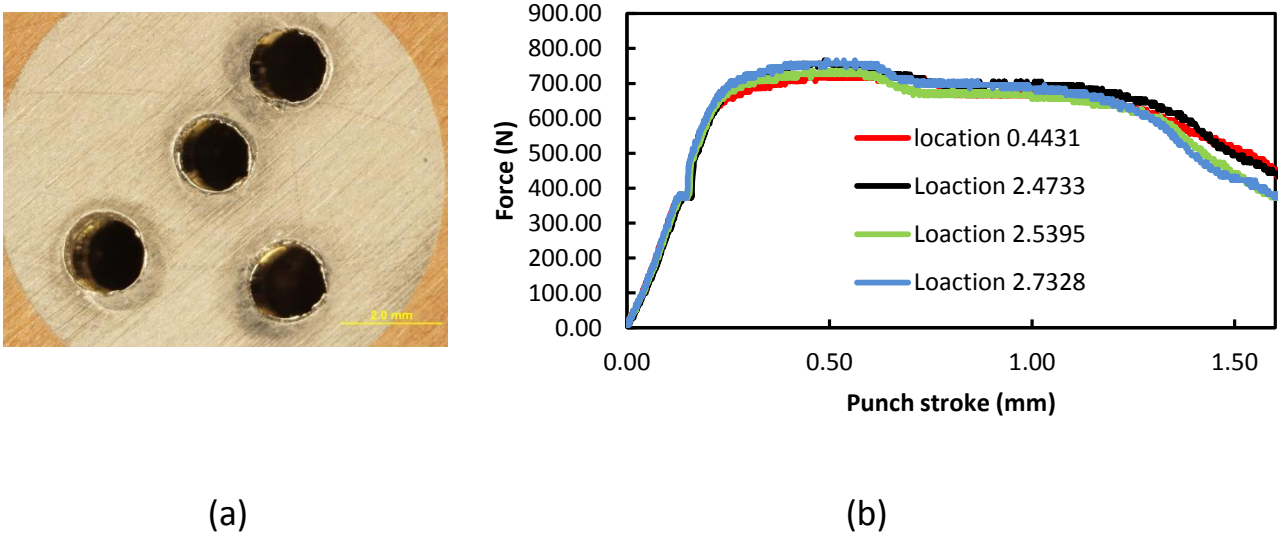

Fig 6-21 (a) CHPT processed sample (1.5 GPa with 2 revolution process condition) after micro shear punch test and (b) Shear stress versus normalized displacement for the CHPT processed sample obtained using micro shear punch test

The sample fabricated under multi-dimensional compaction using 1.5GPa applied pressure was also tested using MSPT. However, reliable data was not obtained as the sample was failed in an overloading fracture fashion. The fractured image of the MSPT sample and the fractography image of the sample are shown in Fig 6-22a and 6-22b respectively. These results confirmed that the torsional straining contributes significantly toward the strength of the powder material in a aluminum/copper composite sample fabricated using CHPT process.

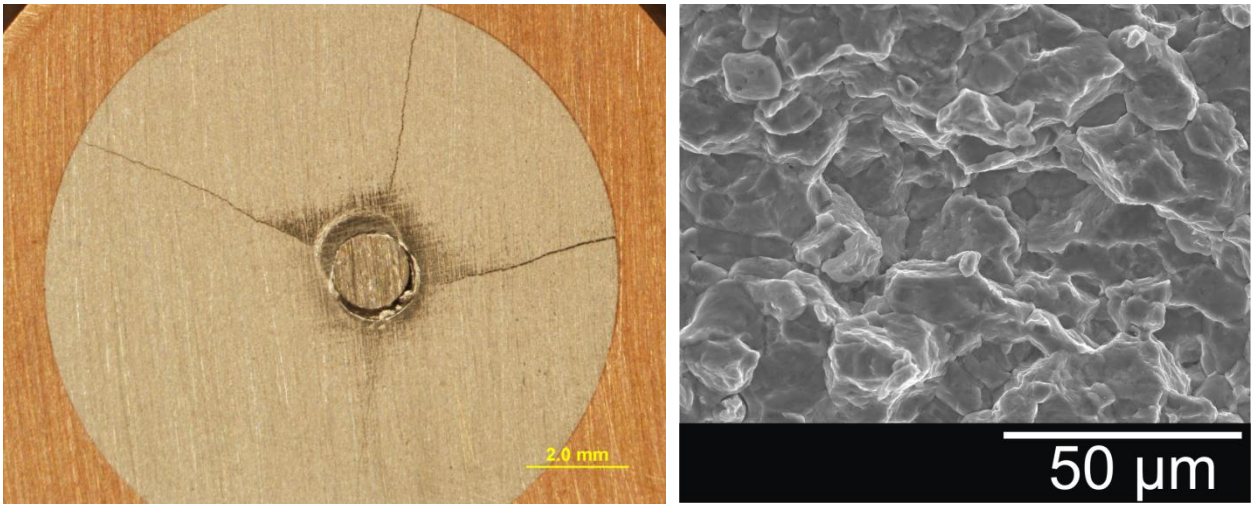

(a) (b)

Fig 6-22 (a) Fractured multi-dimensional compaction sample (1.5 GPa with 0 revolution process condition) after micro shear punch test and (b) Fractography image of the same sample after an overloading fracture.

6.4 Conclusions

A Confined High Pressure Torsion (CHPT) process was proposed to fabricate copper clad aluminum composite samples at room temperature. The Al/Cu composite sample composed of bulk copper ring as the clad and aluminum powder as the filler core material. In order to understand the process parameters, aluminum powder was initially used in this CHPT process to investigate hydrostatic pressure and torsional straining effect of the fabrication process. The preliminary studies showed promising results for the fabrication of high strength compact aluminum powder material, which was having the higher shear strength than that of commercially available aluminum alloy AA5005-H34. In addition to

this, aforementioned samples were fabricated at room temperature with only 1.5GPa hydrostatic pressure and 2 revolution of concurrent torsion. After that the CHPT experiments were performed on Al/Cu clad composite samples. The Al/Cu composite samples fabricated using CHPT were investigated using micro shear punch tests, optical microscopy, FIB-SEM techniques. In order to understand the role of torsional straining in the CHPT composite metal fabrication process, an intermediate step of multi-dimensional compaction stage was studied by applying various hydrostatic pressures to the sample fabrication. The fabricated samples using multi-dimensional compaction showed solid evidence of the porosity elimination and the role of pressure in the CHPT process. The full process of the CHPT (hydro static pressure with concurrent torsion) has significantly improved the mechanical properties of both aluminum power samples and copper clad aluminum samples. This CHPT process is beneficial for industrial applications where manufacturing of hybrid rods with broad range of energy and material saving are considered. Further investigation of the fabricated CHPT sample is required to optimize the process parameters. In this chapter CHPT process has been introduced as another successful fabrication method to produce axi-symmetric metallic composite at room temperature.

Chapter 7:
Conclusions and recommendations

Chapter 7: Conclusions and recommendations

7.1 Summary and conclusions

Alternate solutions to existing materials and novel manufacturing processes are highly demanding to cater for the limitations of the existing materials and the increasing demand to new materials. The existing materials are having limitations in terms of quantity as well as the required property for multiple attributes. Therefore recent years, hybrid materials become attractive alternate solution, which can cater for the existing demand as well as can be designed to provide the required multiple attributes in a single solution. For this purpose, metallic hybrid materials are fabricated using various metals forming and metal joining processes.

In term of hybrid metal fabrication, cladded hybrid rods and tubes have been fabricated using traditional processes, such as extrusion, drawing, hydrostatic extrusion process. A literature survey on existing metal forming and metal joining processes, which have been traditionally used to fabricate the cladded hybrid metal showed that those processing methods having disadvantages. They either required higher extrusion ratios or fluidic environments which make the process expensive, more venerable, non-energy efficient and uncontrollable dimensions of the final product.

Severe plastic deformation (SPD) processes are well known for improving material properties and deliver high strength processed materials due to significant grain refinement. In recent years, the severe plastic deformation (SPD) processes are used in manufacturing of hybrid metals which eliminate the drawbacks of the traditional core clad hybrid manufacturing techniques. Recent examples of hybrid metals fabrication using such SPD processes, such as using equal channel angular (ECAE) process are also reviewed in the literature. The drawbacks of the existing hybrid metal manufacturing using SPD processes and the suitability of the processing methods were analyzed.

Moreover, qualities of the processed hybrid metals using existing manufacturing techniques were also discussed in the literature review. It was identified that much more sophisticated processes are required to eliminate these existing issues in those manufacturing methods and to obtain hybrid metals with multiple attributes in a feasible way. After careful consideration of all those existing issues in the existing

hybrid metal manufacturing processes, two novel processes were proposed to fabricate axi-symmetric hybrid metals with more attractive attributes. Those processes are namely axi-symmetric forward spiral composite extrusion process (AFSCE) and confined high pressure torsion process (CHPT), were presented in this thesis.

The axi-symmetric forward composite spiral extrusion (AFSCE) process was firstly investigated for the fabrication of hybrid metal and which aimed to create a successful bonding at the interface using the process. In order to determine the amount of the strain components in the AFSCE samples, an analytical solution for two extreme boundary conditions of the AFSCE process was derived based on quadratic velocity field in the bimetallic composite during the process. An experimental case study of a hybrid rod fabrication using copper core and aluminum sleeve was investigated to determine the required process parameters of the AFSCE process.

Elevated temperature of 300° C with an applied back pressure of 200MPa was identified as a successful combination to create effective bonding in Al/Cu clad composite rods. A specially designed dedicated blanking test (DBT) was utilized to investigate the shear strength of the bonding which revealed successful bond formation during the AFSCE process. During the DBT test, the bonded interface fails suddenly which was similar to a brittle failure, while the reference pure aluminum failure was in a ductile fashion. It was identified that the presence of two materials at the interface can create a stress discontinuity and stress concentration at the interface which may cause the premature failure of the bonded interface. Further investigation was carried out across the interface region using SEM and EDX technique, and fractography analyses of the fractured surfaces during the blanking tests; the fracture had occurred at the interface which contains both copper and aluminum. These early promising results of a successful bond formation show that the AFSCE process has potential to manufacturing hybrid materials.

In addition to this, AFSCE process provides good dimensional control on the fabricated samples and it can be considered as a near zero shape change process. It is advantage of being a near zero shape change, which can reduce the material wastage during the fabrication process. Moreover the AFSCE process is performed in a single step which does not require additional time for holding the interfaces together or additional heat treatment makes the process more attractive for industrial applications, where it reduces the manufacturing cost and energy requirement.

Further investigation of the samples fabricated using AFSCE was carried out to understand the nature of the bonded interface and strength changes across the transverse section of the processed copper clad aluminum rods. Combinations of FIB, SEM, EDX and XRD techniques were used to characterise the bonding mechanism of the AFSCE processed samples. It was found that the bond was formed most likely by the mechanical interlocking mechanism because there were not any intermetallic compounds (IMCs) or diffusive layers were identified during the interfacial investigations. It was identified that the bond was almost flawless and the bonding shear strength was calculated based on the finding as approximately 50.5 MPa, which is higher than the shear yield strength of the pure aluminum (46 MPa) used in this study. This result demonstrated the potential of this process in a fabrication of copper clad aluminum composite rods.

Moreover, a complicated strain accumulation in those composite samples was observed in hardness results across the transverse section of the processed sample in radial directions, which was explained using an analytical model for both copper and aluminum regions. Hardness values in the copper region was distributed in a cop shape, where the hardness values at the interface and the outer periphery regions of the copper sleeve were found to be significantly higher than those in its middle region. The minimum hardness value in the middle region of the copper sleeve is approximately equal to that of unprocessed copper which is 61 HV10/10. A similar cup shape trend was also found in the extruded aluminum core. This cup shape behavior emphasizes a multidimensional deformation during the AFSCE process which was confirmed using various section views of the processed sample.

In addition to this, a formation of ultra-fine grains (UFGs) in the copper sleeve near the interface with approximately 61% of the grains below 1 μm was also confirmed in the processed samples using EBSD analyses. The grain refinement was identified as the reason for significant increase for hardness in the copper at interface region. In contrast, it was found that the deformation which led to the change in crystal orientation was the dominant mechanism for the hardness increase near the outer periphery of the composite structure. The EBSD crystal orientation results and texture plots, and statistical data of grain size and misorientation angle of those sampling regions revealed that the AFSCE process has the potential to form UFGs as well as change crystal orientation and texture in various locations of its sample. Therefore these investigations suggest that the potential application of the AFSCE process, which can produce architectural hybrid materials with specific localized properties as multiple attributes for modern industrial applications.

Finite element analysis using Abaqus FE package was carried out to identify the required design parameters of the special dedicated blanking test rig was also presented in chapter 5. The finite element (FE) model was conducted for the composite sample to study the effect of sample thickness, punch-die clearance and fillet radius of the blanking tools on the strain distribution near the interface regions during a shear blanking test. Model consists of constitutive models of both aluminum and copper obtained using a torsion test in a hot torsion machine after applying a heating cycle similar to the AFSCE process. Based on the finite element simulations, 1mm sample thickness was identified as the most suitable sample thickness to perform a DBT for a composite sample. The FE simulations also revealed that a 0.6 mm clearance between the punch and die develops a large effective strain at the interface, which is sufficient for failure to occur. The blanking tools (punch and die) fillet radii simulations showed that the non-sharp edges with 0.1mm fillet radii develop shear failure at the interface unlike the the tool with a sharp corner that caused failures at different places which deviates from the interface region. Based on the FE simulations, a test was required to be performed with the configuration of 1mm thick sample with the clearance of 0.6mm and blanking tools with fillet radii to determine the shear strength of a composite bonding to cause the failure exactly at the interface.

In addition to this, the FE simulations enhanced the understanding of composite blanking failure with the prominent effect of stress concentration scenarios which are not the case for a single material shear failure. The shearing load requirements to determine the bond strength of the AFSCE processed composite samples were measured using the designed test rig. Finally, the proposed design delivers an appropriate method that could be used for a composite structure to evaluate bond shear strength of interfacial failures.

In addition to this, a confined high pressure torsion process (CHPT), was also investigated to be used to fabricate axi- symmetric hybrid material. This process has shown to be beneficial and having potential applications compared to that of traditional high pressure torsion process. This confined HPT process can be applied to fabricate net-shape composite materials, where the process does not have any flashout during the processing which eliminates additional machining of the processed samples. The CHPT process was also investigated for a fabrication of copper clad aluminum samples using aluminum powder and bulk copper.

In order to understand the CHPT and the effects of process parameters, only aluminum powder was initially used in this process. The results of fabricated samples at room temperature with only 1.5GPa hydrostatic pressure and 2 revolution of concurrent torsion show the CHPT process having a potential application and eliminate the need for sintering which required for the traditional powder material processes to obtain a high quantity processed sample. The processed samples have the five times higher shear strength than the pure bulk aluminum sample. The fabricated Al powder samples also have higher shear strength than that of commercially available aluminum alloy AA5005-H34.

Then CHPT experiments were carried out to fabricate Al/Cu clad composite samples and investigated using micro shear punch tests, optical microscopy, FIB-SEM and optical microscopy. In order to understand the role of torsional straining in the CHPT composite metal fabrication process, an intermediate step of multi-dimensional compaction stage was investigated by applying various hydrostatic pressures to the composite sample. The fabricated samples using multi-dimensional compaction showed that the porosity elimination increases with the increase of the hydrostatic pressure during CHPT process.

The role of torsional straining on those CHPT processed composite samples and aluminum powder samples were studied using both samples with and without torsional straining. The samples fabricated with the torsional straining in the CHPT (with hydro static pressure) showed significant improvement of the mechanical properties of both aluminum power samples and copper clad aluminum samples.

In conclusion this thesis introduced two new axi-symmetric fabrication processes to produce hybrid metals. These processes have advantages using shear deformation and hydrostatic pressure to fabricate hybrid metals. AFSCE is a near-zero shape change process which has better dimensional control on the core and the clad material. The AFSCE process showed a promising bond formation by a mechanical interlocking and ultrafine grain formation in the copper region at the interface. The CHPT process showed an exceptional improvement in the compacted aluminum powder samples and the powder regions of the aluminum/copper clad samples. The effective compaction of this process is promising for high strength materials fabrication and become more economical as they eliminate the additional sintering process as in the traditional powder compaction methods.

7.2 Recommendations for further research

The mechanism for matching of the flow stresses at the core-clad interface is a key to understanding the hybrid bonding at the core-clad interface during AFSCE. Estimating the flow stresses within the composite sample is extremely difficult because of the presence of two materials during the AFSCE process. Therefore it requires simultaneous solution by trial and error of non-linear stiffness equations and their boundary conditions for core and clad material. The solution should be followed by "stress recovery" based on an accurate constitutive description of core-clad, kinematic equations and equilibrium of the forces at die-clad and core-clad interfaces. A numerical solution could be a solution for this problem, which requires the development of a sophisticated model based on complex and detailed boundary conditions at the interface of the core-clad metals.

Appropriateness of the relative velocity boundary conditions at the interface can affect the final results of the numerical model. Therefore an experiment with a tracing wired sample may be utilized to obtain the velocity distribution at the interface. After that by introducing the appropriate boundary condition to the bi-metallic numerical model the solution can be obtained. In addition to this, an appropriate numerical model for CHPT process can be modelled to predict the strain distribution in powder samples and composite samples. These numerical models can help to understand the role of actual CHPT process parameters and formation of a successful hybrid bonding.

Furthermore, various process conditions may utilize to further identify the potential application of the AFSCE process and CHPT process. For example, higher number of revolutions can have a capacity to produce nanocrystalline structures in the composite materials and single materials using the CHPT process provides opportunity for further investigation.

References

[1] M. F. Ashby, *Materials Selection in Mechanical Design*, 3rd edn ed.: Butterworth-Heinemann, 2004.

[2] M. F. Ashby and Y. J. M. Bréchet, "Designing hybrid materials," *Acta Materialia,* vol. 51, pp. 5801-5821, 2003.

[3] R. Z. Valiev, Y. Estrin, Z. Horita, T. G. Langdon, M. J. Zehetbauer, and Y. T. Zhu, "Producing bulk ultrafine-grained materials by severe plastic deformation," *JOM,* vol. 58, pp. 33-39, 2006.

[4] O. Bouaziz, H. S. Kim, and Y. Estrin, "Architecturing of Metal-Based Composites with Concurrent Nanostructuring: A New Paradigm of Materials Design," *Advanced Engineering Materials,* vol. 15, pp. 336-340, 2013.

[5] O. Bouaziz, Y. Bréchet, and J. D. Embury, "Heterogeneous and Architectured Materials: A Possible Strategy for Design of Structural Materials," *Advanced Engineering Materials,* vol. 10, pp. 24-36, 2008.

[6] D. Embury and O. Bouaziz, "Steel-based composites: driving forces and classifications," *Annual Review of Materials Research,* vol. 40, pp. 213-241, 2010.

[7] B. A. Ewing and M. Herman, "Method of manufacturing a hybrid turbine rotor," ed: Google Patents, 1979.

[8] J. C. Schilling, "Hybrid blade for a gas turbine," ed: Google Patents, 1997.

[9] H. I. H. Saravanamuttoo, G. F. C. Rogers, and H. Cohen, *Gas turbine theory*: Pearson Education, 2001.

[10] W. F. Hosford and R. M. Caddell, *Metal forming*: Prentice Hall, 1993.

[11] G. E. Dieter and D. Bacon, *Mechanical metallurgy* vol. 3: McGraw-Hill New York, 1986.

[12] J. Hu, Z. Marciniak, and J. Duncan, *Mechanics of sheet metal forming*: Butterworth-Heinemann, 2002.

[13] E. P. Degarmo, J. T. Black, and R. A. Kohser, "Materials and processing in manufacturing," 9 ed USA: John Wiley & Sons, 2004, pp. 969-974.

[14] M. P. Groover, *Fundamentals of modern manufacturing: materials processes, and systems*: John Wiley & Sons, 2007.

[15] S. Kumar, *Principles of metal working*: Oxford & IBH Publishing Company, 1985.

[16] I. Suchy, *Handbook of die design"*: Mc Graw-Hill Professional , 2006.

[17] S. Kobayashi, S.-i. Oh, T. Altan, and A. Chaudhary, "Metal forming and the finite-element method," *Journal of Materials Shaping Technology,* vol. 8, pp. 65-65, 1990.

[18] J. Bonet, *Nonlinear continuum mechanics for finite element analysis*: Cambridge university press, 1997.

[19] R. W. Lewis and B. A. Schrefler, *The finite element method in the static and dynamic deformation and consolidation of porous media*: John Wiley, 1998.

[20] S. Kalpakjian, "Manufacturing Engineering and Technology," ed USA: Addison-Wesley Publishing Company, 1992, pp. 888-890.

[21] N. F. Kazakov, *Diffusion Bonding of material*. Moscow: Mir Publishers, 1985.

[22] A. Shirzadi, "Solid-state diffusion bonding," in *Microjoining and nanojoining*, Y. N. Zhou, Ed., ed Cambridge: Woodhead Publishing Limited, 2004, pp. 234-249.

[23] C. JIANQIAO, S. TAKEZONO, L. GUANGXIA, and T. TANAKA, "Effect of laser cladding on fatigue strength of an alloy steel,"*Journal of society of material science(Japan),*vol.44, pp. 343-347, 1995.

[24] X. Wei, B. Vekshin, V. Kraposhin, Y. Huang, J. Shen, and K. Xia, "Full density consolidation of pure aluminium powders by cold hydro-mechanical pressing," *Materials Science and Engineering: A,* vol. 528, pp. 5784-5789, 2011.

[25] R. P. Seelig, "Introduction to Seminar-Review of Literature on Pressing of Metal Powders," *TRANSACTIONS OF THE AMERICAN INSTITUTE OF MINING AND METALLURGICAL ENGINEERS,* vol. 171, pp. 506-534, 1947.
[26] R. P. Seelig and J. Wulff, "The pressing operation in the fabrication of articles by powder metallurgy," *POWDER METALL, UK,* vol. 166, pp. 492-504, 1946.
[27] F. V. Lenel, "Mechanical fundamentals of consolidation," in *Metals handbook*. vol. 7, 9 ed: ASM, 1984, pp. 296-308.
[28] K. Lange and K. Pöhlandt, *Handbook of metal forming*: Ed. Techniques Ingénieur, 1985.
[29] D. Green, "Continuous extrusion-forming of wire sections," *J INST MET,* vol. 100, pp. 295-300, 1972.
[30] A. Azushima, R. Kopp, A. Korhonen, D. Yang, F. Micari, G. Lahoti*, et al.*, "Severe plastic deformation (SPD) processes for metals," *CIRP Annals-Manufacturing Technology,* vol. 57, pp. 716-735, 2008.
[31] C. Wang, F. Li, L. Wang, and H. Qiao, "Review on modified and novel techniques of severe plastic deformation," *Science China Technological Sciences,* vol. 55, pp. 2377-2390, 2012/09/01 2012.
[32] E. Hall, "The deformation and ageing of mild steel: III discussion of results," *Proceedings of the Physical Society. Section B,* vol. 64, p. 747, 1951.
[33] E. Hall, "The deformation and ageing of mild steel: II Characteristics of the Lüders deformation," *Proceedings of the Physical Society. Section B,* vol. 64, p. 742, 1951.
[34] E. O. Hall, *Yield point phenomena in metals and alloys*: Springer-Verlag US, 1970.
[35] N. Petch, "The cleavage strength of polycrystals," *J. Iron Steel Inst.,* vol. 174, pp. 25-28, 1953.
[36] R. Armstrong, I. Codd, R. Douthwaite, and N. Petch, "The plastic deformation of polycrystalline aggregates," *Philosophical Magazine,* vol. 7, pp. 45-58, 1962.
[37] N. J. Petch, "The influence of grain boundary carbide and grain size on the cleavage strength and impact transition temperature of steel," *Acta Metallurgica,* vol. 34, pp. 1387-1393, 7// 1986.
[38] W. F. Smith and J. Hashemi, *Foundations of materials science and engineering*: Mcgraw-Hill Publishing, 2006.
[39] R. Valiev, I. Alexandrov, Y. Zhu, and T. Lowe, "Paradox of strength and ductility in metals processed bysevere plastic deformation," *Journal of Materials Research,* vol. 17, pp. 5-8, 2002.
[40] H. W. Höppel, J. May, and M. Göken, "Enhanced Strength and Ductility in Ultrafine‐Grained Aluminium Produced by Accumulative Roll Bonding," *Advanced engineering materials,* vol. 6, pp. 781-784, 2004.
[41] M. A. Meyers, A. Mishra, and D. J. Benson, "Mechanical properties of nanocrystalline materials," *Progress in Materials Science,* vol. 51, pp. 427-556, 2006.
[42] T. C. Lowe, Y. T. Zhu, S. L. Semiatin, and D. R. Berg, "Overview and Outlook for Materials Processed by Severe Plastic Deformation," in *Investigations and Applications of Severe Plastic Deformation*. vol. 80, T. Lowe and R. Valiev, Eds., ed: Springer Netherlands, 2000, pp. 347-356.
[43] T. Lowe and R. Z. Valiev, *Investigations and applications of severe plastic deformation* vol. 80: Springer, 2000.
[44] M. Zehetbauer and R. Z. Valiev, *Nanomaterials by severe plastic deformation*: Wiley Online Library, 2004.
[45] R. Z. Valiev, M. J. Zehetbauer, Y. Estrin, H. W. Höppel, Y. Ivanisenko, H. Hahn*, et al.*, "The Innovation Potential of Bulk Nanostructured Materials," *Advanced Engineering Materials,* vol. 9, pp. 527-533, 2007.
[46] R. Z. Valiev, R. Islamgaliev, and I. Alexandrov, *Bulk nanostructured materials from severe plastic deformation* vol. 45: Pergamon, 2000.
[47] P. Prangnell, J. R. Bowen, and P. Apps, "Ultra-fine grain structures in aluminium alloys by severe deformation processing," *Materials Science and Engineering: A,* vol. 375, pp. 178-185, 2004.

[48] Y. Estrin and A. Vinogradov, "Extreme grain refinement by severe plastic deformation: A wealth of challenging science," *Acta Materialia,* vol. 61, pp. 782-817, 2013.

[49] J. C. Villegas, K. Dai, L. L. Shaw, and P. K. Liaw, "Nanocrystallization of a nickel alloy subjected to surface severe plastic deformation," *Materials Science and Engineering: A,* vol. 410–411, pp. 257-260, 11/25/ 2005.

[50] R. Z. Valiev, R. K. Islamgaliev, and I. V. Alexandrov, "Bulk nanostructured materials from severe plastic deformation," *Progress in Materials Science,* vol. 45, pp. 103-189, 2000.

[51] V. M. Segal, "Materials processing by simple shear," *Materials Science and Engineering: A,* vol. 197, pp. 157-164, 1995.

[52] H. S. Kim, "Finite element analysis of deformation behaviour of metals during equal channel multi-angular pressing," *Materials Science and Engineering: A,* vol. 328, pp. 317-323, 5// 2002.

[53] Y. Nishida, H. Arima, J.-C. Kim, and T. Ando, "Rotary-die equal-channel angular pressing of an Al – 7 mass% Si – 0.35 mass% Mg alloy," *Scripta Materialia,* vol. 45, pp. 261-266, 8/13/ 2001.

[54] C.-Y. Chou, S.-L. Lee, J.-C. Lin, and C.-M. Hsu, "Effects of cross-channel extrusion on the microstructures and superplasticity of a Zn–22 wt.% Al eutectoid alloy," *Scripta Materialia,* vol. 57, pp. 972-975, 11// 2007.

[55] V. S. Rao, B. Kashyap, N. Prabhu, and P. Hodgson, "T-shaped equi-channel angular pressing of Pb–Sn eutectic and its tensile properties," *Materials Science and Engineering: A,* vol. 486, pp. 341-349, 2008.

[56] B. Talebanpour, R. Ebrahimi, and K. Janghorban, "Microstructural and mechanical properties of commercially pure aluminum subjected to Dual Equal Channel Lateral Extrusion," *Materials Science and Engineering: A,* vol. 527, pp. 141-145, 2009.

[57] E. Cerri, P. P. De Marco, and P. Leo, "FEM and metallurgical analysis of modified 6082 aluminium alloys processed by multipass ECAP: Influence of material properties and different process settings on induced plastic strain," *Journal of Materials Processing Technology,* vol. 209, pp. 1550-1564, 2/1/ 2009.

[58] A. Ma, J. Jiang, N. Saito, I. Shigematsu, Y. Yuan, D. Yang*, et al.*, "Improving both strength and ductility of a Mg alloy through a large number of ECAP passes," *Materials Science and Engineering: A,* vol. 513, pp. 122-127, 2009.

[59] K. Nakashima, Z. Horita, M. Nemoto, and T. G. Langdon, "Development of a multi-pass facility for equal-channel angular pressing to high total strains," *Materials Science and Engineering: A,* vol. 281, pp. 82-87, 2000.

[60] B. Mani, M. Jahedi, and M. H. Paydar, "A modification on ECAP process by incorporating torsional deformation," *Materials Science and Engineering: A,* vol. 528, pp. 4159-4165, 5/15/ 2011.

[61] A. Rosochowski and L. Olejnik, "Finite element analysis of two-turn Incremental ECAP," *International Journal of Material Forming,* vol. 1, pp. 483-486, 2008/04/01 2008.

[62] V. M. Segal, "Engineering and commercialization of equal channel angular extrusion (ECAE)," *Materials Science and Engineering: A,* vol. 386, pp. 269-276, 2004.

[63] V. Segal, "Equal channel angular extrusion: from macromechanics to structure formation," *Materials Science and Engineering: A,* vol. 271, pp. 322-333, 1999.

[64] J.-C. Lee, Y.-H. Chung, H.-K. Seok, J.-Y. Suh, and J.-H. Han, "Structural evolution of a strip-cast al alloy sheet processed by continuous equal-channel angular pressing," *Metallurgical and materials transactions A,* vol. 33, pp. 665-673, 2002.

[65] R. Lapovok, D. Tomus, and C. Bettles, "Shear deformation with imposed hydrostatic pressure for enhanced compaction of powder," *Scripta Materialia,* vol. 58, pp. 898-901, 2008.

[66] V. Varyukhin, Y. Beygelzimer, S. Synkov, and D. Orlov, "Application of twist extrusion," *Materials Science Forum*, 2006, pp. 335-340.

[67] V. Varyukhin, Y. Beygelzimer, R. Kulagin, O. Prokof'eva, and A. Reshetov, "Twist extrusion: fundamentals and applications," *Materials Science Forum*, 2010, pp. 31-37.
[68] Y. Beygelzimer, V. Varyukhin, S. Synkov, and D. Orlov, "Useful properties of twist extrusion," *Materials Science and Engineering: A,* vol. 503, pp. 14-17, 2009.
[69] Y. Beygelzimer, D. Orlov, A. Korshunov, S. Synkov, V. Varyukhin, I. Vedernikova*, et al.*, "Features of twist extrusion: method, structures & material properties," *Solid State Phenomena,* vol. 114, pp. 69-78, 2006.
[70] P. W. Bridgman, "Effects of High Shearing Stress Combined with High Hydrostatic Pressure," *Physical Review,* vol. 48, pp. 825-847, 11/15/ 1935.
[71] A. P. Zhilyaev and T. G. Langdon, "Using high-pressure torsion for metal processing: Fundamentals and applications," *Progress in Materials Science,* vol. 53, pp. 893-979, 2008.
[72] A. P. Zhilyaev, S. Lee, G. V. Nurislamova, R. Z. Valiev, and T. G. Langdon, "Microhardness and microstructural evolution in pure nickel during high-pressure torsion," *Scripta Materialia,* vol. 44, pp. 2753-2758, 2001.
[73] A. Zhilyaev, G. Nurislamova, B.-K. Kim, M. Baró, J. Szpunar, and T. Langdon, "Experimental parameters influencing grain refinement and microstructural evolution during high-pressure torsion," *Acta Materialia,* vol. 51, pp. 753-765, 2003.
[74] A. Vorhauer and R. Pippan, "On the homogeneity of deformation by high pressure torsion," *Scripta Materialia,* vol. 51, pp. 921-925, 2004.
[75] M. Kawasaki, R. B. Figueiredo, and T. G. Langdon, "An investigation of hardness homogeneity throughout disks processed by high-pressure torsion," *Acta Materialia,* vol. 59, pp. 308-316, 2011.
[76] A. Zhilyaev, S. Lee, G. Nurislamova, R. Valiev, and T. Langdon, "Microhardness and microstructural evolution in pure nickel during high-pressure torsion," *Scripta materialia,* vol. 44, pp. 2753-2758, 2001.
[77] J. M. Cubero-Sesin and Z. Horita, "Powder consolidation of Al–10wt% Fe alloy by High-Pressure Torsion," *Materials Science and Engineering: A,* vol. 558, pp. 462-471, 12/15/ 2012.
[78] D. J. Lee, E. Y. Yoon, L. J. Park, and H. S. Kim, "The dead metal zone in high-pressure torsion," *Scripta Materialia,* vol. 67, pp. 384-387, 2012.
[79] Y. Huang, M. Kawasaki, and T. G. Langdon, "Influence of Anvil Alignment on Shearing Patterns in High‐Pressure Torsion," *Advanced Engineering Materials,* vol. 15, pp. 747-755, 2013.
[80] S. Khoddam, A. Farhoumand, and P. D. Hodgson, "Axi-symmetric forward spiral extrusion, a kinematic and experimental study," *Materials Science and Engineering: A,* vol. 528, pp. 1023-1029, 2011.
[81] S. Khoddam, A. Farhoumand, and P. D. Hodgson, "Upper-bound analysis of axi-symmetric forward spiral extrusion," *Mechanics of Materials,* vol. 43, pp. 684-692, 2011.
[82] S. Khoddam, A. Farhoumand, and P. D. Hodgson, "A kinematics study of variable lead axisymmetric forward spiral extrusion," *Materials Science and Engineering: A,* vol. 550, pp. 167-175, 2012.
[83] A. Farhoumand, P. D. Hodgson, and S. Khoddam, "Finite element analysis of plastic deformation in variable lead axisymmetric forward spiral extrusion," *Journal of Materials Science,* vol. 48, pp. 2454-2461, 2013/03/01 2013.
[84] A. Farhoumand, P. D. Hodgson, S. Khoddam, and X. Y. Fang, "Multiple pass axi-symmetrical forward spiral extrusion of interstitial-free (IF) steel," *Materials Science and Engineering: A,* vol. 579, pp. 217-225, 2013.
[85] A. Farhoumand, P. D. Hodgson, and S. Khoddam, "Finite Element Analysis of an Axi-Symmetric Forward Spiral Extrusion of Mg-1.75Mn Alloy," *Materials Science Forum,* vol. 690, pp. 173-176, 2011.

[86] A. Farhoumand, S. Khoddam, and P. Hodgson, "A study of plastic deformation during axisymmetric forward spiral extrusion and its subsequent mechanical property changes," *Modelling and simulation in materials science and engineering,* vol. 20, p. 085005, 2012.
[87] K. Kaneko, T. Hata, T. Tokunaga, and Z. Horita, "Fabrication and Characterization of Supersaturated Al-Mg Alloys by Severe Plastic Deformation and Their Mechanical Properties," *Materials transactions,* vol. 50, p. 76, 2009.
[88] W. Botta Filho, J. Fogagnolo, C. Rodrigues, C. Kiminami, C. Bolfarini, and A. Yavari, "Consolidation of partially amorphous aluminium-alloy powders by severe plastic deformation," *Materials Science and Engineering: A,* vol. 375, pp. 936-941, 2004.
[89] A. Yavari, C. Rodrigues, C. Cardoso, and R. Valiev, "Nanostructured bulk Al< sub> 90</sub> Fe< sub> 5</sub> Nd< sub> 5</sub> prepared by cold consolidation of gas atomised powder using severe plastic deformation," *Scripta Materialia,* vol. 46, pp. 711-716, 2002.
[90] A. Bachmaier and R. Pippan, "Effect of oxide particles on the stabilization and final microstructure in aluminium," *Materials Science and Engineering: A,* vol. 528, pp. 7589-7595, 2011.
[91] Z. Lee, F. Zhou, R. Valiev, E. Lavernia, and S. Nutt, "Microstructure and microhardness of cryomilled bulk nanocrystalline Al–7.5% Mg alloy consolidated by high pressure torsion," *Scripta materialia,* vol. 51, pp. 209-214, 2004.
[92] T. Tokunaga, K. Kaneko, K. Sato, and Z. Horita, "Microstructure and mechanical properties of aluminum–fullerene composite fabricated by high pressure torsion," *Scripta Materialia,* vol. 58, pp. 735-738, 2008.
[93] J. Shang, K. Wang, Q. Zhou, D. Zhang, J. Huang, and G. Li, "Microstructure characteristics and mechanical properties of cold metal transfer welding Mg/Al dissimilar metals," *Materials & Design,* vol. 34, pp. 559-565, 2012.
[94] P. Sammaiah, A. Suresh, and G. R. N. Tagore, "Mechanical properties of friction welded 6063 aluminum alloy and austenitic stainless steel," *Journal of Materials Science,* vol. 45, pp. 5512-5521, 2010/10/01 2010.
[95] B.-M. Li, G.-M. Xu, and J.-Z. Cui, "Inversion Solidification Cladding of H90-Steel," *Journal of Iron and Steel Research, International,* vol. 15, pp. 51-56, 7// 2008.
[96] Y. Lu, J. Song, J. Y. Huang, and J. Lou, "Fracture of Sub‐20nm Ultrathin Gold Nanowires," *Advanced Functional Materials,* vol. 21, pp. 3982-3989, 2011.
[97] Y. Lu, J. Y. Huang, C. Wang, S. Sun, and J. Lou, "Cold welding of ultrathin gold nanowires," *Nature nanotechnology,* vol. 5, pp. 218-224, 2010.
[98] L. W. Shi and X. Y. Zhang, "Design of Copper-Clad Aluminum Winding Alternator for Vehicle Application," *Advanced Materials Research* vol. Volumes 282 - 283, pp. 322-325, 2011.
[99] J. Lee, D. Bae, W. Chung, K. Kim, J. Lee, and Y. Cho, "Effects of annealing on the mechanical and interface properties of stainless steel/aluminum/copper clad-metal sheets," *Journal of Materials Processing Technology,* vol. 187, pp. 546-549, 2007.
[100] J. Nilson, "Method of manufacturing extruded rods of wire from compound material," Sweden Patent 3,780,554, 1973.
[101] K. Osakada, M. Limb, and P. Mellor, "Hydrostatic extrusion of composite rods with hard cores," *International Journal of Mechanical Sciences,* vol. 15, pp. 291-307, 1973.
[102] N. Ahmed, "Extrusion of copper clad aluminum wire," *Journal of Mechanical Working Technology,* vol. 2, pp. 19-32, 1978.
[103] R. Sliwa, "A test determining the ability of different materials to undergo simultaneous plastic deformation to produce metal composites," *Materials Science and Engineering: A,* vol. 135, pp. 259-265, 1991.

[104] R. Sliwa, "Plastic zones in the extrusion of metal composites," *Journal of materials processing technology,* vol. 67, pp. 29-35, 1997.
[105] K. Y. Rhee, W. Y. Han, H. J. Park, and S. S. Kim, "Fabrication of aluminum/copper clad composite using hot hydrostatic extrusion process and its material characteristics," *Materials Science and Engineering: A,* vol. 384, pp. 70-76, 2004.
[106] T. K. J. H. C. Kwon , S. C. Lim, M. S. Kim, "Fabrication of Copper Clad Aluminum Wire(CCAW) by Indirect Extrusion and Drawing," *Materials Science Forum,* vol. 449-452, pp. 317-320, 2004.
[107] A. R. Eivani and A. K. Taheri, "A new method for producing bimetallic rods," *Materials Letters,* vol. 61, pp. 4110-4113, 2007.
[108] P. Eslami and A. K. Taheri, "An investigation on diffusion bonding of aluminum to copper using equal channel angular extrusion process," *Materials Letters,* vol. 65, pp. 1862-1864, 2011.
[109] M. Zebardast and A. K. Taheri, "The cold welding of copper to aluminum using equal channel angular extrusion (ECAE) process," *Journal of Materials Processing Technology,* vol. 211, pp. 1034-1043, 2011.
[110] C. S. Hartley, "Upper bound analysis of extrusion of axisymmetric, piecewise homogeneous tubes," *International Journal of Mechanical Sciences,* vol. 15, pp. 651-663, 1973.
[111] H. Tokuno and K. Ikeda, "Analysis of deformation in extrusion of composite rods," *Journal of Materials Processing Technology,* vol. 26, pp. 323-335, 1991.
[112] B. Avitzur, R. Wu, S. Talbert, and Y. Chou, "Criterion for the prevention of core fracture during extrusion of bimetal rods," *Journal of Manufacturing Science and Engineering,* vol. 104, pp. 293-304, 1982.
[113] B. Avitzur, R. Wu, S. Talbert, and Y. Chou, "Criterion for the prevention of sleeve fracture during extrusion of bimetal rods," *Journal of Manufacturing Science and Engineering,* vol. 108, pp. 205-212, 1986.
[114] N. Chitkara and A. Aleem, "Extrusion of axi-symmetric bi-metallic tubes: some experiments using hollow billets and the application of a generalised slab method of analysis," *International Journal of Mechanical Sciences,* vol. 43, pp. 2857-2882, 2001.
[115] S. Berski, H. Dyja, G. Banaszek, and M. Janik, "Theoretical analysis of bimetallic rods extrusion process in double reduction die," *Journal of materials processing technology,* vol. 153, pp. 583-588, 2004.
[116] H. Haghighat and G. R. Asgari, "A generalized spherical velocity field for bi-metallic tube extrusion through dies of any shape," *International Journal of Mechanical Sciences,* vol. 53, pp. 248-253, 2011.
[117] P. Kazanowski, M. E. Epler, and W. Z. Misiolek, "Bi-metal rod extrusion—process and product optimization," *Materials Science and Engineering: A,* vol. 369, pp. 170-180, 2004.
[118] A. Khosravifard and R. Ebrahimi, "Investigation of parameters affecting interface strength in Al/Cu clad bimetal rod extrusion process," *Materials & Design,* vol. 31, pp. 493-499, 2010.
[119] D. G. Brandon and W. D. Kaplan, *Joining processes:an introduction*: Wiley, 1997.
[120] S. KHODDAM, LAM, Y. C., THOMSON, and P. F., *The effect of specimen geometry on the accuracy of the constitutive equation derived from the hot torsion test* vol. 66. Düsseldorf, ALLEMAGNE: Stahleisen, 1995.
[121] P. C. King, S. H. Zahiri, and M. Jahedi, "Focused ion beam micro-dissection of cold-sprayed particles," *Acta Materialia,* vol. 56, pp. 5617-5626, 2008.
[122] T. T. Sasaki, R. A. Morris, G. B. Thompson, Y. Syarif, and D. Fox, "Formation of ultra-fine copper grains in copper-clad aluminum wire," *Scripta Materialia,* vol. 63, pp. 488-491, 2010.
[123] H. D. Manesh and A. K. Taheri, "Bond strength and formability of an aluminum-clad steel sheet," *Journal of Alloys and Compounds,* vol. 361, pp. 138-143, 2003.

[124] T. K. Varadan and K. Bhaskar, in *Analysis of Plates: Theory and Problems*, ed Delhi: Narosa Publishing House, 1999, pp. 153-163.
[125] A. K. Noor and W. Scott Burton, "Stress and free vibration analyses of multilayered composite plates," *Composite Structures,* vol. 11, pp. 183-204, 1989.
[126] M. Drozdov, G. Gur, Z. Atzmon, and W. D. Kaplan, "Detailed investigation of ultrasonic Al-Cu wire-bonds: I. Intermetallic formation in the as-bonded state," *Journal of Materials Science,* vol. 43, pp. 6029-6037, 2008.
[127] H. J. Kim, J. Y. Lee, K. W. Paik, K. W. Koh, J. Won, S. Choe*, et al.*, "Effects of Cu/Al intermetallic compound (IMC) on copper wire and aluminum pad bondability," *Components and Packaging Technologies, IEEE Transactions on,* vol. 26, pp. 367-374, 2003.
[128] D. S. Bae, S. K. Kim, S. L. Lee, T. Shibayama, and D. H. Bae, "Interface Properties of Copper/Aluminum/Stainless Steel Clad Materials," *Key Engineering Materials,* vol. 345, pp. 1497-1500, 2007.
[129] J. Feng, X. Songbai, and D. Wei, "Reliability studies of Cu/Al joints brazed with Zn–Al–Ce filler metals," *Materials & Design,* vol. 42, pp. 156-163, 2012.
[130] F. Ji, S.-b. Xue, J.-y. Lou, Y.-b. Lou, and S.-q. Wang, "Microstructure and properties of Cu/Al joints brazed with Zn–Al filler metals," *Transactions of Nonferrous Metals Society of China,* vol. 22, pp. 281-287, 2012.
[131] Y. Xiao, H. Ji, M. Li, and J. Kim, "Ultrasound-assisted brazing of Cu/Al dissimilar metals using a Zn–3Al filler metal," *Materials & Design,* vol. 52, pp. 740-747, 2013.
[132] A. Farhoumand, P. Hodgson, and S. Khoddam, "Finite element analysis of an axi-symmetric forward spiral extrusion of Mg-1.75 Mn alloy," *Materials Science Forum*, 2011, pp. 173-176.
[133] N. Llorca-Isern, A. M. Escobar, A. Roca, and J. M. Cabrera, "Equal Channel Angular Pressing of Cu-Al Bimetallic Rod," *Materials Science Forum*, 2012, pp. 1811-1816.
[134] C. L. Bauer and G. G. Lessmann, "Metal-joining methods," *Annual Review of Materials Science,* vol. 6, pp. 361-387, 1976.
[135] T. Sasaki, M. Barkey, G. Thompson, Y. Syarif, and D. Fox, "Microstructural evolution of copper clad steel bimetallic wire," *Materials Science and Engineering: A,* vol. 528, pp. 2974-2981, 2011.
[136] U. Fischer, R. Gomeringer, M. Heinzler, R. Kilgus, F. Naher, S. Oesterle*, et al.*, *Mechanical and Metal Trades Handbook*, 2nd ed. Germany: Verlag Europa-Lehrmittel Nourney, Vollmer GmbH & C, 2010.
[137] D. Banabic, *Sheet metal forming processes: constitutive modelling and numerical simulation*: Springer, 2010.
[138] M. A. Sokolov, J. D. Landes, and G. E. Lucas, *Small Specimen Test Techniques* vol. 4: ASTM International, 2002.
[139] R. K. Guduru, K. A. Darling, R. Kishore, R. O. Scattergood, C. C. Koch, and K. L. Murty, "Evaluation of mechanical properties using shear–punch testing," *Materials Science and Engineering: A,* vol. 395, pp. 307-314, 2005.
[140] R. K. Guduru, A. V. Nagasekhar, R. O. Scattergood, C. C. Koch, and K. L. Murty, "Finite element analysis of a shear punch test," *Metallurgical and Materials Transactions A: Physical Metallurgy and Materials Science,* vol. 37, pp. 1477-1483, 2006.
[141] G. E. Lucas, J. W. Sheckherd, G. R. Odette, and S. Panchanadeeswaran, "Shear punch tests for mechanical property measurements in TEM disc-sized specimens," *Journal of Nuclear Materials,* vol. 122, pp. 429-434, 1984.
[142] J. Elambasseril, R. N. Ibrahim, and R. Das, "Evaluation of fracture characteristics of ceramic coatings on stainless steel substrates using circumferentially notched tensile specimens," *Composites Part B: Engineering,* vol. 42, pp. 1596-1602, 2011.

[143] J. Elambasseril and R. N. Ibrahim, "Validity requirements of circumferentially notched tensile specimens for the determination of the interfacial fracture toughness of coatings," *Composites Part B: Engineering,* vol. 43, pp. 2415-2422, 2012.

[144] G. L. Hankin, M. B. Toloczko, M. L. Hamilton, and R. G. Faulkner, "Validation of the shear punch–tensile correlation technique using irradiated materials," *Journal of Nuclear Materials,* vol. 258–263, Part 2, pp. 1651-1656, 1998.

[145] M. B. Toloczko, R. J. Kurtz, A. Hasegawa, and K. Abe, "Shear punch tests performed using a new low compliance test fixture," *Journal of Nuclear Materials,* vol. 307, pp. 1619-1623, 2002.

[146] M. B. Toloczko, K. Abe, M. L. Hamilton, F. A. Garner, and R. J. Jurtz, "The effect of specimen thickness and grain size on mechanical obtained for the shear punch test," in *Small specimen test techniques*. vol. 4, M. A. Sokolov, J. D. Landes, and G. E. Lucas, Eds., ed USA: ASTM International, 2002, pp. 371-379.

[147] M. B. Toloczko, M. L. Hamilton, and G. E. Lucas, "Ductility correlations between shear punch and uniaxial tensile test data," *Journal of Nuclear Materials,* vol. 283–287, Part 2, pp. 987-991, 2000.

[148] C. A. León and R. A. L. Drew, "Small punch testing for assessing the tensile strength of gradient Al/Ni–SiC composites," *Materials Letters,* vol. 56, pp. 812-816, 2002.

[149] A. Shamdani, S. Khoddam, P. Thomson, and A. Dehghan-Manshadi, "Microstructure and mechanical properties of IF steel deformed during plane stress local torsion," *Journal of Materials Science,* vol. 47, pp. 1582-1587, 2012.

[150] M. Abbasi Gharacheh, A. Kokabi, G. Daneshi, B. Shalchi, and R. Sarrafi, "The influence of the ratio of “rotational speed/traverse speed”(ω/< i> v</i>) on mechanical properties of AZ31 friction stir welds," *International Journal of Machine Tools and Manufacture,* vol. 46, pp. 1983-1987, 2006.

[151] S. A. Hosseini, M. Hosseini, and H. Danesh Manesh, "Bond strength evaluation of roll bonded bi-layer copper alloy strips in different rolling conditions," *Materials & Design,* vol. 32, pp. 76-81, 2011.

[152] M. Eizadjou, H. Danesh Manesh, and K. Janghorban, "Investigation of roll bonding between aluminum alloy strips," *Materials & Design,* vol. 29, pp. 909-913, 2008.

[153] A. F1044-05, "Standard Test Method for Shear Testing of Calcium Phosphate Coatings and Metallic Coatings," ed. USA: Conshohocken, PA, 2010.

[154] J. Mackerle, "Finite element analysis and simulation of welding: a bibliography (1976-1996)," *Modelling and Simulation in Materials Science and Engineering,* vol. 4, p. 501, 1996.

[155] J. Mackerle, "Finite element analysis and simulation of welding-an addendum: a bibliography (1996-2001)," *Modelling and Simulation in Materials Science and Engineering,* vol. 10, p. 295, 2002.

[156] J. Mackerle, "Finite element analysis and simulation of adhesive bonding, soldering and brazing: A bibliography (1976-1996)," *Modelling and Simulation in Materials Science and Engineering,* vol. 5, p. 159, 1997.

[157] S. Khoddam and P. D. Hodgson, "Post processing of the hot torsion test results using a multi-dimensional modelling approach," *Materials & Design,* vol. 31, pp. 2578-2584, 2010.

[158] S. Khoddam and P. D. Hodgson, "A heuristic model selection scheme for representing hot flow data using the hot torsion test results," *Materials & Design,* vol. 31, pp. 2011-2017, 2010.

[159] R. Lapovok, H. P. Ng, D. Tomus, and Y. Estrin, "Bimetallic copper–aluminium tube by severe plastic deformation," *Scripta Materialia,* vol. 66, pp. 1081-1084, 2012.

[160] M. Manahan, A. Argon, and O. Harling, "The development of a miniaturized disk bend test for the determination of postirradiation mechanical properties," *Journal of Nuclear Materials,* vol. 104, pp. 1545-1550, 1981.

[161] A. Shamdani and S. Khoddam, "A combined upper-bound and elastic-plastic finite element solution for a fastener hole subjected to internal torsion," *Archive of Applied Mechanics,* vol. 82, pp. 445-459, 2012.

[162] A. H. Shamdani and S. Khoddam, "A computer-aided specimen design to induce shearing strain around a hole," *Proceedings of the Institution of Mechanical Engineers, Part C: Journal of Mechanical Engineering Science,* p. 0954406212440909, 2012.